

**Pharmacological manipulation of the purinergic P2X₇
receptor: effects on tumor and host cells**

Dissertation

Submitted to the Department of Chemistry,
Faculty of Mathematics, Informatics and Natural Sciences,
University of Hamburg
for the degree of
Doctor of Natural Sciences
(Dr. rer. nat.)

by

Sana Javed

From Faisalabad, Pakistan

Hamburg, January 2020

Supervisor:

Prof. Dr. med. Friedrich Haag

University Medical Center Hamburg-Eppendorf

Department of Diagnostic

Institute of Immunology,

Martinistrasse 52,

20246 Hamburg, Germany

Co-supervisor:

Prof. Dr. rer.nat Peter Heisig

University of Hamburg

Department of Chemistry

Institute of Biochemistry and Molecular Biology

Bundesstrasse 45

20146 Hamburg, Germany

Defense date: 28.02.2020

The present work was carried out in the period from October 2014 to December 2019 at the Institute for Immunology at the University Clinic Hamburg-Eppendorf in the working group of Prof. Dr. Friedrich Haag.

Table of Contents

Zusammenfassung	6
Abstract	8
Abbreviation.....	10
1 Introduction	13
1.1. Purinergic receptors	13
1.1.1. P2X ₇ ion channel	13
1.2. Purinergic signaling	14
1.3. P2X ₇ in cancer	16
1.4. P2X ₇ blocking and potentiating nanobodies.....	17
1.5. Immunogenic cell death (ICD)	17
1.5.1. Unfolded Protein response.....	20
1.5.2. Autophagy.....	21
2 Aims of the project	22
3 Results.....	23
3.1. <i>In-vitro</i> results.....	23
3.1.1. P2X ₇ expression in Yac-1 cells.....	23
3.1.2. P2X ₇ -mediated CD62L shedding, PS flashing and DAPI uptake.....	24
3.1.3. ATP-mediated cytotoxicity is blocked by P2X ₇ antagonist 13A7	25
3.1.4. Gating of P2X ₇ enhances the uptake and cytotoxicity of doxorubicin in Yac-1 lymphoma cells	26
3.1.5. Doxorubicin cytotoxicity in Yac-1 cells is independent of P2X ₇ activation.	27
3.1.6. Gating of P2X ₇ enhances uptake of doxorubicin at early timepoints. .	27
3.1.7. ATP-induced cell death is rapid, but death due to ATP/DOX synergism is a late event.....	28
3.1.8. Transient activation of P2X ₇ marks cells for doxorubicin-induced death	29
3.1.9. Synergistic effects of P2X ₇ signaling on doxorubicin toxicity are dependent on the P2X ₇ isoform.....	31
3.1.10. P2X ₇ (k)-expressing A20 B lymphoma cells also show enhanced doxorubicin cytotoxicity in the presence of ATP	33
3.1.11. P2X ₇ and doxorubicin co-operate in the induction of phagocytosis-promoting signals	35
3.1.12. P2X ₇ also enhances the cytotoxicity of Bortezomib, a known inducer of the unfolded protein response.....	38
3.1.13. P2X ₇ and doxorubicin synergize to activate Caspase-3.....	39
3.1.14. Gating of P2X ₇ alone results in Calreticulin (CRT) translocation	39

3.1.15.	P2X ₇ -mediated CRT translocation, PS exposure, and pore formation are regulated by the PERK pathway.....	40
3.1.16.	Inhibition of PERK blocks the synergistic effect of P2X ₇ on doxorubicin-mediated cytotoxicity.....	42
3.2.	<i>In-vivo</i> results	43
3.2.1.	Expression of P2X ₇ inhibits tumor growth.....	43
3.2.2.	Expression of functional P2X ₇ R slows 4T1 tumor growth <i>in-vivo</i>	45
3.2.3.	P2X ₇ enhancing nanobody slows down the tumor growth.....	48
3.2.4.	Subsets of tumor-infiltrating lymphocytes.....	49
3.2.5.	Phenotypic analysis of tumor-infiltrating lymphocytes.....	50
3.2.6.	Subsets of lymphocytes in the spleen.....	54
3.2.7.	Phenotypic analysis of T cells in the spleen.....	56
3.2.8.	Increased co-expression of CD39 and CD73 on tumor infiltrating Lymphocytes (TIL)	57
4	Discussion	59
4.1.	Synergistic cytotoxic effects	59
4.2.	Possible mechanisms of synergistic cell death	61
4.2.1.	Increased Drug uptake	61
4.2.2.	ER stress and immunogenic cell death	61
4.3.	P2X ₇ expression on tumor cells	64
5	Materials and Methods.....	68
5.1.	Materials.....	68
5.2.	Methods	76
5.2.1.	Methods in Molecular Biology.....	76
5.2.2.	Methods in cell biology	81
5.2.3.	<i>In-vitro</i> assays	85
5.2.4.	Methods in animal experiments	87
5.3.	Statistical analysis	89
6	References:.....	90
7	Appendix	99
7.1.	List of Figures.....	99
7.2.	List of tables	101
7.3.	Safety and Disposal.....	102
7.4.	Curriculum vitae	106
7.5.	Acknowledgement.....	108
7.6.	Declaration	110

Zusammenfassung

Der purinerge P2X₇-Rezeptor ist ein ATP-gesteuerter Kationenkanal, der sowohl von hämatopoetischen als auch von vielen Tumorzellen exprimiert wird. Die Expression von P2X₇ bietet einen Wachstumsvorteil für Tumorzellen, indem der mitochondriale Calciumgehalt erhöht und der Zellstoffwechsel stimuliert wird. Andererseits kann eine starke Stimulierung von P2X₇ zum Tod von Tumorzellen führen, und die Expression von P2X₇ durch Wirtsimmunenzen ist für den Tumor schädlich, indem sie die Antitumor-Immunantwort verstärkt. Über die Rolle von P2X₇ in der Chemotherapie ist wenig bekannt. Ich untersuchte daher die Auswirkungen der P2X₇-Stimulation in Gegenwart von Chemotherapeutika die einen immunogenen Zelltod auslösen, wie z.B. doxorubicin (DOX) und bortezomib (BTZ).

Zur Untersuchung der In-vitro-Toxizität wurden Yac-1-Lymphomzellen, die P2X₇ endogen exprimieren, sowie weitere mit P2X₇-Varianten stabil transduzierte Zelllinien (A20 B-Lymphom, 4T1 Mammakarzinom) verwendet. Niedrige Dosen von extrazellulärem ATP (eATP), die selbst eine geringe Toxizität verursachten, erhöhten die Empfindlichkeit gegenüber DOX um das 7- bis 8-fache. Eine einstündige vorübergehende Exposition gegenüber eATP und DOX reichte aus, um den Zelltod nach einer Kultur über Nacht auszulösen. Mechanistisch erhöhte das Gating von P2X₇ zwar die anfängliche Aufnahme von DOX in Zellen. Der verstärkte Zelltod konnte jedoch durch Blockade von PERK, einer zentralen Kinase des ER-Stress Signalweges abgeschwächt werden, was darauf hindeutete, dass der Synergismus eher auf einer Wechselwirkung nachgeschalteter Signalwege beruhte. Die Aktivierung von P2X₇ durch ATP führte zur Phosphorylierung des PERK-Substrats eIF2 α und zur Translokation von Calreticulin an die Zelloberfläche, zwei Kennzeichen des immunogenen Zelltodes.

Als Tumormodelle für *in vivo* Untersuchungen wurden Yac-1 T-Lymphom Zellen nach i.v. Injektion in SCID Mäuse sowie 4T1 Mammakarzinom-Zellen (stabil retroviral transduziert mit funktionalem oder nicht-funktionalem P2X₇) nach lokaler Injektion in das Brustfettgewebe von Balb/C Mäusen verwendet. Dabei wurde die Tumorgroße im Yac-1 Modell durch Bildgebung, im 4T1 Modell durch einen Messchieber gemessen. In beiden Modellen verlangsamte die Expression von funktionalem P2X₇ durch Tumorzellen das Tumorstadium

Meine Ergebnisse zeigen, dass P2X₇ auf Tumorzellen zum Erfolg der Chemotherapie beitragen kann, und legen nahe, dass die Modulation der P2X₇ Aktivität eine mögliche therapeutische Strategie zur Erhöhung der Zytotoxizität von Chemotherapeutika darstellt.

Abstract

The purinergic P2X₇ receptor is an ATP-gated cation channel expressed by various immune and tumor cells. Expression of P2X₇ by tumor cells can favor tumor growth by raising mitochondrial calcium levels and stimulating the cell metabolism. On the other hand, strong stimulation of P2X₇ can cause cell death. Expression of P2X₇ by antigen presenting cells (APCs) results in maturation of dendritic cells and thus is detrimental to the tumor by enhancing the anti-tumor immune response. Little is known about the role of P2X₇ in the context of chemotherapy. Therefore, I studied the effects of P2X₇ stimulation in the presence of chemotherapeutic agents that induce immunogenic cell death (i.e., doxorubicin (DOX) and bortezomib (BTZ)).

For *in-vitro* cytotoxic studies I used Yac-1 lymphoma cells that express P2X₇ endogenously and also other cell lines (A20 B lymphoma cell line, 4T1 mammary carcinoma cell line) that were transduced with P2X₇ variants. Low doses (100 to 200 μM) of extracellular ATP (eATP) that were not toxic by their own synergistically enhanced the sensitivity to DOX and BTZ. Transient exposure to eATP and DOX for one hour was sufficient to induce cell death after overnight culture. Mechanistically, gating of P2X₇ augmented the initial uptake of DOX into cells. However, a decrease in cell death was observed when an important pathway of unfolded protein response, PKR ER kinase (PERK) was blocked by using PERK inhibitor, suggesting that the synergism was rather due to an interaction of downstream signaling pathways. I observed that ATP mediated P2X₇ activations resulted in the phosphorylation of eIF2 α as well as calreticulin (CRT) translocation to the cell surface, which are important hallmarks of immunogenic cell death.

For *in-vivo* studies, tumor graft models were prepared using Yac-1 lymphoma cells (injected i.v. in SCID mice) and 4T1 breast cancer cell line (stably transduced with functional or nonfunctional P2X₇ by using retroviral vector) injected in mammary fat pad of Balb/C mice. In Yac-1 injected mice, tumor size was measured using optical image system while in the 4T1 injected mice, tumor volume was assessed by using caliper. In both animal models expression of P2X₇ receptor by tumor cells slowed down the tumor growth.

My results showed that P2X₇ activation synergistically enhance the cytotoxic effects of chemotherapy *in vitro*. Expression of P2X₇ by tumor cells helped in tumor cell killing, both *in-vivo* and *in-vitro*. Therefore, P2X₇ receptor activation on tumor cells could be considered as a combination therapy for better therapeutic outcomes.

Abbreviation

°C	degrees centigrade
ADP	Adenosine diphosphate
AMP	Adenosine monophosphate
APC	Allophycocyanin
APC	Antigen presenting cells
ART2	ADP-ribosyl transferase 2
ATF4	Activating transcription factor 4
ATF6	Activating transcription factor 6
ATP	Adenosine triphosphate
BIP	Binding immunoglobulin protein
BSA	Bovine serum albumin
BTZ	Bortezomib
cAMP	Cyclic adenosine monophosphate
CD	Cluster of differentiation
cDNA	Cyclic deoxyribonucleic acid
CHOP	CAAT/enhancer-binding protein (C/EBP) homologous protein
CRT	Calreticulin
DAMP	Damage associated molecular pattern
DC	Dendritic cells
DOX	Doxorubicin
DMEM	Dulbecco's modified eagle medium
DNA	Deoxyribonucleic acid
dNTPs	Deoxyribonucleotide triphosphate
EDTA	Ethylenediaminetetraacetic acid
eGFP	Enhanced green fluorescent protein
eIF2 α	Eukaryotic initiation factor 2 alpha
ER	Endoplasmic Reticulum
ELISA	Enzyme linked immunosorbent assay
FACS	Fluorescence activated cell sorting
FCS	Fetal calf serum
FITC	Fluorescein

Foxp3	Forkhead box protein 3
FSC	Forward scatter
HEPES	4-(2-hydroxyethyl)-1-piperazineethanesulfonic acid
g	gram
HLE	Half-life extended
i.p.	intraperitoneal
IFN- γ	Interferon γ
Ig	Immunoglobulin
IL	Interleukin
IL-1 β	Interleukin 1 β
IRE1	Inositol-requiring enzyme-1
i.v.	Intravenous
Da	Daltons
l	Liter
Lb	Luria broth
M	Molar
mg	milligram
MHC	Major histocompatibility complex
min	Minute
ml	milliliter
mM	millimolar
mP2X ₇	Mouse P2X ₇
mRNA	Messenger ribonucleic acid
NAD	Nicotinamide adenine dinucleotide
NTPDase	Ectonucleoside triphosphate diphosphohydrolase
NPP	Nucleotide pyrophosphatase phosphodiesterase
ns	Non-significant
PBS	Phosphate buffered saline
PCR	Polymerase chain reaction
PERK	PRK like ER kinase
RNA	ribonucleic acid
ROS	Reactive oxygen species
RPMI	Roswell Park Memorial Institute (medium)

RT	Room temperature
s.c.	Subcutaneous
SOC	Super optimal broth with catabolite repression
SSC	Sideward scatter
TACE	Tumor necrosis factor converting enzyme
TAE	Tris-acetate-EDTA
TNF- α	Tumor necrosis factor α
Treg	Regulatory T cells
UPR	Unfolded protein response
wt	Wild type
μg	microgram
μl	microliter

1 Introduction

1.1. Purinergic receptors

Purinergic receptors are ligand-gated plasma membrane proteins expressed by almost all mammalian tissues that mediate several physiological and pathophysiological effects including neurotransmission, pain and inflammation (Burnstock 2007; Di Virgilio et al. 2018). These receptors are mainly activated by extracellular nucleotides, i.e., nicotinamide adenine dinucleotide (NAD) and adenine triphosphate (ATP). These nucleotides are released from the cells under physiological and pathological conditions (inflammation and cell death) (Kroemer et al. 2013).

Purine receptors belong to two subfamilies (Boeynaems et al. 2005), termed P1 and P2, that are activated by adenosine (nucleoside) or ADP/ATP (nucleotide), respectively. The P2 receptors are subdivided in P2X and P2Y receptors on the basis of structural differences and cellular functions, upon activation. P1 and P2Y are G protein coupled metabotropic receptors while the P2X subfamily belongs to ionotropic receptors (Burnstock 2007; Bilbao et al. 2012). The functional P2X receptors are able to form trimeric ion channels, either homomeric or heteromeric (Boeynaems et al. 2005; Burnstock 2007; Rissiek et al. 2015). Activation of P2X receptors results in influx of Ca^{2+} and Na^{+} ions and efflux of K^{+} ions. The P2X receptors differ in sensitivity to ATP from nanomolar (nm) to micromolar (μM) concentration (Burnstock 2007).

1.1.1. P2X₇ ion channel

The P2X₇ receptor is predominantly expressed by various immune and tumor cells. P2X₇ is a unique member within the P2X family, structurally by the presence of a long intracellular carboxy-terminal tail that contains several signaling motifs, and biochemically by its requirement for comparatively high (upper micromolar to low millimolar) concentrations of ATP (North 2002). P2X₇ channel consists of three subunits that self-assemble in homomeric trimer during translation and make stable complexes. The channel is composed of 595 amino acids which makes it the largest member of P2X family (Surprenant et al. 1996).

Gating of P2X₇ usually occurs by extracellular ATP, but ADP-ribosyltransferase-C2 (ARTC2) expressing cells can also be gated by NAD-dependent ADP-ribosylation (Adriouch et al. 2002). The N-terminal domain of P2X₇ is subject to alternative splicing. The mP2X₇ (a) and (k) isoforms differ in the N-terminal 42 (a) and 39 (k) amino acids comprising the N terminal domain and most of the first transmembrane domain (Fig. 1A). In addition, C57BL/6 mice distinguish from Balb/c and wild-type mice by a functionally relevant polymorphism in the cytosolic domain (L451P) (Schwarz et al. 2012).

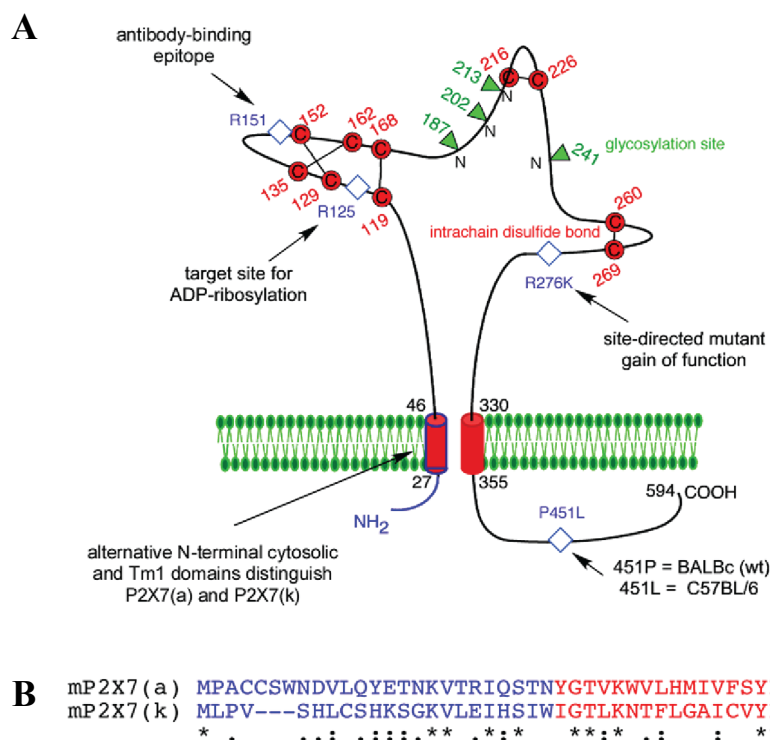


Figure 1. P2X₇ structure, splice variants and mutants: P2X₇ structure consists of homotrimer sub units, with two transmembrane domains connected with an extracellular domain. The two mouse P2X₇ (mP2X₇) splice variants (a) and (k) differ at the first transmembrane domain with 42 amino acids in (a) isoform replaced with 39 amino acids in (k) isoform (Fig A & B). C57BL/6 mice differ from Balb/c mice with a single amino acid at 451 position where leucine in C57BL/6 mice is replaced with proline in Balb/c (Fig.1A) (Schwarz et al. 2012).

1.2. Purinergic signaling

ATP release from cells can serve as a paracrine signal for intercellular functions. ATP is present at millimolar concentrations within the cells, but only in nanomolar concentrations in the extracellular milieu. Under steady-state conditions, activation of the TCR/CD3 complex results in cellular ATP release; as a result, the extracellular

ATP concentration reaches $>60 \mu\text{M}$ within 2 min after cell stimulation (Yip *et al.*, 2009). These ATP concentrations are sufficient to stimulate P2X receptors (Klapperstück *et al.* 2001; North 2002; Gever *et al.* 2006). Following its release, ATP hydrolyzes gradually to ADP, AMP and adenosine by the action of ectonucleotidases (NTPDases and NPPs), ecto-5'-nucleotidase and alkaline phosphatases (Joseph *et al.* 2004; Robson *et al.* 2006; Zimmermann *et al.* 2012). This process prevents the desensitization of receptor and facilitates rapid and sustained purinergic signaling (Yegutkin 2008).

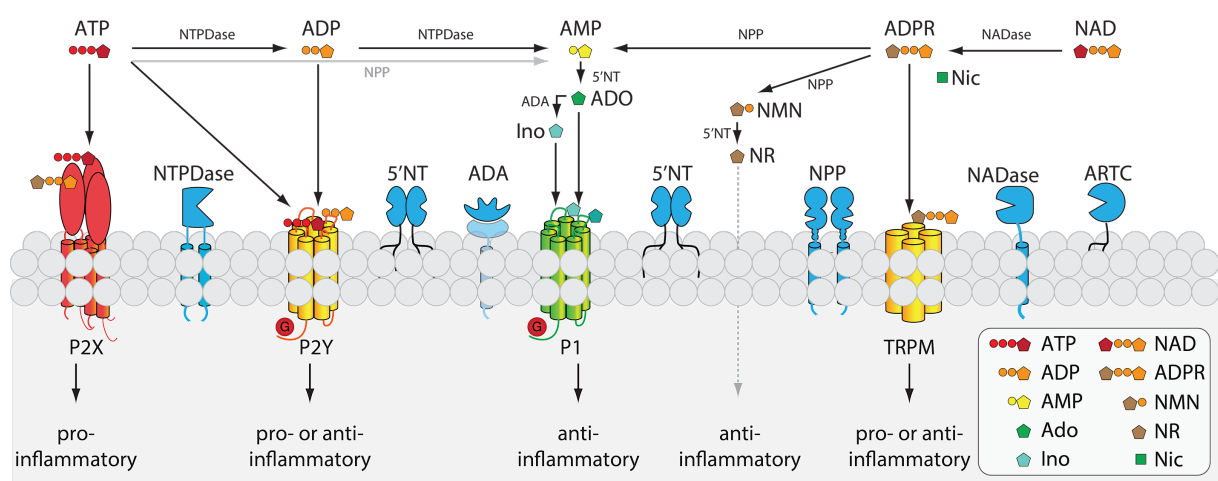


Figure 2. Purinergic signaling: Nucleotides such as adenosine triphosphate (ATP) and nicotinamide adenine dinucleotide (NAD) are released from the cells in inflammatory conditions. ATP binds and activates the P2X receptors (mainly involved in proinflammatory responses) and NAD acts as a substrate for ARTC (ecto-ADP-ribosyl transferase) receptors. ATP is quickly degraded by Ectonucleoside triphosphate diphosphohydrolase-1 (NTPDase-1) to AMP which is further dephosphorylated to a potent anti-inflammatory and immune suppressor adenosine in the presence of ecto-5'-nucleotidase (5' NT). Modified from Stephan Menzel (unpublished figure).

Binding of the extracellular ATP to the P2X₇ receptor induces a conformational change within milliseconds that allows the influx of extracellular Ca²⁺ and Na⁺ and the efflux of K⁺. Prolonged stimulation of P2X₇ for seconds to minutes results in the formation of molecularly ill-defined pores that permit the passage of substrates up to 900 Daltons. This is accompanied by activation of membrane metalloproteases like ADAM17 (TACE, TNF-alpha converting enzyme) that cleave certain substrates such as the homing receptor L-selectin (CD62L) from the cell surface, as well as by the

phosphatidylserine (PS) exposure on the outer surface of the cell membrane as an early indicator of the induction of apoptosis (Haag et al. 2007).

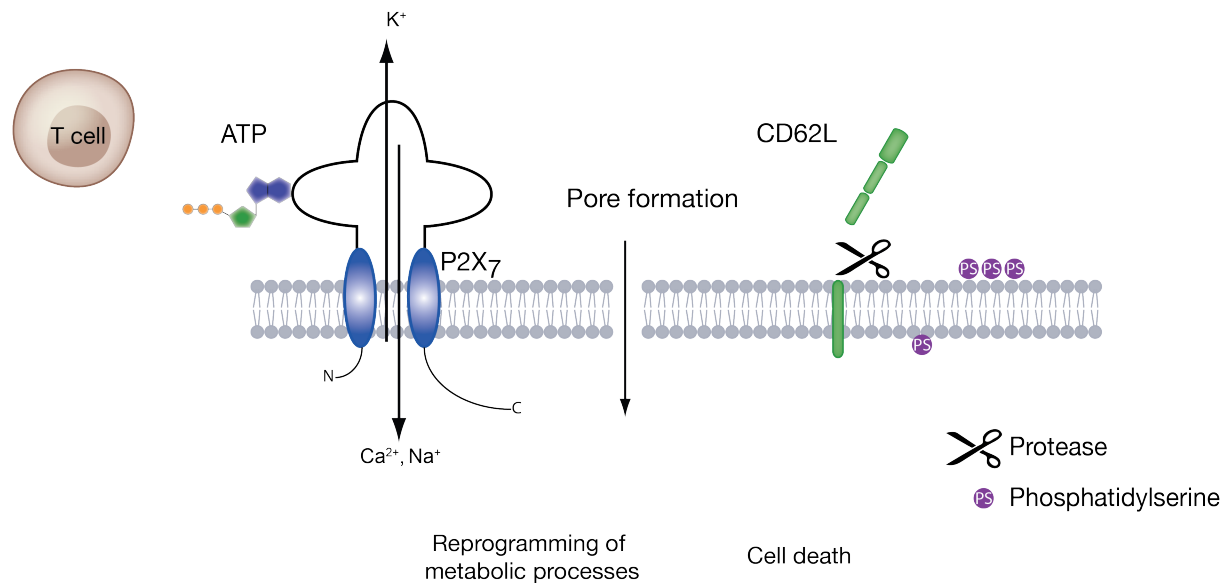


Figure 3. P2X₇ activation: P2X₇ is an ATP-gated cation channel expressed in the plasma membrane of many immune cells and tumors that have been linked to inflammation and tumor growth. Stimulation of P2X₇ induces channel opening, influx of Ca²⁺ and Na⁺ ions; and efflux of K⁺ ions and the membrane pores formation that enable the influx of molecules up to 900Da. Upon P2X₇ stimulation, activation of metalloproteases results in CD62L shedding from the cell surface as well as phosphatidylserine (proapoptotic marker) flipping from inner face of cell membrane to the outer membrane. Prolonged and strong stimulation of P2X₇ leads to cell death (Scheuplein et al. 2009).

1.3. P2X₇ in cancer

Beyond its importance for energy metabolism within the cell, ATP can be released from cells to play an important role as an extracellular signaling molecule under conditions of inflammation, tissue damage, and cell death (Pellegatti et al. 2008; Eltzschig et al. 2012). In tumor microenvironment, the concentration of ATP is remarkably high, which exerts multiple effects, including the conduction of survival signals as well as regulation of immune response via purinergic receptors (P2X or P2Y) (Seman et al. 2003; Di Virgilio et al. 2018). Among these, the P2X₇ receptor has gained attention because it is expressed on a wide range of hematopoietic cells and also by many tumors (Di Virgilio et al. 2009).

The expression of the P2X₇ receptor by tumor cells can have ambivalent effects for the tumor. Strong and prolonged stimulation of P2X₇ has cytolytic effects on many

cells, presumably, due to its capability to induce membrane pores. Nonetheless, under steady-state conditions, the expression of P2X₇ reportedly has a trophic effect on tumor cells by stimulating cell metabolism and increasing ATP production (Adinolfi *et al.*, 2012; Di Virgilio, 2012).

1.4. P2X₇ blocking and potentiating nanobodies

Nanobodies are heavy chain only antibodies from camelids (Danquah *et al.* 2016). They consist of smallest antigen binding domains that can be used for therapeutic purposes. These single domain antibodies have various advantages over conventional antibodies i.e., nanobodies can interact with conformational epitopes that are not available to conventional antibodies. The monomeric nanobodies have superior tissue penetration and rapid effect compared to antibodies (Wesolowski *et al.* 2009; Van Bockstaele *et al.* 2009; Muyldermans 2013). The half-life of nanobodies can be increased by fusing them with albumin-specific nanobody (Tijink *et al.* 2008).

13A7 HLE (half-life extended) nanobody is a potent blocker of ATP mediated P2X₇ activation, whereas 14D5 potentiates the effects of ATP on the P2X₇ receptor. The blocking of P2X₇ helps in attenuation of various inflammatory conditions i.e., glomerulonephritis (Danquah *et al.* 2016).

1.5. Immunogenic cell death (ICD)

Cell death by the apoptosis or necrosis pathways has been known for decades. Under steady state conditions, cell death mainly occurs via apoptosis, which is either tolerogenic or ignored by the immune system. In last two decade, the concept of immunogenic cell death (ICD) has evolved, which refers to a regulated cell death pathway that is able of activating an adaptive immune response against dead cell antigens derived from cancer cells (Kroemer *et al.* 2013; Bezu *et al.* 2015; Serrano-del Valle *et al.* 2019). Such antigens allow a strong antitumor immune response when presented to T cells (Chen and Mellman 2013).

A series of events is required for the effective removal of tumor cells by anticancer immune response. At the start, the released neoantigens are taken by dendritic cells (DCs) for processing. This may be accompanied by the release of danger signals such

as proinflammatory cytokines or the liberation of intracellular molecules. In the next step, captured antigens by DCs are presented on major histocompatibility class I (MHC I) and major histocompatibility class II (MHC II) molecules to T cells, which leads to priming and activation of effector T cell response against cancer specific antigens (Chen and Mellman 2013). At this stage, the type of immune response is determined by the ratio of effector T cell vs regulatory T cells (Motz and Coukos 2013). At the last stage, if the ratio of effector T cells is higher than the regulatory T cells, the cytotoxic T cells infiltrate the tumor bed and kill the target cancer cell (Zhu and Lang 2016).

Four different types of ICD have been described to date, each associated with a specific type of stimulus and danger signal. 1) pathogen driven ICD, which is one of the shielding mechanisms against pathogens; 2) necroptosis, an alternative form of regulated cell death, which requires RIPK3, a well-known regulator of inflammation in health and disease, 3) ICD-induced by physical signals such as irradiation, Hyp-PDT (Hypericin-Photodynamic-therapy) and HHP (High hydrostatic pressure) and 4) some chemotherapeutic drugs i.e., anthracyclines also induce immunogenic cell death by targeting ER stress and release of reactive oxygen species (Apetoh et al. 2007; Obeid et al. 2007; Michaud et al. 2011; Zitvogel et al. 2015).

Several mediators of immunogenic cell death have been well-known. These include the exposure of endoplasmic reticulum (ER)-resident protein calreticulin (CRT) on the cell surface, the cell death-associated release of high-motility group box 1 (HMGB1) protein, and the secretion of ATP (Panaretakis et al. 2009; Michaud et al. 2011; Garg et al. 2012). Not all chemotherapeutic drugs induce calreticulin translocation, ATP secretion and release of HMGB1. Doxorubicin (DOX) is an anthracycline produced by *Streptomyces peucetius*. The structure of DOX contains a planar aromatic chromophore portion that intercalates between two base pairs of the DNA. As a result, replication is stopped and DOX-treated cells die. Due to its fluorescent activity, the accumulation of this chemotherapeutic drug in cells can be detected using flow cytometry. DOX is used as a common treatment against cancer of the hematopoietic system as well as cancer of internal organs (Gewirtz 1999). DOX induces

immunogenic cell death by a mechanism that involves the release of ATP by dying tumor cells (Kroemer et al. 2013).

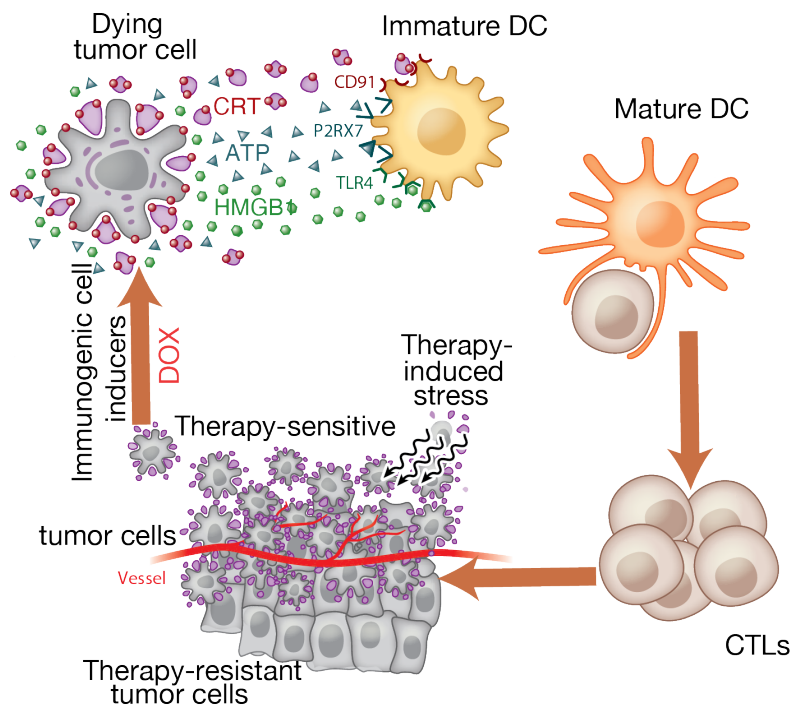


Figure 4: Immune activation by chemotherapeutic drugs (i.e., DOX): Increase in endoplasmic reticulum (ER) stress by chemotherapeutic drugs may lead to ATP and high mobility group box 1 protein (HMGB1) release, and calreticulin (CRT) exposure on cell surface. CRT, ATP and HMGB1 bind to receptors on immature DCs, initiating the maturation and recruitment of DCs and antigen presentation to T cells. This process can lead to strong immune responses that can help in killing of chemotherapy resistant cancer cells. Modified from Kroemer *et al.*, 2013.

Immunogenic cell death is regulated by two types of stress: ER stress and autophagy. Chemotherapy-induced ER stress results in the translocation of CRT to the cell surface from the ER lumen, and this occurs before the cell undergoes apoptotic cell death and marked by the exposure of phosphatidylserine on outer leaflet of cell membrane (Panaretakis et al. 2009). Calreticulin on outer leaflet of cell membrane acts as a strong phagocytic signal and enables dendritic cells to engulf stressed and dying tumor cells (Gardai et al. 2005; Chao et al. 2010). In immunocompetent mice, blockade of cell surface exposure of CRT negatively regulates the antitumor response of anthracyclines (Panaretakis et al. 2008). Therefore, ER stress-mediated immunogenic signal is necessary for the induction of anticancer immune responses by chemotherapeutic drugs (Obeid et al. 2007; Tesniere et al. 2010).

1.5.1. Unfolded Protein response

Tumor cells are continuously exposed to various stress factors i.e, environmental (hypoxia or nutrient deficiency) and genetic (genetic alteration, oncogene activation) factors. These factors are conventional initiators of ER stress (Urrea et al. 2016). To deal with this stress, cells activate a well-defined process called the unfolded protein response (UPR). The UPR is controlled by three membrane-bound ER sensors, inositol-requiring enzyme-1 (IRE1), protein kinase R-like endoplasmic reticulum kinase (PERK), and activating transcription factor (ATF6) (Liu et al. 2015). Under steady state conditions, these sensors bind to BIP (binding immunoglobulin protein), which keeps them in an inactive form. Under stress conditions, BIP dissociates from the sensors and allow their self-activation and oligomerization. The activation of sensors help to restore the cell homeostasis by protein synthesis inhibition, degradation of misfolded proteins, and increase levels of redox enzymes that help in enhancing protein folding capacity (Szegezdi et al. 2006; Garg et al. 2012; Walter et al. 2018).

If ER stress sustains, the UPR can elicit a pro-apoptotic response controlled mainly by the IRE1 and PERK pathways. Activation of PERK results in phosphorylation of the eIF2 α (eukaryotic initiation factor 2 α), which leads to inhibition of global protein translation to reduce protein load. However, some transcripts, like activating transcription factor 4 (ATF4), are translated proficiently in the presence of ER stress. Increased expression of ATF4 activates downstream pathways that involve the expression of genes responsible for amino acid and redox metabolism and apoptosis. ATF4 and the transcription factor CHOP (CAAT/enhancer-binding protein (C/EBP) homologous protein) are the vital factors of ER stress- mediated cell death (Serrano-del Valle *et al.* 2019). Activation of P2X₇ receptor leads to phosphorylation of eIF2 α ,

induction of CHOP, and cleavage of caspase 3 with subsequent apoptosis (Chao et al. 2012).

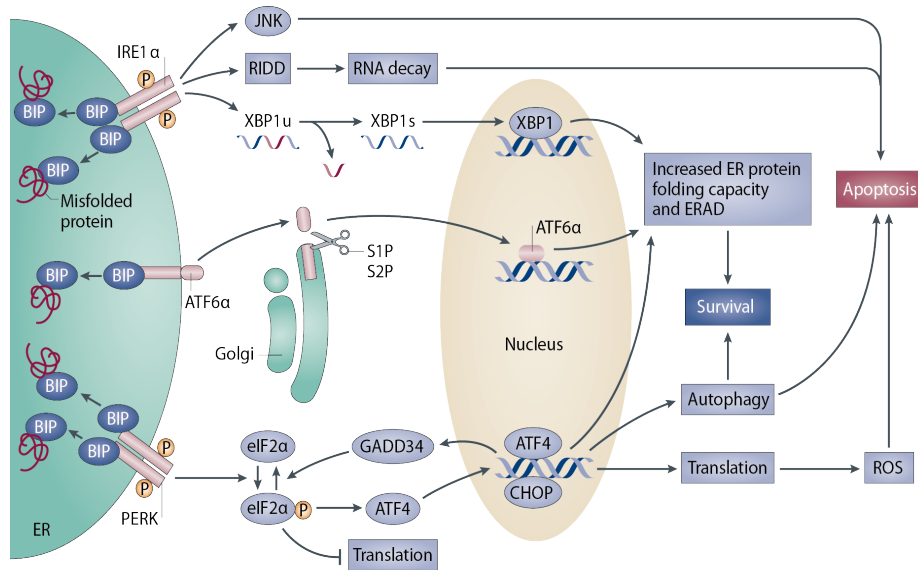


Figure 5: Unfolded protein response: Under endoplasmic reticulum (ER) stress conditions, the unfolded protein response (UPR) is activated which causes the activation of three branches of UPR: 1) PERK which results in phosphorylation of eIF2 α , 2) IRE1 which activates the X-box binding protein (XBP1), and 3) activation of ATF6 to recover from this stress. The consequence of UPR response increases the protein folding, degradation of ER and transport proteins and shuts down the global mRNA translation. If the stress is not resolved, it leads to cell apoptosis. PERK, PRK like ER kinase. IRE1, Inositol-requiring protein 1. CHOP, C/EBP homologous protein; ROS, reactive oxygen species; XBP1s, transcriptionally active XBP1; XBP1u, unspliced XBP1. GAAD34, growth arrest and DNA damage-inducible protein 34 (Wang and Kaufman 2014).

1.5.2. Autophagy

Autophagy is also mandatory for immunogenic cell death. It does not interfere with the translocation of CRT and HMGB1 release, but it does positively affect the secretion of ATP. Only autophagy competent tumors recruit the DCs and T lymphocytes in response to chemotherapy. Inhibition of extracellular ATP degrading enzymes or high concentrations of extracellular ATP can help to restore a chemotherapeutic response in autophagy-deficient cancers. Therefore, autophagy plays a crucial role in the immunogenic cell death by releasing ATP (Michaud et al. 2011; Kroemer et al. 2013).

2 Aims of the project

It is still unclear whether activation of P2X₇ under the conditions of chemotherapy will be beneficial to the tumor or the host. The aim of my project is to study the effects of P2X₇ gating in different cancer cell lines (Yac-1, 4T1 and A20 cells) under treatment with the chemotherapeutic agents that induce immunogenic cell death (doxorubicin and Bortezomib).

This includes the following specific objectives:

- To assess the impact of P2X₇ expression and gating for the growth and survival of tumor cells
- To evaluate the impact of P2X₇ gating on tumor cells in the presence of chemotherapy
- To evaluate the consequences of P2X₇ expression in tumor cells *in-vivo* by generating mouse models

3 Results

The results are divided into two sections. In section 3.1, the *in-vitro* synergistic cytotoxic effects of DOX in the presence of P2X₇ receptor activation are presented. Additionally, the possible mechanisms i.e., enhanced ER stress and drug uptake are also shown. In section 3.2 the *in-vivo* role of P2X₇ on tumor cells is presented, showing that expression of P2X₇ (k) by tumor cells slowed down the tumor growth compared to tumors expressing non-functional P2X₇ or treated with P2X₇ blocking nanobody (13A7 half-life extended). Moreover, treatment of solid tumors with P2X₇ potentiating nanobody (14D5 half-life extended) further reduced the tumor growth.

3.1. *In-vitro* results

3.1.1. P2X₇ expression in Yac-1 cells

P2X₇ receptors are expressed by most of immune and tumor cells. Here I investigated the expression of P2X₇ on the murine lymphoma cell line Yac-1 by flow cytometry using anti-mouse P2X₇ specific antibody. The anti-human P2X₇-specific antibody was used as an isotype control. Results showed that Yac-1 cells have noticeable surface expression of P2X₇ (**Fig. 6A**). To find out the splice variant of P2X₇ in Yac-1 cells, DNA from Yac-1 cells was amplified by using P2X₇ (a) and (k) specific primers (**Fig. 6B**). Yac-1 cells express the (k) variant, which is mainly expressed by T cells and is more sensitive to ATP compared to the (a) variant (Schwarz et al. 2012).

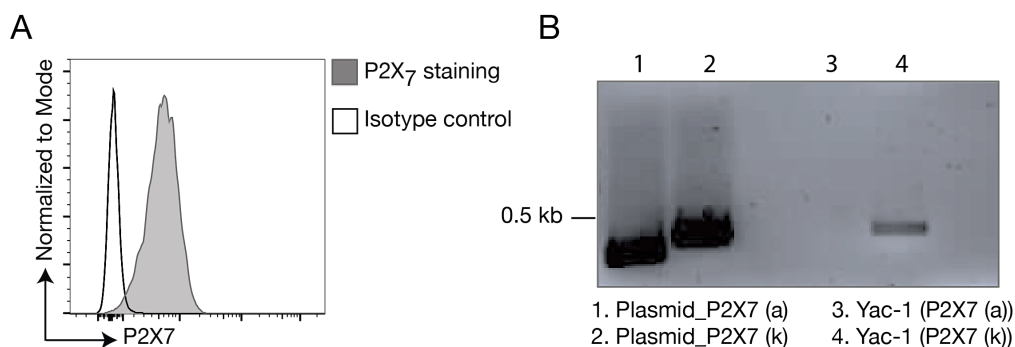


Figure 6. Cell surface expression and splice variants of P2X₇ in T cell lymphoma (Yac-1): **A)** To check the expression of P2X₇ on Yac-1 cells, cells were stained with fluorochrome-conjugated anti-P2X₇ monoclonal antibody RH23-A44-Alexa 647 (shaded histogram) or anti human antibody L4, an isotype control (open histogram) and analyzed by flow cytometry. **B)** cDNA from Yac-1-cells was amplified by PCR using primers specific for the (a) or (k) splice variants of P2X₇ (lanes 3 and 4). Plasmids encoding P2X₇ (a) or (k) were used as positive controls (lanes 1 and 2).

3.1.2. P2X₇-mediated CD62L shedding, PS flashing and DAPI uptake

It has previously been shown that short-term (20-30 min) treatment of P2X₇-transfected HEK cells with ATP resulted in P2X₇ mediated CD62L shedding, translocation of phosphatidylserine (PS) to the outer surface of the cell membrane, and low-level uptake of DAPI as an indicator of pore-formation (Schwarz et al. 2012). To determine whether Yac-1 cells also exhibit similar responses upon ATP treatment, cells were incubated with various concentrations of ATP (50 μ M - 800 μ M) for 30 min, and samples were measured by flow cytometry. CD62L shedding (**Fig. 7A-B**) and PS translocation (**Fig. 7C**) were observed at relatively low concentrations of ATP (50 μ M), while DAPI uptake required ATP concentrations > 200 μ M (**Fig. 7D**).

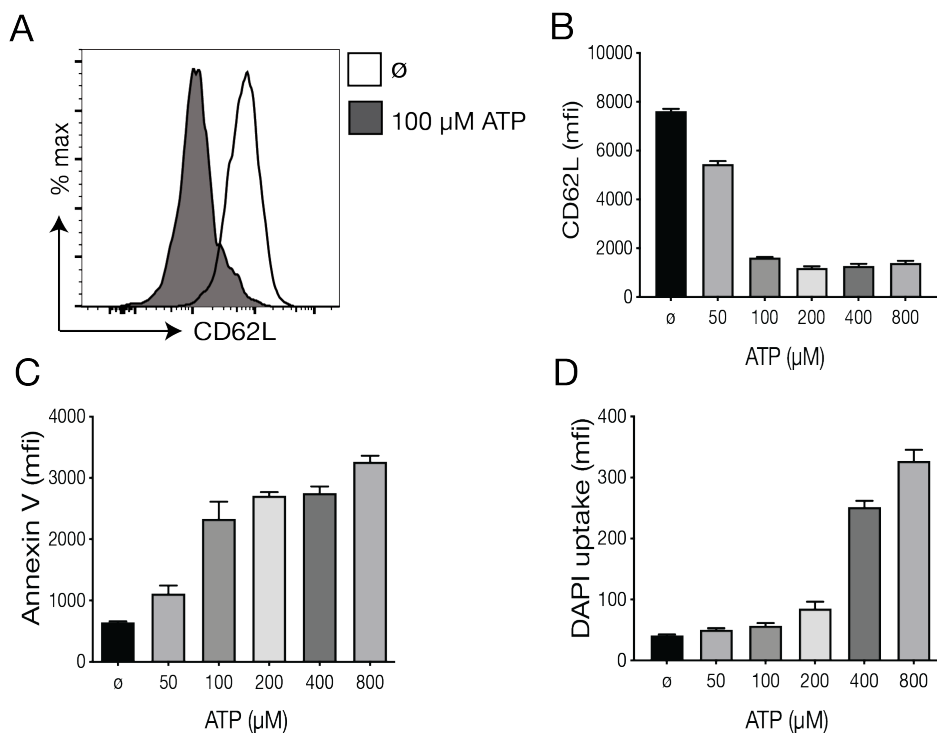


Figure 7. P2X₇R mediates ATP-induced CD62L shedding, PS exposure, and dye uptake: A-D) Yac-1 cells were stained with an anti-CD62L antibody and DNA-staining dye, and incubated for 30 min at 37°C in the presence of the indicated concentrations of ATP. Cells were washed with annexin-V buffer and stained with annexin-V antibody to detect the surface exposure of phosphatidylserine (PS) for 15 min at room temperature in dark. Samples were analyzed by flow cytometry and mean fluorescence intensity (mfi) was calculated by flowjo software. ATP induced CD62L shedding (**A-B**), PS exposure (**C**), and DAPI uptake (**D**). Data presented as mean \pm SEM

3.1.3. ATP-mediated cytotoxicity is blocked by P2X₇ antagonist 13A7

It has been demonstrated that the prolonged activation of P2X₇ by ATP results in cell death (detected by propidium iodide staining) which was prevented by the P2X₇ blocking nanobody 13A7 (Farrell et al. 2010; Danquah et al. 2016). I investigated here whether this effect can also be observed in Yac-1 cells. Overnight incubation of Yac-1 cells at 37 °C with the indicated concentrations of ATP resulted in cytotoxicity with an EC₅₀ around 300 μM. ATP cytotoxicity was mediated by the P2X₇ receptor, since pre-incubating the cells with the P2X₇-specific nanobody 13A7 blocked this effect. The inhibitory effect is dose dependent as it is overcome at high concentrations of ATP **Fig. 8A-B**). Cells were also stained for annexin V to check the apoptotic cell death via phosphatidylserine (PS) flashing. Interestingly, P2X₇ activation did not only induce necrotic cell death that is shown as DAPI and annexin V double positive cells but also induce apoptotic cell death, annexin V only positive cells (**Fig. 8A**). The presence of P2X₇ blocking nanobody more strongly blocks apoptotic effects (**Fig. 8C**) compared to overall cell death (**Fig. 8B**).

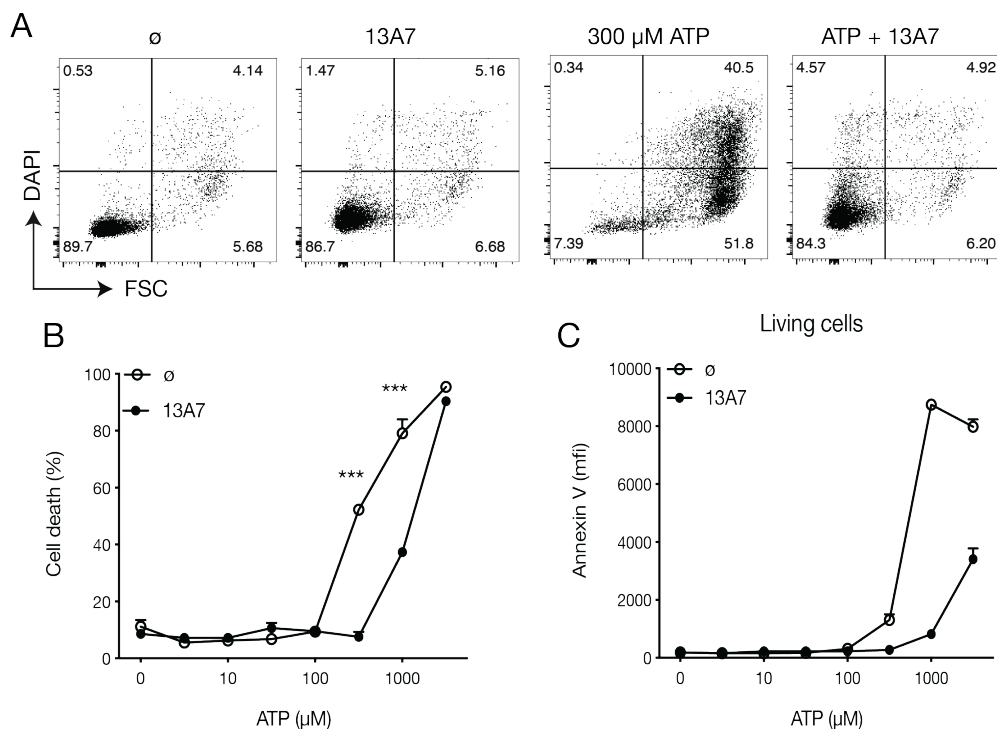


Figure 8. ATP induced toxicity in Yac-1 cells: A-C) Yac-1 cells were preincubated with the P2X₇ blocking nanobody 13A7 for 15min at room temperature on a roller in 500 μl of RPMI complete medium, and incubated for 24 h at 37 °C and 5% CO₂ with the indicated concentrations of ATP. After washing with annexin V buffer cells were stained with annexin V for 15 min at room temperature in the dark. To stain dead cells, DAPI was added immediately before flow cytometry analysis. **A)** Representative FACS plots for DAPI uptake vs annexin V staining in untreated samples (0) and 300μM ATP treated samples in the presence and absence of P2X₇ blocking nanobody 13A7. **B)**

XY graph shows the dose response curve for ATP induced cell death which is blocked by 13A7 in a dose dependent manner. **C)** Mean fluorescence intensity of annexin V in ATP \pm 13A7 treated samples is shown. The experiment was performed in triplicate for each condition. This figure is representative of three independent experiments with similar results. Statistics: two-way analysis of variance; posttest: Bonferroni test. ***, $p < 0.001$.

3.1.4. Gating of P2X₇ enhances the uptake and cytotoxicity of doxorubicin in Yac-1 lymphoma cells

Doxorubicin (DOX) is an anthracycline drug used in the treatment of lymphomas and various solid tumors (Gewirtz 1999). To assess the effect of P2X₇ gating on DOX cytotoxicity, Yac-1 cells were incubated overnight with various concentrations of DOX in the presence of 200 μ M ATP (**Fig. 9A-B**). While DOX at a concentration of 30 nM induced death in about 8% of cells, the combination with 200 μ M ATP increased cell death to above 80%. This increase in cell death was completely blocked by pre-treating the cells with the nanobody 13A7. Importantly, gating of P2X₇ by 200 μ M ATP in the absence of DOX caused only low levels of cell death (15-20%).

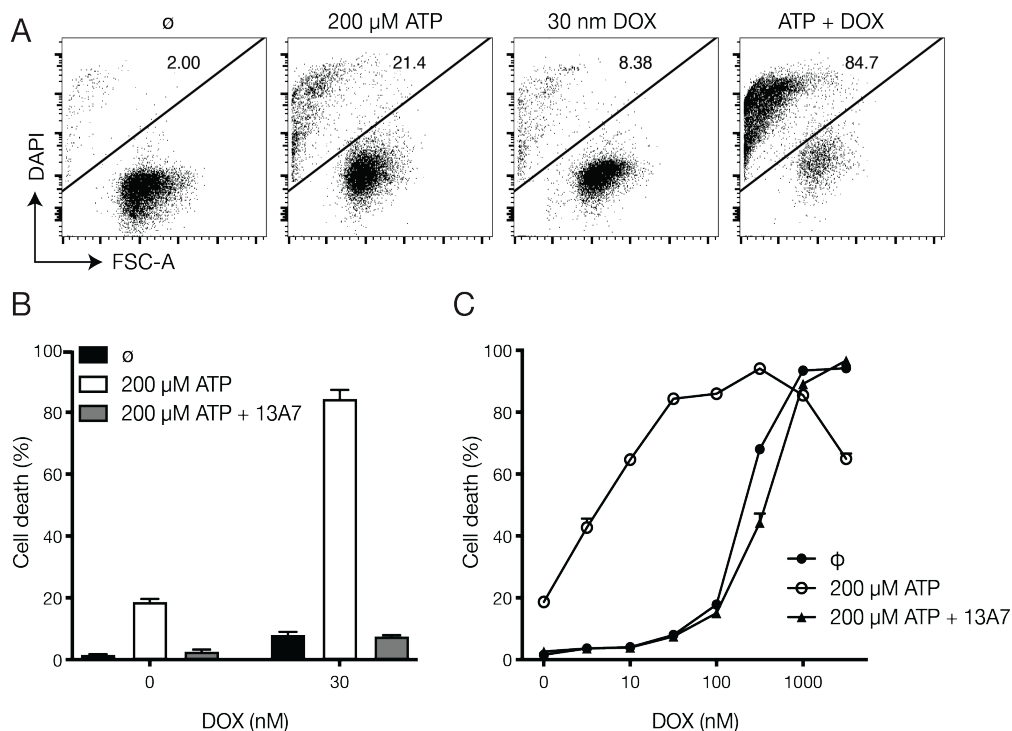


Figure 9. Gating of P2X₇ enhances the cytotoxicity of doxorubicin in Yac-1 cells: The cytotoxic effects of ATP and DOX on Yac-1 cells after overnight incubation were determined by flow cytometry. **A-C)** Cells were incubated with 200 μ M ATP and varying concentrations of DOX in the presence or absence of the P2X₇-inhibitory nanobody 13A7. To assess vitality, DAPI was added immediately before analysis. Cell death was defined as the uptake of DAPI combined with a reduction in forward scatter as shown in **A)**. Representative FACS plots and bar graph are shown in Fig. **A** and **B** respectively. **C)** summary of the data from **A** and **B**. Assay was performed in triplicate.

Error bars represent standard deviations from the mean. The results are representative of at least three independent experiments.

3.1.5. Doxorubicin cytotoxicity in Yac-1 cells is independent of P2X₇ activation.

Fig. 9 showed that Yac-1 cells are sensitive to DOX-induced toxicity. Twenty-four hours treatment is enough to kill the cells with EC₅₀ 150nM (**Fig. 9B**) and apoptosis is the dominant pathway of DOX-induced cell death (**Fig.10 A and C**). To investigate the role of P2X₇ in DOX-induced toxicity, cells were preincubated with P2X₇ blocking nanobody 13A7. Results showed that blocking of P2X₇ did not affect the DOX cytotoxicity (**Fig. 10A-C**).

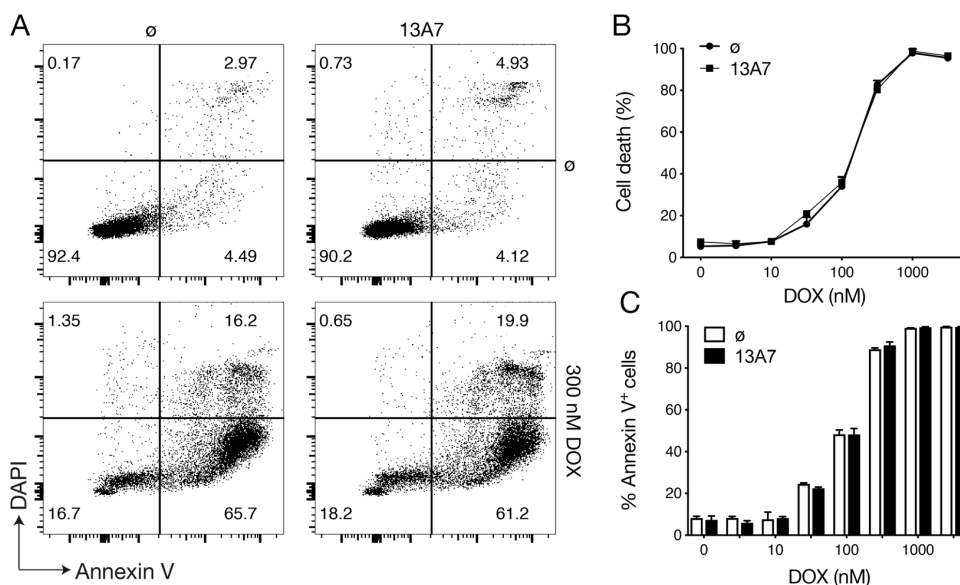


Figure 10. Doxorubicin cytotoxicity: Yac-1 cells were preincubated with 13A7 for 15 min on a roller. Cells were treated with the indicated concentrations of Doxorubicin \pm 13A7 overnight. Cells were then washed with annexin V buffer and stained for the exposition of PS with APC conjugated annexin V for 15 min in the dark at room temperature. The DNA-staining dye DAPI was added 2 min before analysis. Data collection was carried out by flow cytometry. **A)** Representative FACS plots for DAPI⁺ vs annexin V⁺ cells. **B)** Dose response curve for DOX toxicity in the presence and absence of 13A7. **C)** Summary of percentage of annexin V⁺ cells.

3.1.6. Gating of P2X₇ enhances uptake of doxorubicin at early timepoints.

Activation of the P2X₇ receptor is known to induce the pore formation that allows passage of substances up to a molecular weight of 900 Dalton through the plasma membrane (Surprenant *et al.* 1996). I therefore considered the possibility that gating of P2X₇ might enhance the cytotoxicity of DOX by facilitating the entry of DOX into the cells. Since DOX is a fluorescent compound, its content in cells can be determined conveniently by flow cytometry. Thus, the effect of ATP on DOX uptake was examined. Indeed, ATP at concentrations as low as 100 μ M facilitated the entry of

DOX into the cells within 1 h (**Fig. 11A**). However, at the end of the overnight assay the total DOX content was only marginally increased in the presence of ATP (**Fig. 11B**).

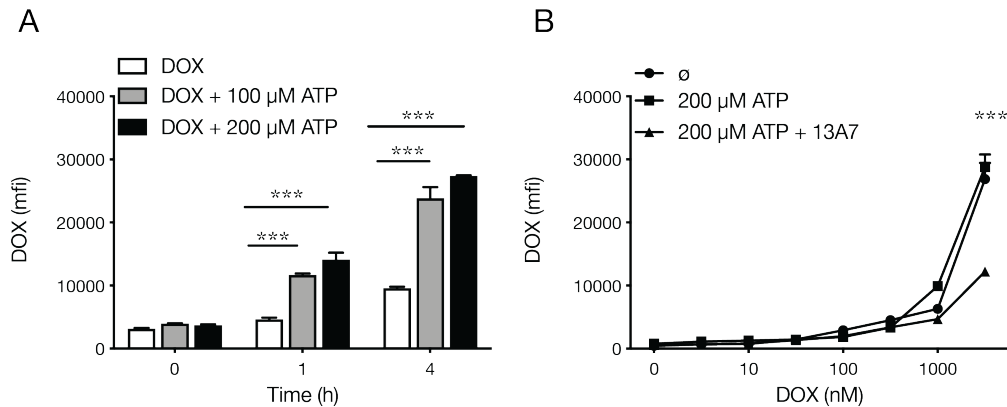


Figure 11. Gating of P2X₇ enhances uptake of doxorubicin at early timepoints: A) Yac-1 cells were incubated for 1 and 4 h with 1 μM DOX, ATP (100 and 200 μM), or a combination of both. The accumulation of fluorescent DOX was monitored by flow cytometry. **B)** Yac-1 cells were treated overnight with increasing concentrations of DOX in the presence or absence of 200 μM ATP and the P2X₇ inhibitory nanobody 13A7. The DOX uptake was measured by FACS. Statistics: Two-way analysis of variance; posttest: Bonferroni test. ***, p<0.001.

3.1.7. ATP-induced cell death is rapid, but death due to ATP/DOX synergism is a late event

Signaling through P2X₇ induces rapid cell death in primary T lymphocytes that is apparent within 30 min (Seman *et al.* 2003), presumably associated with the opening of the large non-selective membrane pore (Di Virgilio *et al.* 2001). By contrast, apoptosis mediated by DOX is a slow process requiring intracellular signal transduction and *de novo* synthesis of pro-apoptotic proteins (Gewirtz 1999; Peidis *et al.* 2011). I asked whether cell death caused by the synergistic interaction of ATP and DOX occurred early or late after exposure to the two substances. Using low concentrations of ATP just above the threshold for ATP-mediated cell death (100 and 200 μM), and a high concentration of DOX (1 μM) that is highly cytotoxic (see **Fig. 10**), I investigated the effects of ATP and DOX 60 min after exposure to the two substances (**Fig. 12A**). The results confirmed that at one-hour low-dose ATP had killed some of the cells, while even high-dose DOX had no cytotoxic effect. I then followed the time course of cytotoxicity, using concentrations of ATP (100 μM) and DOX (30nM) that were at or just below the threshold for inducing cell death by themselves (**Fig. 12B**). The results showed that 100 μM ATP alone killed a small percentage of cells that were

detectable within the first four hours after incubation. At 16 hours, however, this effect was no longer visible, presumably due to degradation of ATP and proliferation of cells in this time period. No cytotoxicity was observed at any time-point for 30 nM DOX. Of note, the presence of 30 nM DOX did not add to the toxicity of ATP during the first four hours. However, after 16 hours of incubation, the combination of ATP and DOX killed 80% of the cells. Together, these observations suggest that gating of P2X₇ strongly enhances DOX-mediated death, but that the presence of DOX does not affect the early cytotoxicity mediated by ATP.

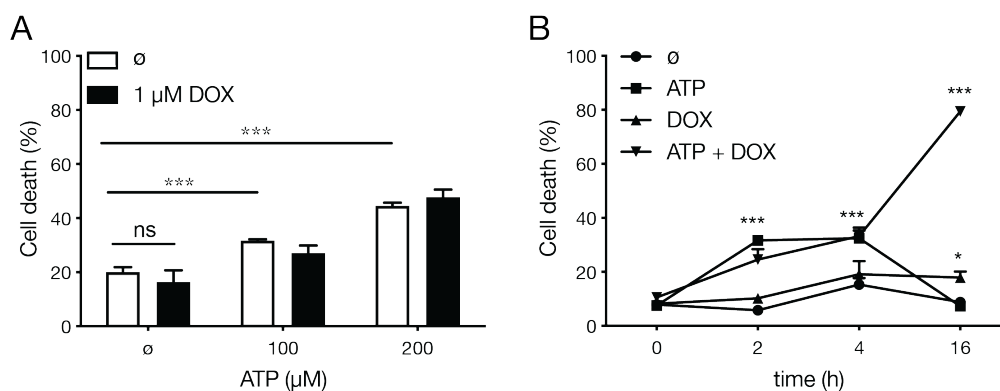


Figure 12. ATP-induced cell death is rapid, but death due to ATP/DOX synergism is a late event: A) Yac-1 cells were treated with 1 μM DOX in the presence or absence of 100 or 200 μM ATP for 1 h. Cell death was determined by adding DAPI before analysis by flow cytometry. **B)** Cells were treated with 100 μM ATP, 30nM DOX, or a combination of both for 2, 4 and 16 h. Cell viability was determined by staining with DAPI. Data is shown as mean± SEM. Statistics: two-way analysis of variance; posttest: Bonferroni test. *, p<0.05, ***, p<0.001.

3.1.8. Transient activation of P2X₇ marks cells for doxorubicin-induced death

The signal transmitted by gating of P2X₇ is rapid, and the ligand ATP is not stable for long periods of time in the extracellular milieu. By contrast, DOX accumulates within cells, and presumably DOX signaling for death is the result of a long process. I wondered whether the enhancement of DOX-mediated cell death by ATP required long-lasting signals at the P2X₇ receptor. To address this question, Yac-1 cells were co-incubated with ATP and DOX for varying periods of time between 1 h and 16 h, then washed and resuspended in fresh medium for further culture overnight. I found that a 1h co-incubation with ATP and DOX sufficed for cytotoxic synergism, i.e. to induce death of > 80% of cells after further incubation overnight, as evidenced by reduction in FSC signals and intense staining with DAPI. In contrast, exposure of cells

to ATP or DOX alone for one hour caused only low levels of cell death (**Fig. 13A and C**).

At the same time, I monitored the uptake of DOX into the cells (**Fig. 13B**). The results show that the presence of ATP significantly increased the incorporation of DOX into the cells

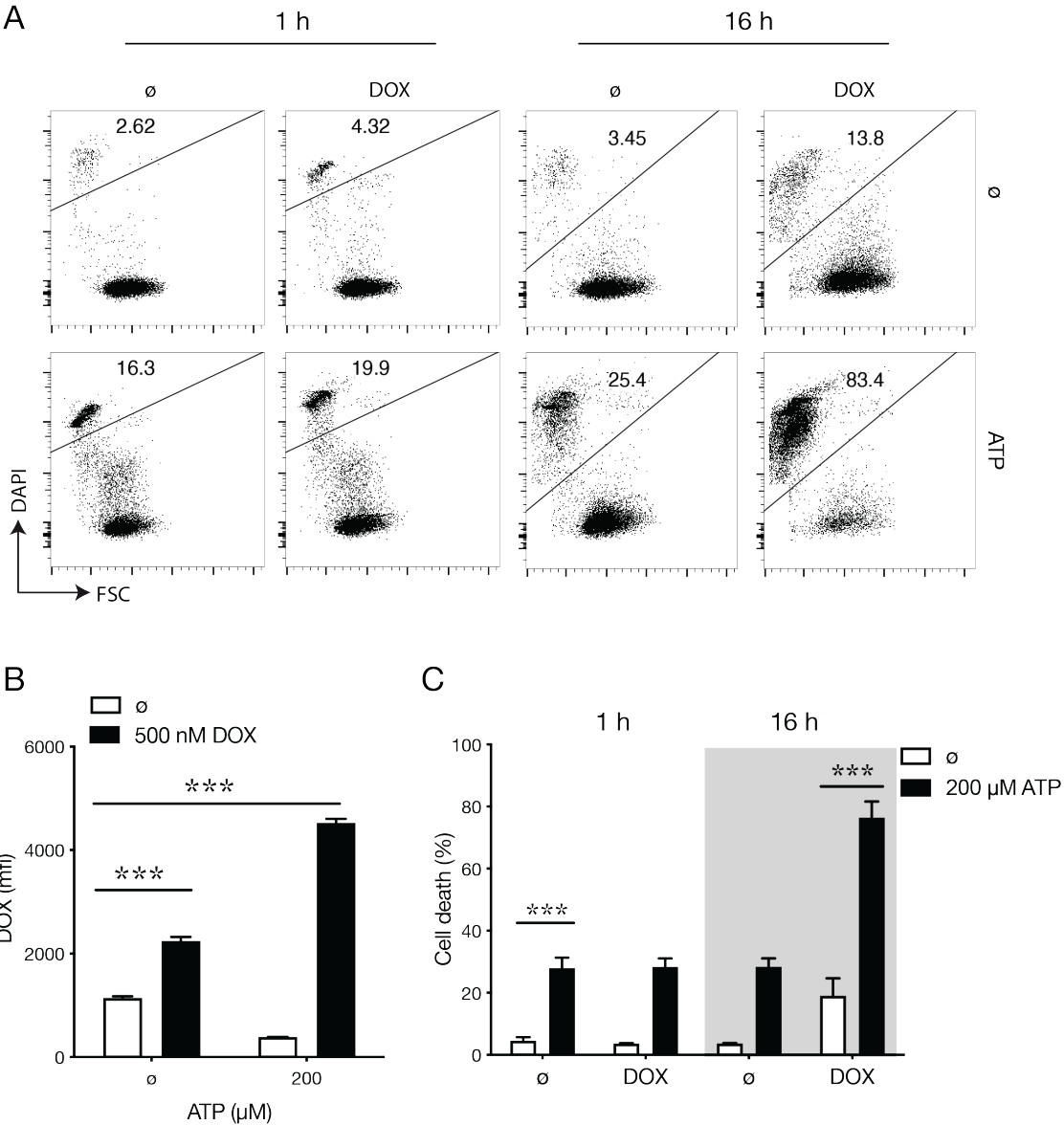


Figure 13. Transient gating of P2X₇ marks cells for doxorubicin-induced death: A-C) Yac-1 cells were incubated for 1 h with 500 nM DOX, 100 μM ATP, 200 μM ATP, or the indicated combinations of ATP and DOX. The cells were then washed and cultured overnight in complete RPMI medium. Cell death and DOX accumulation were determined by flow cytometry. **A-C)** Representative FACS plots and bar graph showing cell death in relationship to the duration of treatment with DOX and/or ATP. **B)** DOX uptake by cells treated for 1h. This experiment is representative of three separate experiments with similar outcome. Data shown as mean ± SEM. Statistics: two-way analysis of variance; posttest: Bonferroni test. ***, p<0.001

3.1.9. Synergistic effects of P2X₇ signaling on doxorubicin toxicity are dependent on the P2X₇ isoform

In the first phase of the project, I found that Yac-1 cells were sensitive to ATP and DOX with EC50s of 300 μ M and 200 nM, respectively. Treatment with ATP increased the cytotoxic effects of DOX in a synergistic manner. To further support our results, we cloned P2X₇ splice variants (a) and (k) into the retroviral vector pMXs. Retroviral vectors have the ability to transform their single strand RNA to double stranded DNA that stably incorporates into the target cell genome (Anson 2004).

4T1 cells are a mouse mammary carcinoma cell line. Various characteristics of 4T1 cell line make it suitable for *in-vivo* studies of breast cancer. It is easily transplantable, highly tumorigenic and invasive. Metastatic spread of 4T1 cells is very similar to that of human mammary cancer (Pulaski et al. 2000a). In recent studies, 4T1 cell line was also used to evaluate immunotherapy strategies focussed on tumor specific CD8 and CD4 lymphocytes (Pulaski and Ostrand-Rosenberg 1998; Pulaski et al. 2000b). Therefore, I used 4T1 cell line to check the role of P2X₇ in tumor cells.

To see if P2X₇ also synergistically enhances the effects of DOX in this cell line, I transduced the breast tumor cell line with the P2X₇ (a) and (k) splice variants, as well as with a non-functional variant of P2X₇, which has a point mutation at position 294 that makes it insensitive to ATP (Adriouch et al. 2009). FACS analyses revealed a high level of P2X₇ expression in 4T1 cells transfected with both P2X₇ variants and the dead mutant when stained with the monoclonal antibody RH23-A44-Alexa 647, which is specific for murine P2X₇ (**Fig.14A**). I treated the 4T1 wild type and P2X₇-transduced cell lines with increasing concentrations of DOX in the presence of 300 μ M ATP for 48 h. Interestingly, I found that ATP increased the cytotoxic effects of DOX in the 4T1 P2X₇ (k) cell line in a similar fashion as in Yac-1 cells (**Fig. 14D**), while the 4T1 P2X₇ (a) cells did not show any synergism between DOX and ATP at this concentration (**Fig. 14C**).

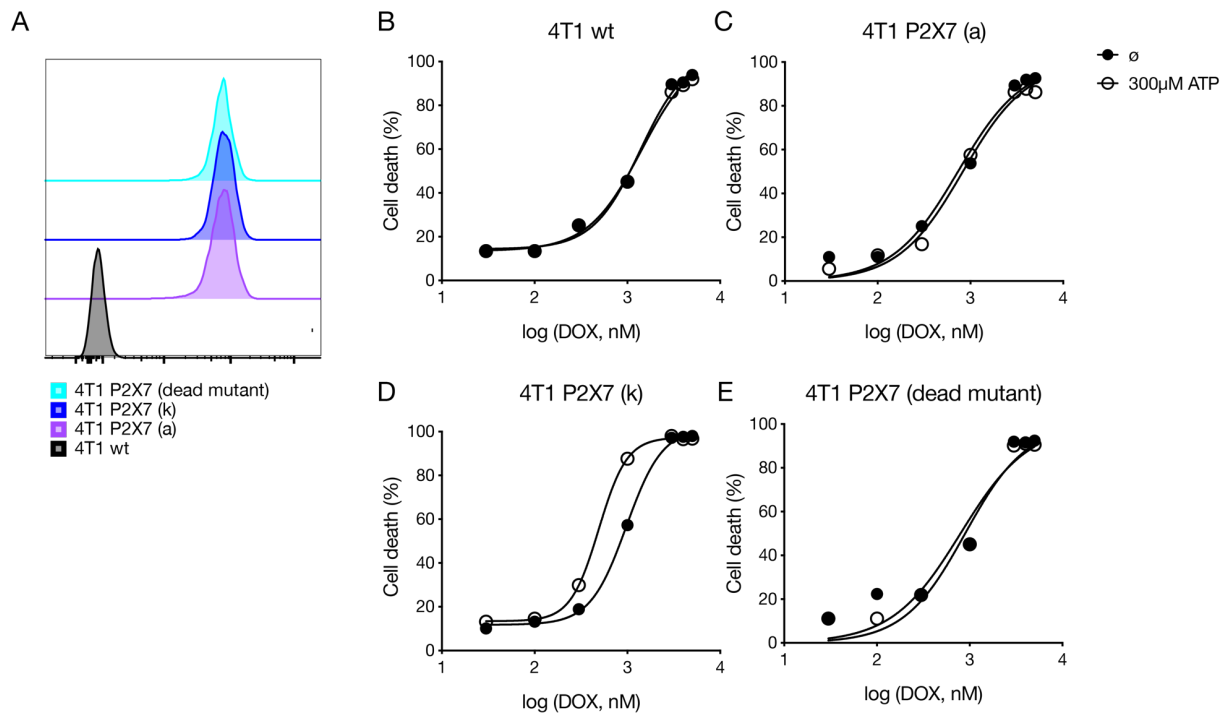


Figure 14. The synergistic effect of P2X₇ on doxorubicin cytotoxicity is dependent on the P2X₇ isoform: A) 4T1 mammary carcinoma cells were retrovirally transduced with P2X₇ (a) and (k) splice variants, as well as with a non-functional P2X₇ variant (dead mutant). **B-E)** cells were treated for 48 hours with various concentrations of DOX and 300 μM ATP in the presence or absence of 13A7. Cell death was measured by the acid phosphatase assay. Histograms in **Fig. A** show the expression of P2X₇ in different 4T1 cell lines. 4T1 wt (gray) does not express any P2X₇, while 4T1 cells transduced with P2X₇ (a) (purple), P2X₇ (k) (blue) and P2X₇ R294A (turquoise) show the similar expression levels of P2X₇. Dose response curves for DOX cytotoxicity in the presence or absence of ATP are shown in 4T1_wt (**B**), 4T1 P2X7 (a) (**C**), P2X7 (k) (**D**) and 4T1 P2X7 R294A (**E**).

3.1.10. P2X₇ (k)-expressing A20 B lymphoma cells also show enhanced doxorubicin cytotoxicity in the presence of ATP

I generated a further model system by transducing the A20 B lymphoma cell line with the P2X₇ (a) and (k) splice variants. The rationale for doing so was twofold. Firstly, A20/P2X₇ provides a second lymphocyte model that allows for direct comparison of P2X₇ variants; and secondly, as a B cell-derived tumor they might provide a good model to study the unfolded protein response. FACS analyses showed a high level of P2X₇ expression in A20 cells transfected with both P2X₇ variants (a) and (k) when stained with RH23-A44-Alexa 647 (**Fig. 15A**). Therefore, this cell line is appropriate to investigate P2X₇ signaling in tumor cells as well as to find out the role of the two splice variants in the DOX/ATP synergism. I tested all the cell lines for ATP sensitivity. 30 min treatment with different concentrations of ATP showed that A20 P2X₇ (k) is very sensitive to ATP (IC₅₀: 300µM) and PS exposure on living cells (gated on DAPI negative cells) was observed at 100 µM ATP (**Fig. 15B-D**). A20 P2X₇ (a) cells were much less sensitive to ATP (IC₅₀: 1mM). A20 wt did not respond to ATP treatment. I also tested all the cell lines for DOX sensitivity in presence of ATP and the P2X₇ blocking nanobody 13A7. I observed enhanced DOX sensitivity only in P2X₇ (k) transduced cells in the presence of 200 µM ATP (**Fig. 15E-G**). A20 wt and A20 cells transfected with P2X₇ (a) variant did not show any additive toxic effects. I have also used higher concentration of ATP in the presence of DOX to check if A20 P2X₇ (a) shows any synergistic effects, and I observed that P2X₇ (a) required more than 500µM ATP for synergistic toxic effects (data not shown).

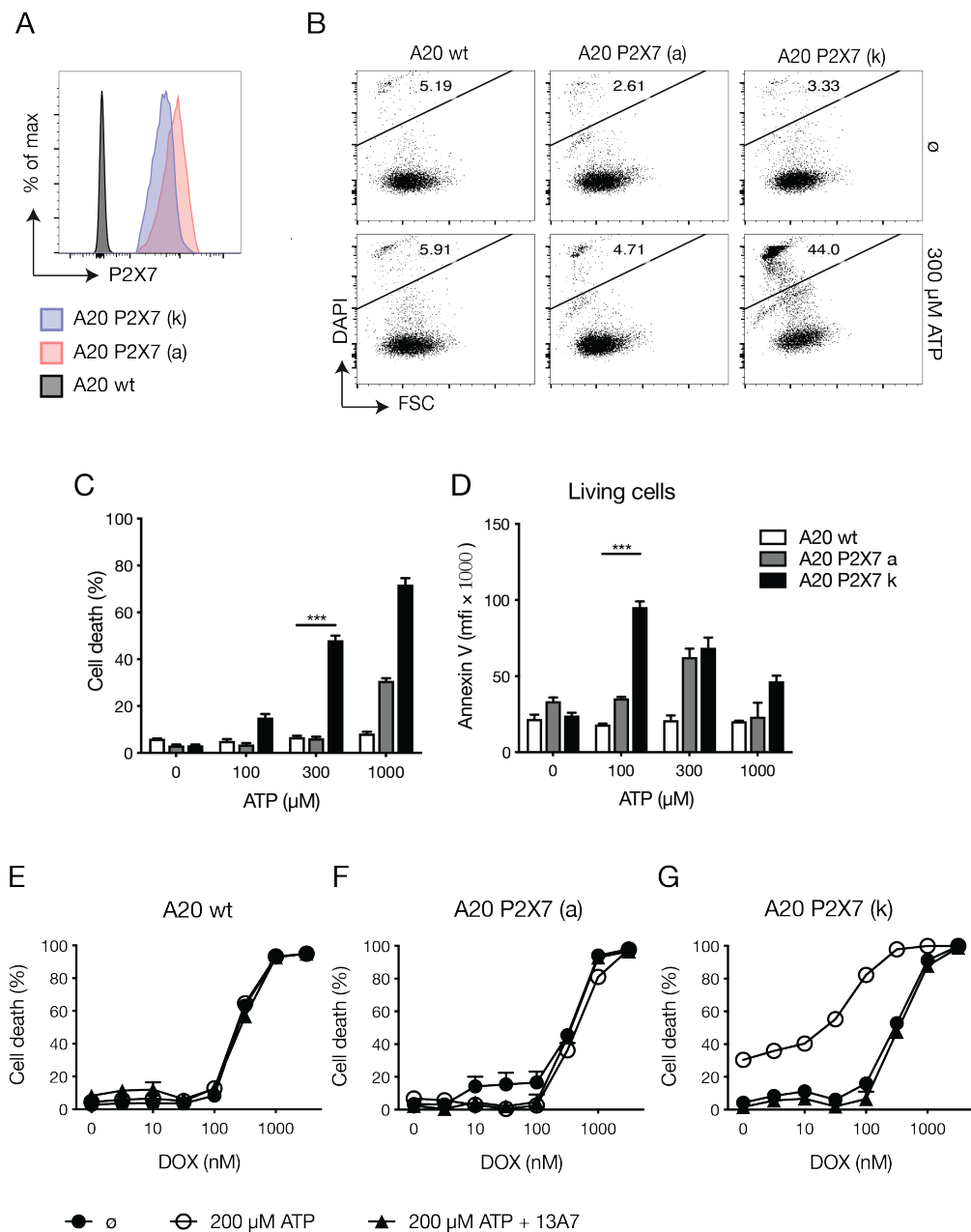


Figure 15. P2X₇ splice variants differ in their effects on synergistic cytotoxicity:

A) The B lymphoma cell line A20 was transduced with the two P2X₇ splice variants (a) and (k) and the expression was checked by flow cytometry as explained in figure 14. A20-wt does not express P2X₇ (gray shaded histogram), P2X₇ (a) and (k) transduced A20 cells showed similar expression of P2X₇ as shown in orange shaded (P2X₇ (a)) and blue shaded (P2X₇ (k)) histograms. **B-C)** 30min incubation with various concentrations of ATP showed that P2X₇ (k) has a higher sensitivity to ATP than P2X₇ (a), while un-transfected cells were completely insensitive to ATP. **B)** Representative FACS plots for cell death after 30 min and summary of **Fig. B** is shown **C. D)** PS flashing (increase in mean fluorescence intensity (mfi) of annexin V) in un-transfected and P2X₇ transfected A20 cells. **E-G)** Acid phosphatase assay was performed to check the cell viability in all A20 cell line treated with DOX +/- ATP and 13A7. The presence of ATP (300μM) did not affect DOX induced cell death in A20_wt (**E**) and

A20 P2X₇ (a) cell line **(F)**. LC50 for doxorubicin was significantly reduced in A20/P2X₇ (k) cells treated with 200 μM ATP **(G)**.

3.1.11. P2X₇ and doxorubicin co-operate in the induction of phagocytosis-promoting signals

Anthracycline drugs are known inducers of type 1 immunogenic cell death (Garg et al. 2016). A hallmark of ICD is the translocation of calreticulin (CRT) from the ER to the cell surface. Cell surface CRT provides a phagocytosis signal to APCs, which together with the release of danger signals stimulates the immune reaction against the dying cell (Kroemer et al. 2013). On the other hand, P2X₇ signaling causes the translocation of phosphatidylserine (PS) to the exterior leaflet of the plasma membrane, which facilitates the recognition and uptake of the cell by professional phagocytes (Adriouch *et al.* 2002). I therefore asked whether P2X₇ and DOX also co-operate in the induction of these phagocytosis-promoting signals. A six-hour culture in the presence of 100 μM ATP did not induce the exposure of PS or CRT on live cells. Co-incubation with the P2X₇-enhancing nanobody 14D5 (Danquah et al. 2016) led to a small increase in PS, but not CRT exposure. DOX alone (300 nM) induced exposure of both PS and CRT, which was not affected by co-incubation with 100 μM ATP alone, but strongly enhanced in the presence of ATP + 14D5 **(Fig.16 B)**. Incubation with DOX also caused some cell death, which was also slightly increased in the presence of ATP and 14D5 **(Fig. 16A)**. Interestingly, incubation with DOX alone for 6 hours caused an increase in membrane permeability in living cells, as shown by an increase in low-level DAPI uptake **(Fig.16A)**.

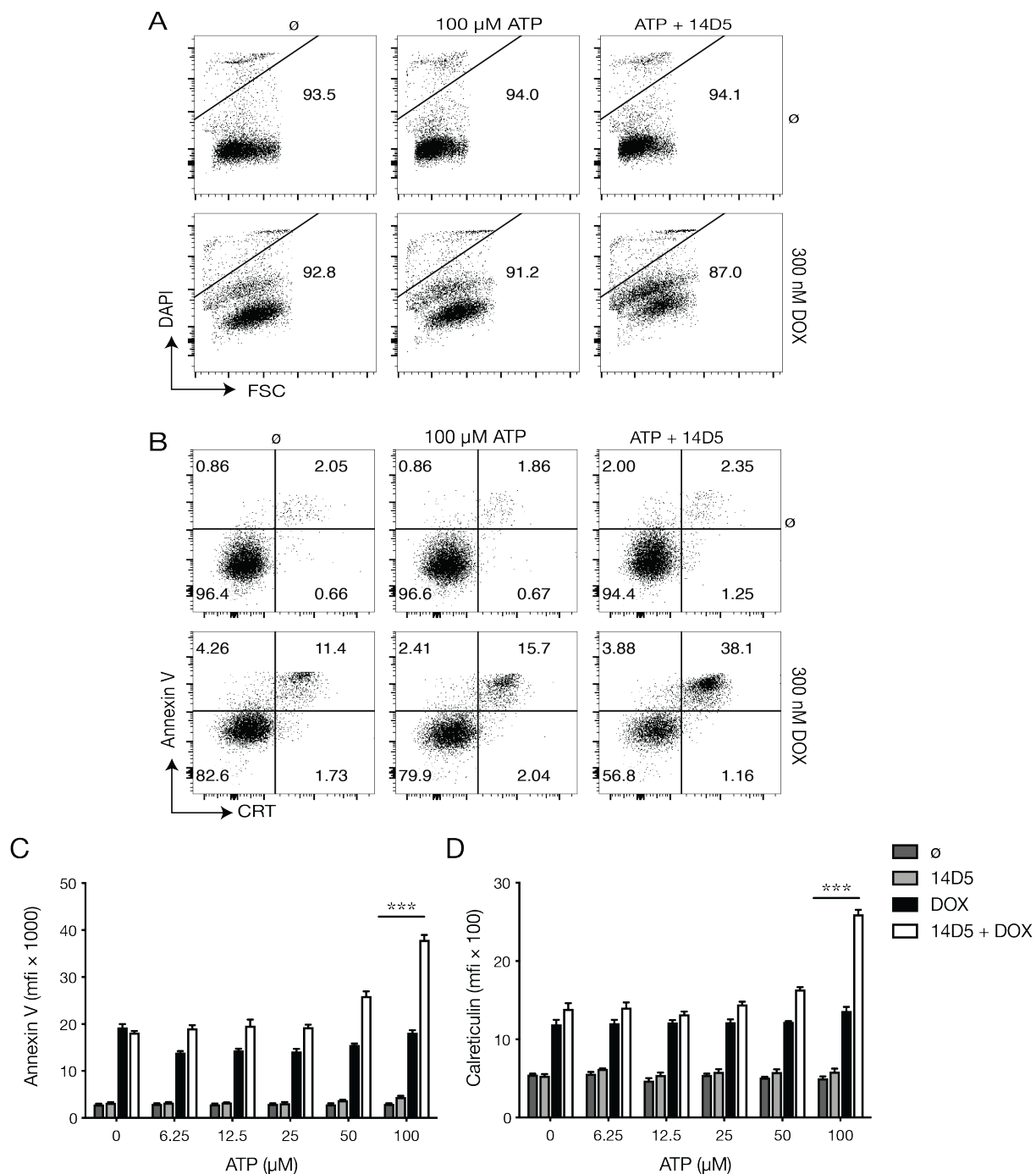


Figure 16: P2X₇ and doxorubicin co-operate in the induction of phagocytosis-promoting signals: Yac-1 cells were incubated for 6 h with 300 nM DOX and various concentrations of ATP (0 - 100 μM) in the presence or absence of the P2X₇-enhancing nanobody 14D5, and analyzed for cell vitality (**A**), binding of annexin V or surface expression of calreticulin (**B**) by flow cytometry on a FACS Canto2. In **B** live cells are shown. Staining for calreticulin (CRT) was performed with unlabeled rabbit monoclonal antibody (clone D3E6) followed by secondary staining with AF647-coupled anti-Rabbit-Ig antiserum. Annexin V staining was done by incubating the cells with annexin V antibody for 30 min at room temperature in dark. Cell vitality was determined by co-staining with DAPI (**A**). Mean fluorescence intensity of annexin V and calreticulin are shown in **C** and **D** respectively. Statistics: two-way analysis of variance; posttest: Bonferroni test. ***, p<0.001.

I further confirmed the increase in ER stress in the presence of ATP and DOX by microscopy. Fibroblast cell line 3T3 transfected with P2X₇ (k) was further stably transduced with calreticulin fused to GFP. The expression of CRT was checked by flow cytometry and under the microscope. Cells were treated with DOX, ATP or combination of both for 4 h. A decrease in CRT at the ER was observed in the combined therapy (**Fig. 17 D**) as well as stress granules were formed in the treated cells compared to control.

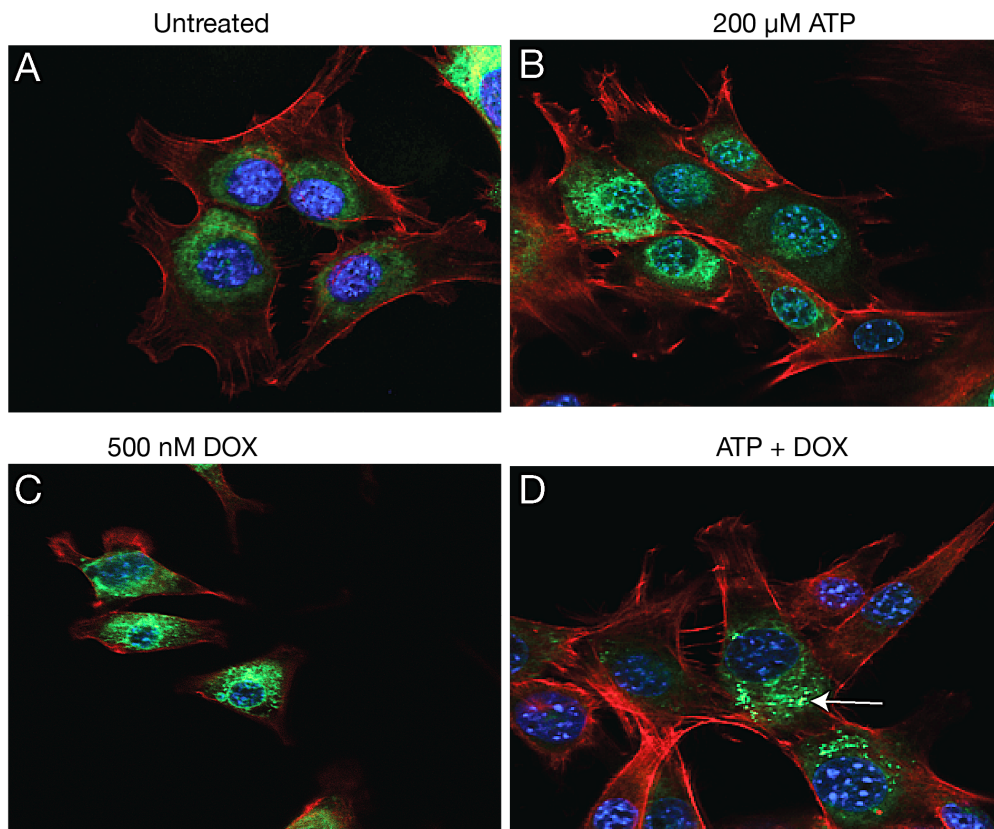


Figure 17. Enhanced ER stress in fibroblast cell line: A-D) To check the calreticulin surface translocation, P2X₇ (k) transfected 3T3 cells that were retrovirally transduced with calreticulin eGFP were seeded (5×10^4 / sample) on cover slips (previously treated with 0.1 mg /ml poly L lysin (PLL), treated with 500 nM DOX in the presence and absence of 200 μM ATP for 4 h. Cells were permeabilized with 1% Triton for 5 min and blocked with blocking buffer (1% BSA and 0.1 % triton) for 40 min at room temperature and stained with Phalloidin (1:50) for 30min to visualize the actin cytoskeleton. Cover slips were mounted with mounting medium containing DAPI on slides. Stress granule formation was observed by using confocal Microscope (sp5). Untreated sample (\emptyset) showed intact cytoskeleton (red) and nucleus (blue). No surface translocation of calreticulin (green) was observed (**A**). Treatment with ATP alone (**B**) and in the combination with DOX (**D**) resulted in stress granule formation. **Fig. C** shows that treatment with DOX alone caused cell shrinkage.

3.1.12. P2X₇ also enhances the cytotoxicity of Bortezomib, a known inducer of the unfolded protein response

Surface exposure of calreticulin induced by DOX or other mediators of immunogenic cell death results from ER stress and consequent triggering of the unfolded protein response (UPR) (Garg et al. 2012). I therefore investigated the effect of P2X₇ gating on the UPR induced in A20 cells by overnight treatment with Bortezomib (BTZ). BTZ is a known type 1 immunogenic cell death inducer that causes protease inhibition in the ER, resulting in ER stress and triggering of UPR (Ri 2016). I evaluated the survival of A20 cells transduced with P2X₇ (k) in the presence or absence of ATP (**Fig. 18 A-B**). Treatment with 3 nM BTZ alone caused death in approximately 10 % of cells, while only few cells died in response to 100 μ M ATP alone. However, in the presence of 100 μ M ATP, 3 nM BTZ was toxic for more than 60% of the cells. This effect was blocked entirely by pre-treatment with the P2X₇-antagonistic nanobody 13A7.

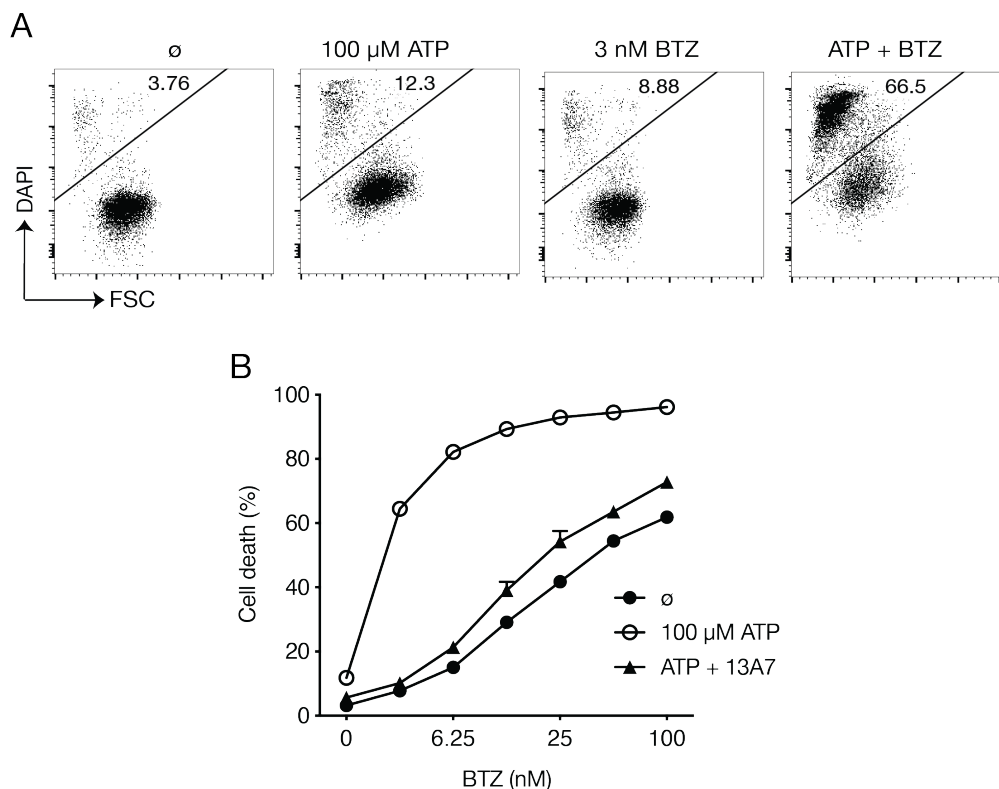


Figure 18. P2X₇ activation results in enhanced Bortezomib toxicity: A-B) A20/P2X₇ (k) cells were treated overnight with different concentrations of Bortezomib (3-100 nM) or in the combination of 100 μ M ATP in the presence or absence of 13A7 nanobody. DAPI was added immediately before analysis to stain the dead cells. Cell viability was assessed by flow cytometry. Representative FACS plots for cell death and summary of data are shown in **A** and **B** respectively.

3.1.13. P2X₇ and doxorubicin synergize to activate Caspase-3

It has been reported that activation of caspase-3 is an important step in the pathway that mediates apoptotic cell death resulting from ER stress (Hitomi et al. 2004). I therefore investigated the role of P2X₇ signaling in caspase-3 activation. Treatment of Yac-1 cells with either 200 μ M ATP or 300 nM DOX for 6 h induced activation of caspase-3 in live cells (**Fig. 19A-B**). This was supra-additively enhanced when the two compounds were given together. The synergistic effect of ATP was blocked by pre-incubation of the cells with the P2X₇-inhibitory nanobody 13A7. Staurosporin (STR), a known inducer of caspase-3-dependent apoptosis was used as a positive control (**Fig. 19C**).

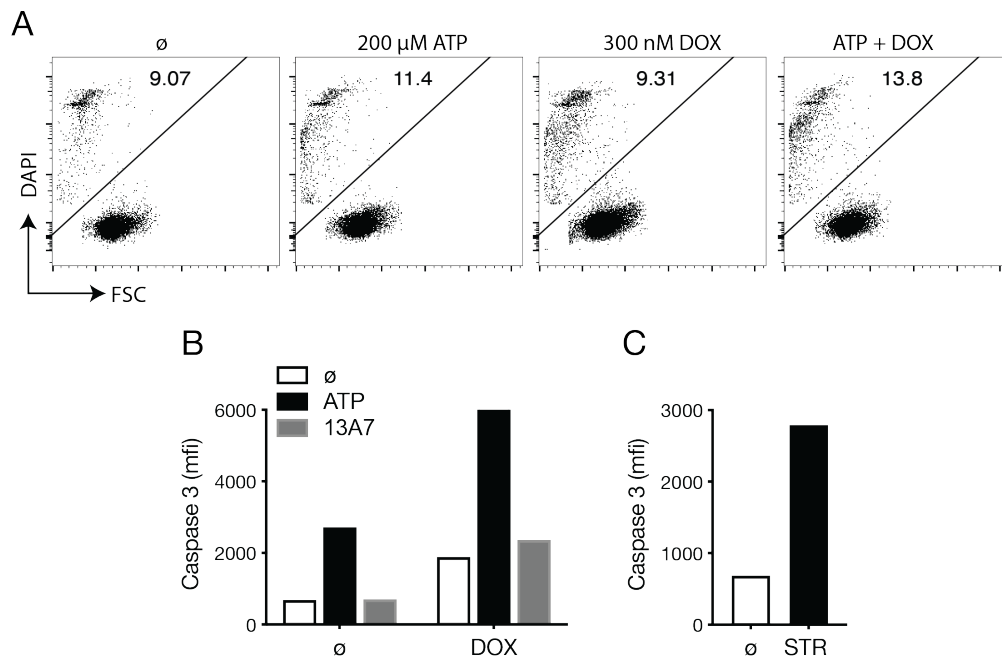


Figure 19. P2X₇ and doxorubicin synergize to activate caspase-3: A-B) Yac-1 cells were incubated at 37°C for 6 h with 200 μ M ATP, 300 nM DOX, or a combination of both, or 300 nM staurosporin (STR), washed, and stained with the FLICA caspase-3 kit to detect activated caspase-3. DAPI was added immediately before analysis to monitor cell death. **A)** Representative FACS plots for cell viability. **B)** Mean fluorescence intensity (mfi) for caspase 3 in live cells (DAPI negative cells). **C)** STR was used as a positive control for caspase-3-dependent apoptosis.

3.1.14. Gating of P2X₇ alone results in Calreticulin (CRT) translocation

The previous experiments established that P2X₇ synergistically co-operates with DOX in the induction of the ER stress/UPR pathway. In light of these observations I asked whether gating of P2X₇ by itself was also sufficient to trigger the UPR. To do so, I investigated whether ATP alone could induce CRT translocation to the cell membrane (**Fig. 20**). Indeed, 30 min treatment with 100 – 200 μ M ATP in the case of A20 P2X₇

(k) cells and more than 1 mM ATP in the case of A20 P2X₇(a) was sufficient to induce CRT surface exposure in a concentration-dependent manner.

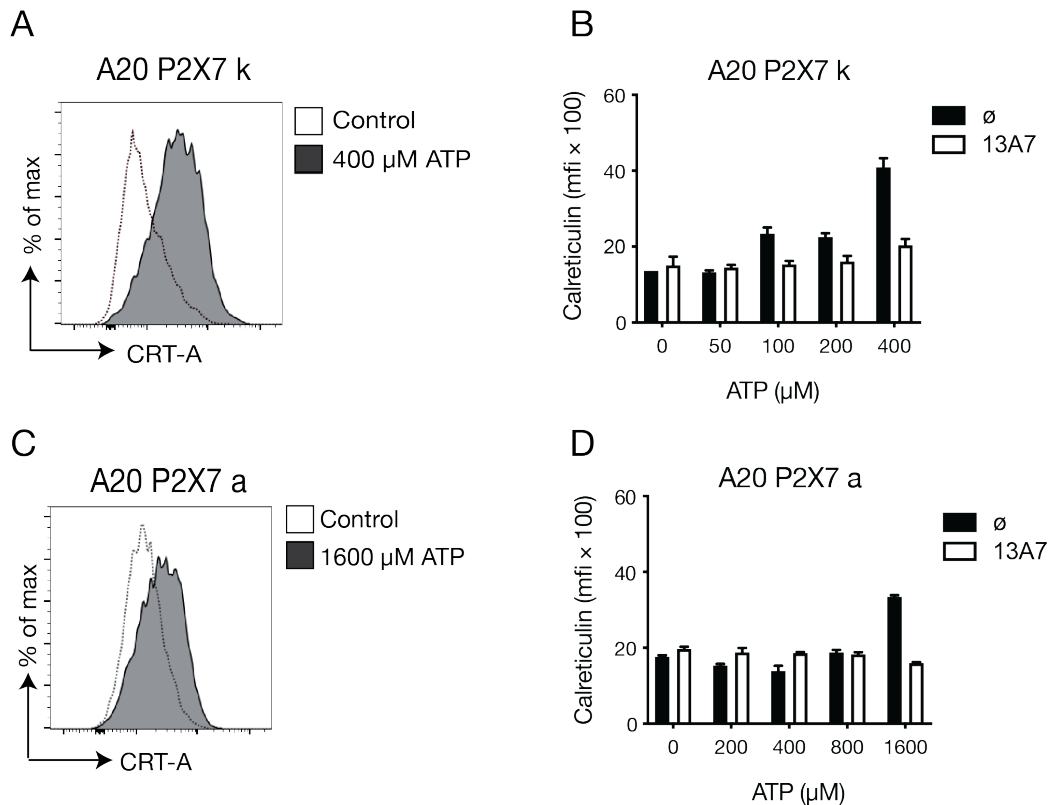


Figure 20. P2X₇ activation results in CRT surface translocation: A-D) A20/P2X₇ (a) or (k) cells were incubated with various concentrations of ATP for 30min. Cells were stained for calreticulin (CRT) using the unlabeled rabbit monoclonal antibody (clone D3E6) for 1 h on ice, followed by secondary staining with AF647-coupled anti-Rabbit-Ig antiserum for 30 min at 4 °C. Cell vitality was determined by co-staining with DAPI. Representative histogram for calreticulin translocation in A20 P2X₇ (k) is shown in **A** and summarized data in **B**. Calreticulin surface translocation in A20 P2X₇ (a) cell line is shown in **C** and **D**.

3.1.15. P2X₇-mediated CRT translocation, PS exposure, and pore formation are regulated by the PERK pathway

The PKR-like ER kinase (PERK) is an important mediator of the immunogenic cell death pathway. Under conditions of ER stress, activation of PERK leads to phosphorylation of its substrate eukaryotic initiation factor-2 α (eIF2 α) and externalization of CRT (Panaretakis et al. 2009; Kepp et al. 2015). I therefore tested if P2X₇-induced ER stress is regulated by PERK activation.

For this, cells were pre-treated with the PERK inhibitor GSK2606414 for 1 h and then incubated with ATP for short time periods (2-10 min). Interestingly, I found that, p-eIF2 α , CRT translocation, PS exposure, and DAPI uptake induced by short-term

exposure to ATP were all blocked by inhibition of PERK (**Fig. 21A-E**). However, CD62L shedding did not block by PERK inhibitor in the presence of 400 μ M ATP (**Fig. 21F**).

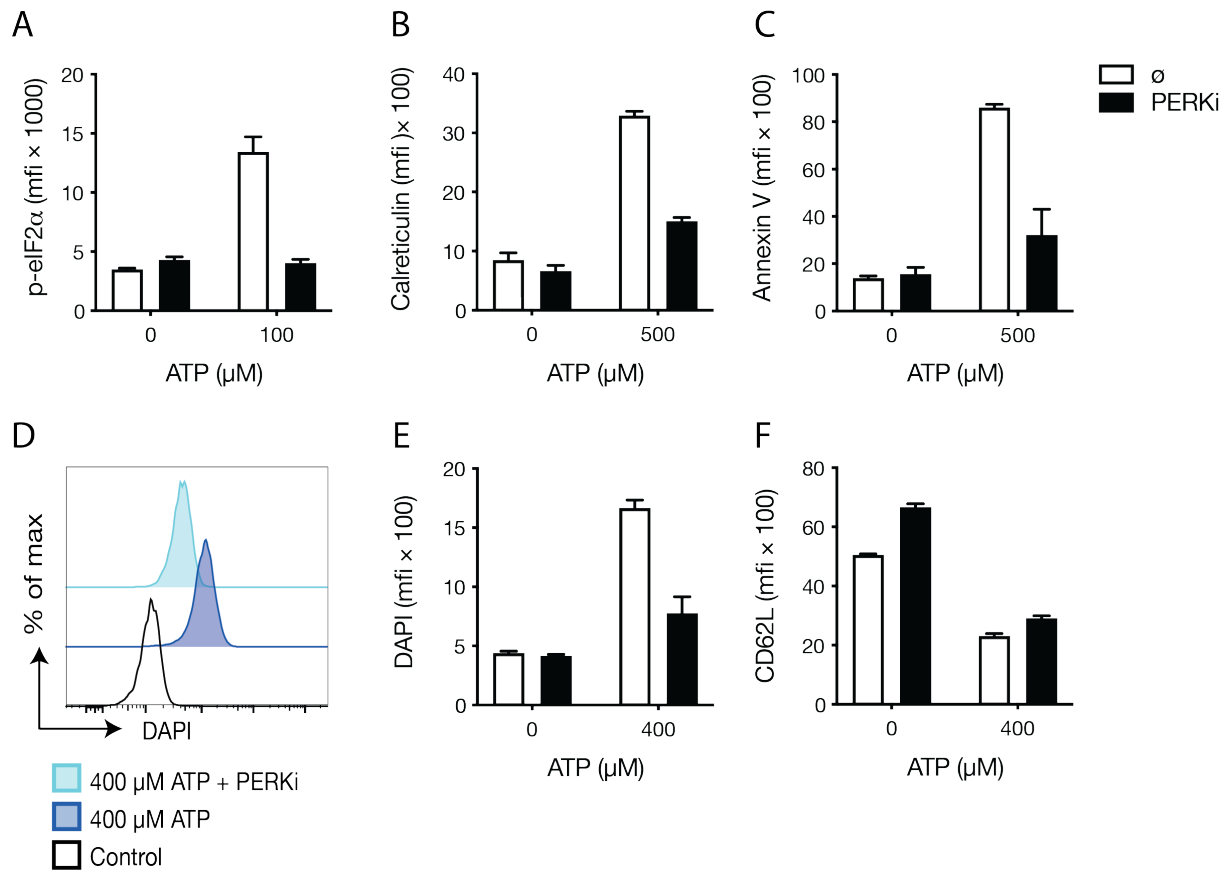


Figure 21. P2X₇-mediated DAPI uptake, PS flashing and CRT translocation are blocked by inhibition of PERK: A-F) Yac-1 cells were pre-incubated with 10 μ M of the PERK inhibitor GSK2606414 (PERKi) for 1 h, and then cells were treated with 100 μ M ATP for 10 min (**A**), 500 μ M ATP for 10 min (**B & C**) and 400 μ M ATP for 2 min (**D-F**). Cells were washed and stained for p-eIF2 α , surface CRT, PS exposure, CD62L shedding and DAPI uptake (explained in previous sections). Representative bar graphs show increase in phosphorylation of eIF2 α (**A**), surface translocation of CRT (**B**) and PS flashing (**C**) in ATP treated samples, all these affects are blocked in the presence of PERK inhibitor. A representative FACS histogram for DAPI uptake is shown in **Fig. D** and summarized data in **Fig E**. Presence of PERK inhibitor blocks ATP mediated DAPI Uptake. **F**) ATP mediated CD62L shedding did not affected in the presence of PERK inhibitor. Statistics: two-way analysis of variance; posttest: Bonferroni. ***, $p < 0.001$

3.1.16. Inhibition of PERK blocks the synergistic effect of P2X₇ on doxorubicin-mediated cytotoxicity

In previous experiments I found that PERK inhibition negatively regulates the P2X₇ mediated effects i.e., DAPI uptake, CRT surface translocation and PS translocation. Here I investigated if the PERK pathway also affects the cytotoxic effects of DOX in the presence or absence of subthreshold eATP. Interestingly, inhibition of PERK had the opposite effects on the DOX-mediated cytotoxicity and the P2X₇-mediated cytotoxic synergism (**Fig. 22 A-B**), showing that gating of P2X₇ did not merely amplify DOX signaling by increasing its uptake.

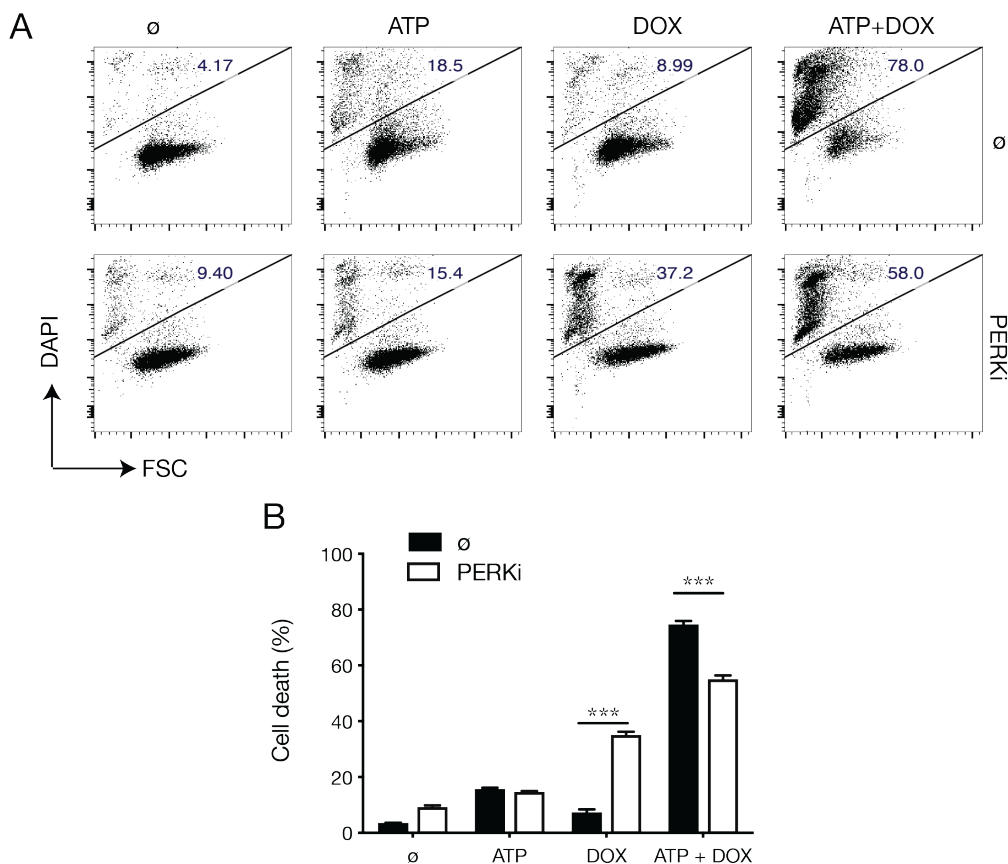


Figure 22. Inhibition of PERK blocked the synergistic effect of P2X₇ on doxorubicin-mediated cytotoxicity: A-B) Yac-1 cells were treated with 10 μ M PERK inhibitor (GSK2606414) for 1 h and then indicated concentrations of ATP, DOX or a combination of DOX and ATP were added overnight at 37°C and 5% CO₂. Cells were washed and stained with DAPI immediately before analysis by flow cytometry. Each condition was performed in triplicate. **A)** Representation of cell viability (DAPI+ cells) in the presence of different treatments with and without PERK inhibitor. **B):** Bar graph representing the mean values \pm SEM. Statistics: two-way analysis of variance; posttest: Bonferroni. ***, $p < 0.001$

3.2. *In-vivo* results

3.2.1. Expression of P2X₇ inhibits tumor growth.

Bioluminescence imaging (BLI) technology has become a powerful tool for real time monitoring of diverse molecules and tumor growth *in-vivo*, based on the generation of light by the luciferase/luciferin reaction. For *in-vivo* imaging of tumor growth, I transduced the Yac-1 cells with the Lentivirus LeGo-iG2-Puro+luc2+GFP, provided by Dr. Kristoffer Riecken, Center for Oncology, Interdisciplinary Clinic and Polyclinic for Stem Cell Transplantation, University Medical Center, Hamburg-Eppendorf, Germany), which encodes luciferase in combination with the enhanced green fluorescent protein (eGFP). To study the effect of P2X₇ on tumor growth, luciferase transduced Yac-1 cells (that endogenously express P2X₇) were injected intravenously into SCID mice, which were then treated with the P2X₇-antagonistic nanobody 13A7-HLE (half-life extended) twice a week (**Fig. 23A**). Bioluminescence (BLI) imaging was performed twice a week with the help of Mr. Michael Horn-Glander, IVIS Facility, University Medical Center Hamburg-Eppendorf, using small animal imaging system (IVIS-200, Caliper Life Sciences, Hopkinton, Massachusetts, USA). D-luciferin was injected in anesthetized mice 15 min before image acquisition. Mice (max. 5) were placed in imaging system and imaged. The total flux is calculated by photons per sec (p/s) in the region of interest (ROI) (**Figure 23 B-C**), by using Living image 4.2 software. Results showed that blocking of P2X₇ resulted in accelerated tumor growth compared to placebo (**Fig. 23 B-F**).

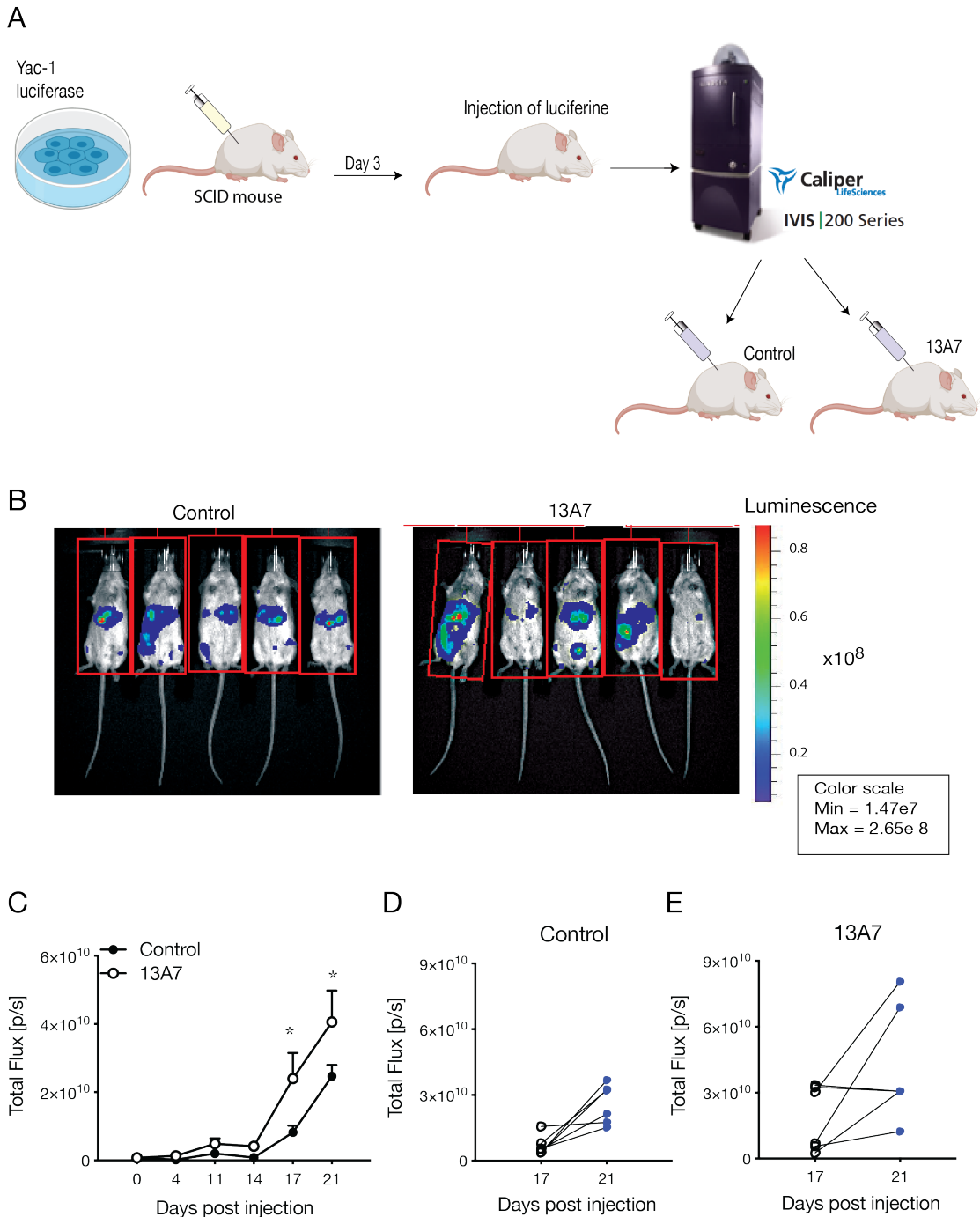


Figure 23. Inhibition of P2X₇ in Yac-1 cells promotes tumor growth: **A)** 2.5×10^5 Yac-1 cells were injected i.v. in SCID mice. At day 3, mice were randomized in 2 groups after *in-vivo* imaging using small animal imaging system (IVIS-200, Caliper Life Sciences). Mice were injected (i.p.) with PBS (placebo) or P2X₇ antagonist nanobody, 13A7 HLE (50 μ g), twice a week. **B-C)** *in vivo* imaging of placebo and 13A7 HLE injected mice at day 14. Images were captured 15 min after intraperitoneal D-luciferin injection. Red rectangles around mice in figure **B** and **C** represent the region of interest (ROI). **D)** Comparison of tumor growth in 13A7.HLE- and placebo-injected mice is shown as total flux (p/s). Data presented as mean \pm SEM. **E-F)** Tumor size, measured as total flux (p/s), in individual mice treated with placebo (PBS) or 13A7 at day 17 and day 21.

3.2.2. Expression of functional P2X₇R slows 4T1 tumor growth *in-vivo*

To confirm the role of P2X₇ in tumor growth, I performed a similar experiment using the 4T1 breast tumor model with the assistance of Dr. Isabel Ben Batalla, Department of Oncology, University Medical Clinic, Hamburg-Eppendorf, Germany. As previously described, 4T1 cells were transfected with P2X₇(k) or the non-functional mutant of P2X₇ that is unable to bind ATP as a control. The 4T1 cells were injected into syngeneic Balb/c mice. Interestingly, 4T1/P2X₇(k) tumors grew significantly slower compared to controls (**Fig. 24A**), supporting the findings from *in-vivo* experiment (Figure 23) showing that expression of P2X₇ slows down tumor growth. The tumor samples were analyzed for T cell infiltration and apoptosis by histology. P2X₇-expressing tumors exhibited higher degrees of T cell infiltration (CD3 staining) and apoptosis than the controls (**Fig. 24 B-D**)

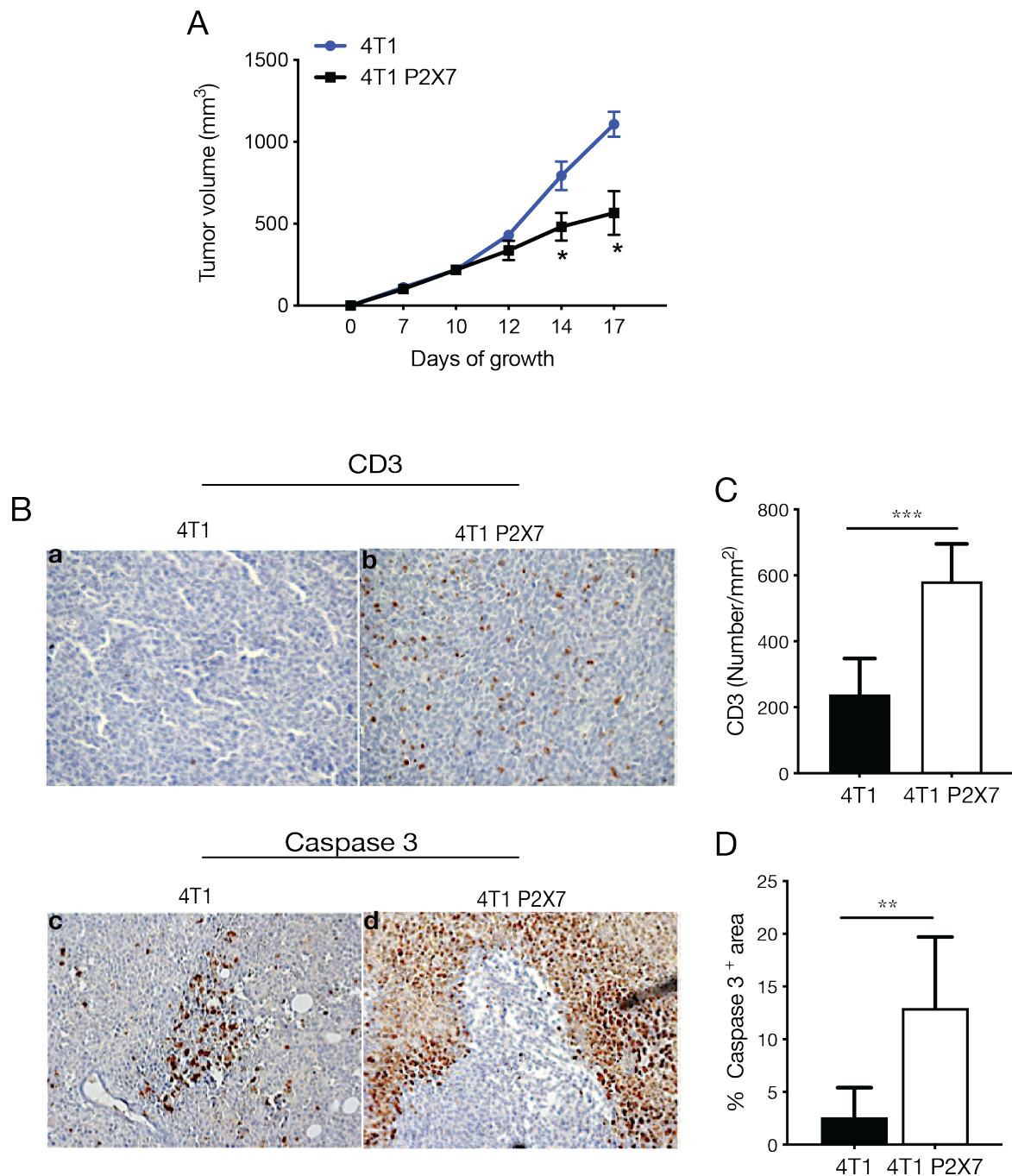


Figure 24. Tumors carrying a functional P2X₇R exhibit slower growth in-vivo: 4T1 cells (5×10^5) carrying either a non-functional P2X₇ mutant (4T1) or P2X₇(k) (4T1_P2X₇) were injected into mammary fat pads of Balb/c mice. **A)** Tumor volume was assessed *in-vivo* by caliper at the indicated time points. **B-D)** Tumor samples were stained for CD3 and caspase-3. Data show the average \pm SEM.

The 4T1-injected mice were then treated with chemotherapy (DOX) when a tumor size of 100mm³ was reached. Significant tumor reduction was observed in DOX-treated control mice (**Fig. 25 A**). Surprisingly, DOX had no effect on the growth of P2X7-expressing tumors (**Fig. 25 B**). Histological results showed that the presence of DOX did not affect the infiltration of T cells in control and P2X7-expressing tumors (**Fig. 25 C**) while it significantly increased apoptosis in control group (**Fig. 25 D**).

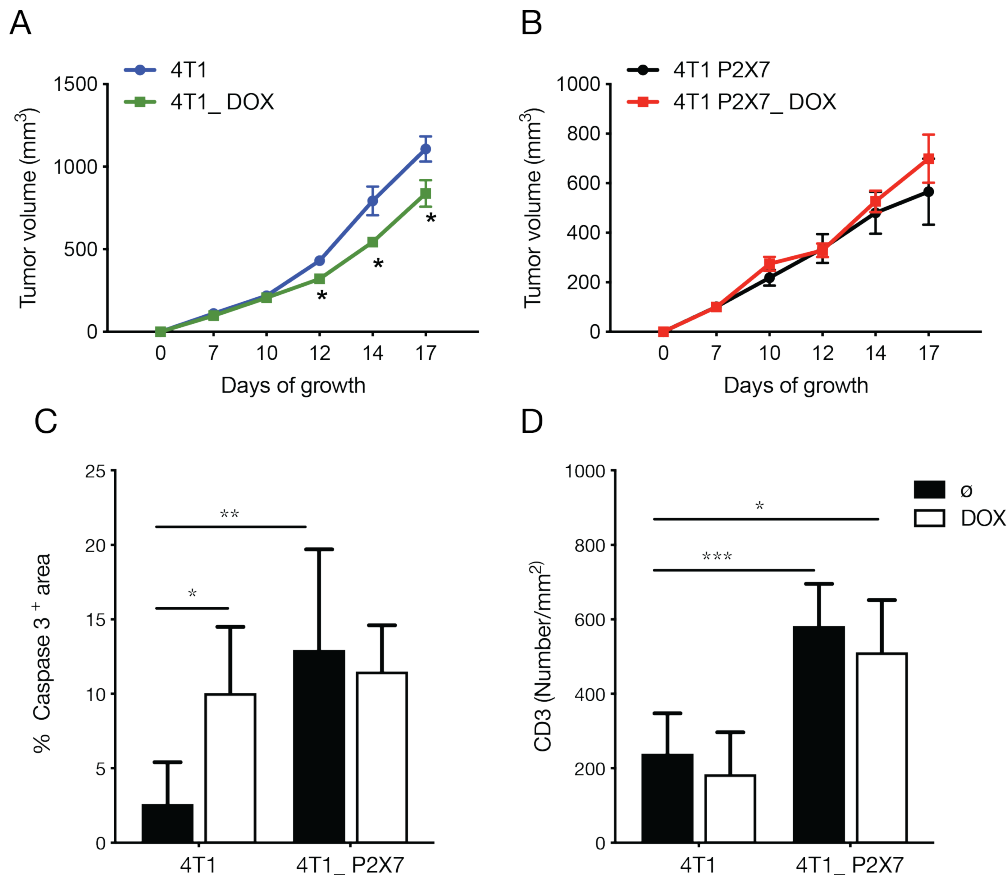


Figure 25. Doxorubicin does not affect the tumor growth in P2X₇ (k) expressing tumors: A-B) 4T1 (P2X/ dead mutant) and 4T1(P2X₇_k) cells (5×10^5) were injected in mammary fat pads of Balb/c mice and treated with 3mg/kg DOX at day 10 and 13. **A-B)** Tumor volume was assessed *in-vivo* assessed by caliper at the indicated time points. **C-D)** For histology, tumor samples were stained for CD3 and caspase 3. Statistics: two-way analysis of variance; posttest: Bonferroni. *, $p < 0.05$, **, $p < 0.01$, ***, $p < 0.001$.

3.2.3. P2X7 enhancing nanobody slows down the tumor growth.

The tumor microenvironment contains a high concentration of extracellular ATP (eATP). It has been shown that eATP levels in tumors are in the range of 100-500 μ M which is much higher than the usual concentration of ATP in healthy tissues (Di Virgilio et al. 2018). 100-500 μ M ATP is enough to activate the purinergic receptor P2X7. To investigate the impact of P2X7 activation on the immune system in the tumor microenvironment, I injected 4T1 cells expressing P2X7(k) into Balb/C mice. When the tumor size reached 100mm³, the mice were randomized into four different groups and treated with intraperitoneal injections of PBS, an agonistic P2X7 nanobody (14D5.HLE), DOX or the combination of 14D5 and DOX. The tumor size was measured every second day. Interestingly, the tumors grew slower in the 14D5 treated group compared to placebo (**Fig. 26A**), supporting our previous observations that the presence of P2X7 (k) on tumors is beneficial for the host (**Section 3.2.1 and 3.2.2**). DOX alone did not show any decrease in tumor size while combination therapy (14D5+DOX) caused a slight decrease in tumor growth compared to placebo (**Fig. 26B**).

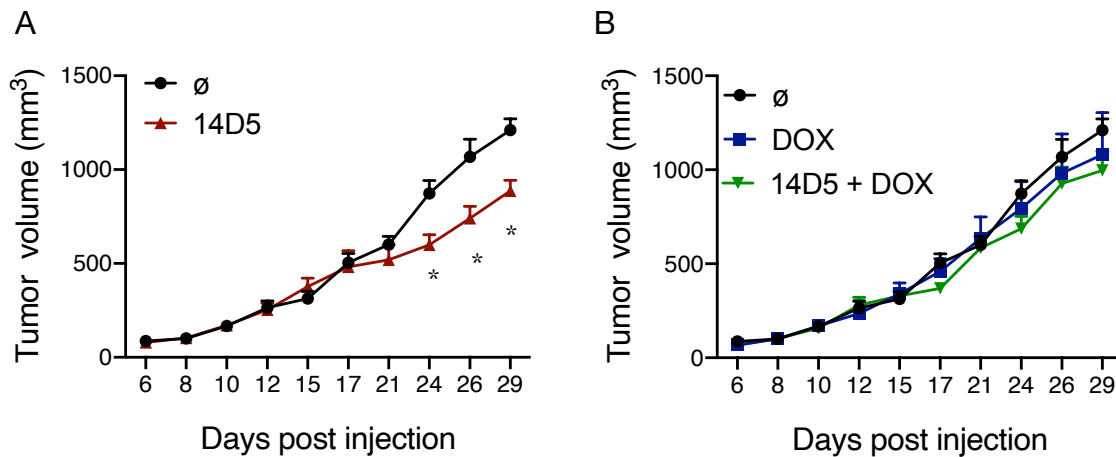
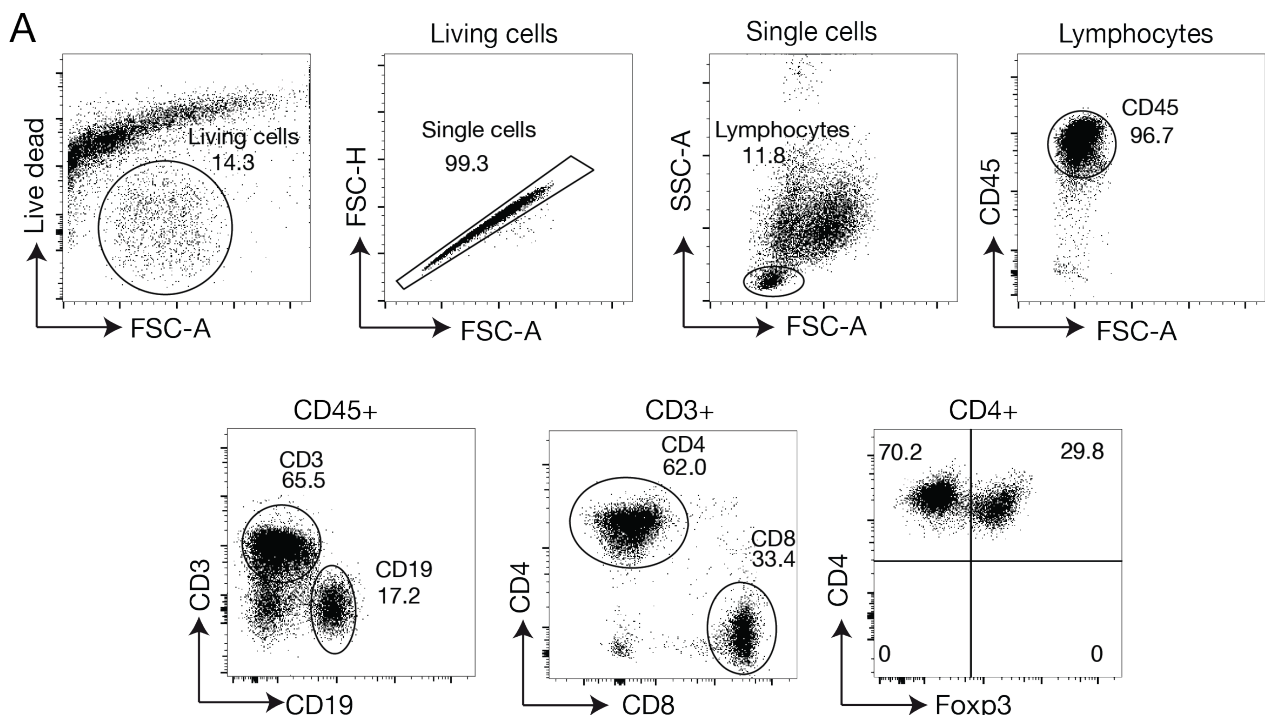


Figure 26. P2X₇ enhancing nanobody slows down the tumor growth: 4T1/P2X7(k) cells (5×10^5) were injected into the mammary fat pads of Balb/c mice. At day 8, when the tumor growth reached 100mm³, the mice were randomized into different groups and injected intraperitoneally twice a week with PBS, DOX (3mg/kg), 14D5 HLE (2mg/kg) or a combination of DOX and 14D5. Tumor volume was assessed *in-vivo* by caliper at the indicated time points. XY graph in the figure represents the increase in tumor volume vs days post 4T1 P2X₇ (K) cells injection. **A**) 14D5 treated mice (red curve) showed slower tumor growth compared to Placebo (black curve). **B**) DOX treated mice did not show any reduction in tumor size. Statistics: Two-way analysis of variance; posttest: Dunnett's test. *, $p < 0.05$.

3.2.4. Subsets of tumor-infiltrating lymphocytes

Tumor infiltrating T cells are an imprint of an ongoing immune response in cancer. A higher presence of tumor infiltrating T lymphocytes is generally an indication of better clinical outcome (Cohen and Blasberg 2017). Therefore, I checked the T and B cell infiltration in solid tumors. At day 31, 4T1 breast cancer bearing mice treated with various treatments (**section 3.2.3**) were injected with S+16 nanobody (an ARTC2 blocker) to protect the cells from NAD induced cell death, 30 min before sacrifice. The solid tumors were collected and prepared for single cell analysis by flow cytometry. The gating strategy used for flow cytometry analyses is shown in **Fig. 27 A**. 40-70% of lymphocytes were positive for CD3 (a marker for T cells) while no significant differences were observed among different treatments (**Fig. 27 B**). 40-60% T cells were positive for CD4 and about 20-40% tumor infiltrating T cells were CD8+ T cells (**Fig. C-D**).

Gating strategy for analysis of lymphocytes from tumor samples



Forkhead Box P3 (Foxp3) positive regulatory T cells (Tregs) cells have the ability to regulate immune responses and immune homeostasis (Fantini et al. 2007; Sakaguchi et al. 2009; Sambucci et al. 2018). I also stained the cells for Foxp3. About 40% of CD4⁺ cells were positive for Foxp3 (**Fig. 27 E**).

CD69 is a marker for early T cell activation and tissue resident memory cells (Cibrián and Sánchez-Madrid 2017). 15 - 35% of CD4⁺ T cells and 40 - 80% of CD8⁺ cells expressed CD69, confirming the high degree of activation of the T cell population as well as differentiating these cells from the circulating lymphocytes (**Fig. 27 F-G**).

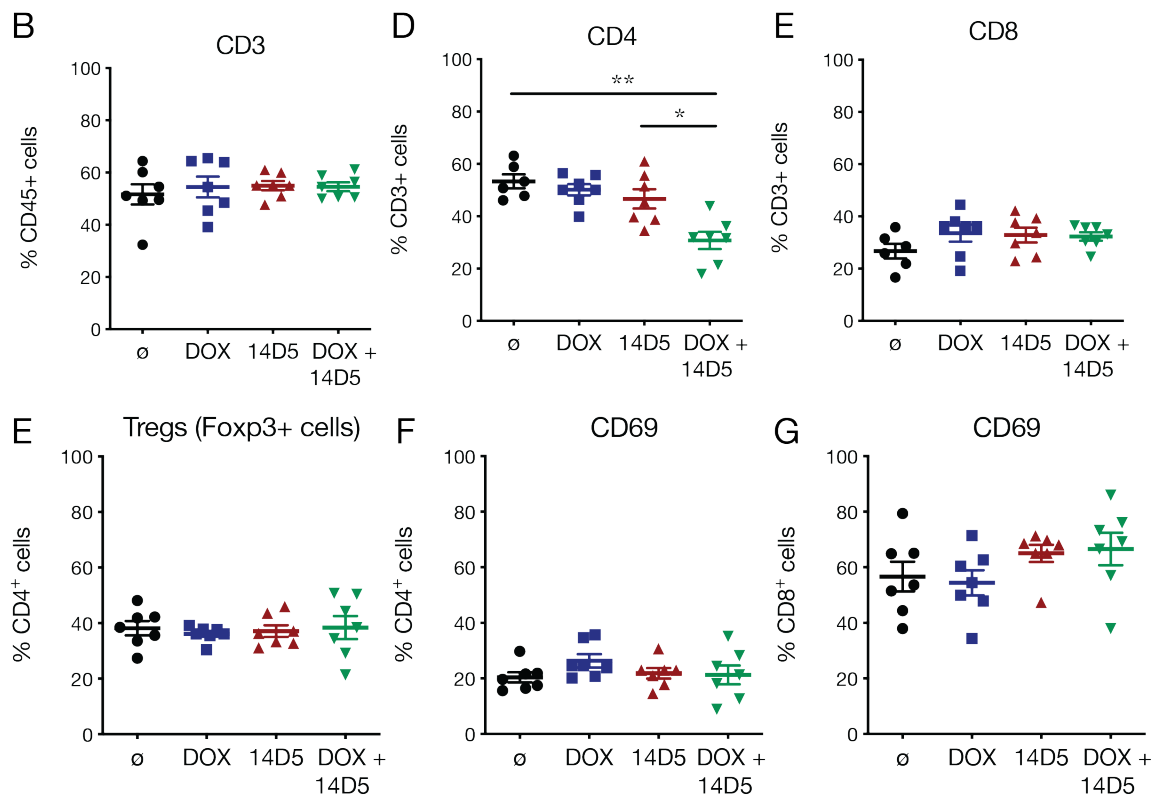


Figure 27. T cell infiltration in solid tumors: After 31 days post injection, mice bearing 4T1 tumors (**section 3.2.3**) were anesthetized and intraperitoneally injected with the ARTC2 blocker S+16, 30 min before euthanizing them. Single cell suspensions from tumors were stained for FACS analysis. Panel **A** shows the gating strategy used to define lymphocyte subsets. Numbers in each gate or quadrant represent % positive cells. Graphs **B-G** show a comparison among treatment groups, % frequencies of cells expressing certain markers within the indicated subpopulations: T cells as percentage of lymphocytes (**B**), CD4⁺ and CD8⁺ cells as percentage of T cells (**C, D**), Tregs as percentage of CD4⁺ T cells (**E**), and the percentages of CD69⁺ cells within CD4⁺ and CD8⁺ T cells (**F, G**). Statistics: one-way analysis of variance; posttest: Tukey. *, p<0.5, **, p<0.01.

3.2.5. Phenotypic analysis of tumor-infiltrating lymphocytes

To address the question of whether P2X7 activation results in a change of the phenotype of T cells, i.e., expression of CD39, CD73, PD1, and granzyme B (GRZB), I analyzed the tumor-infiltrating lymphocytes by flow cytometry.

The presence of high levels of CD39 and CD73 in the tumor microenvironment are crucial for adenosine accumulation (Di Virgilio et al. 2018), particularly, the ATP is converted to ADP and AMP in the presence of CD39, and further dephosphorylated to adenosine by CD73. Increased levels of adenosine results in activation of A2A receptors and rise in the cAMP levels, which impairs the ability of cytotoxic T cells and promotes the infiltration of immunosuppressive cells i.e., Tregs, myeloid derived suppressor cells (MDSCs) and B cells (Allard et al. 2017).

Analysis of CD39 expression showed that Tregs and CD8⁺ cells expressed this marker to a higher degree than conventional (Foxp3⁻) CD4⁺ cells (**Fig. 28A-C**). The expression of CD39 on this subset was decreased by treatment with DOX, either alone or in combination with 14D5 (**Fig 28A**). Interestingly, treatment with DOX also decreased the expression of CD39 on CD8⁺ cells, while the expression of CD39 was increased by treatment with 14D5 (**Fig. 28C**). The expression of CD73 by T cell subpopulations was high in all groups and was not influenced by any of the treatment regimens (**Fig. 28D-F**).

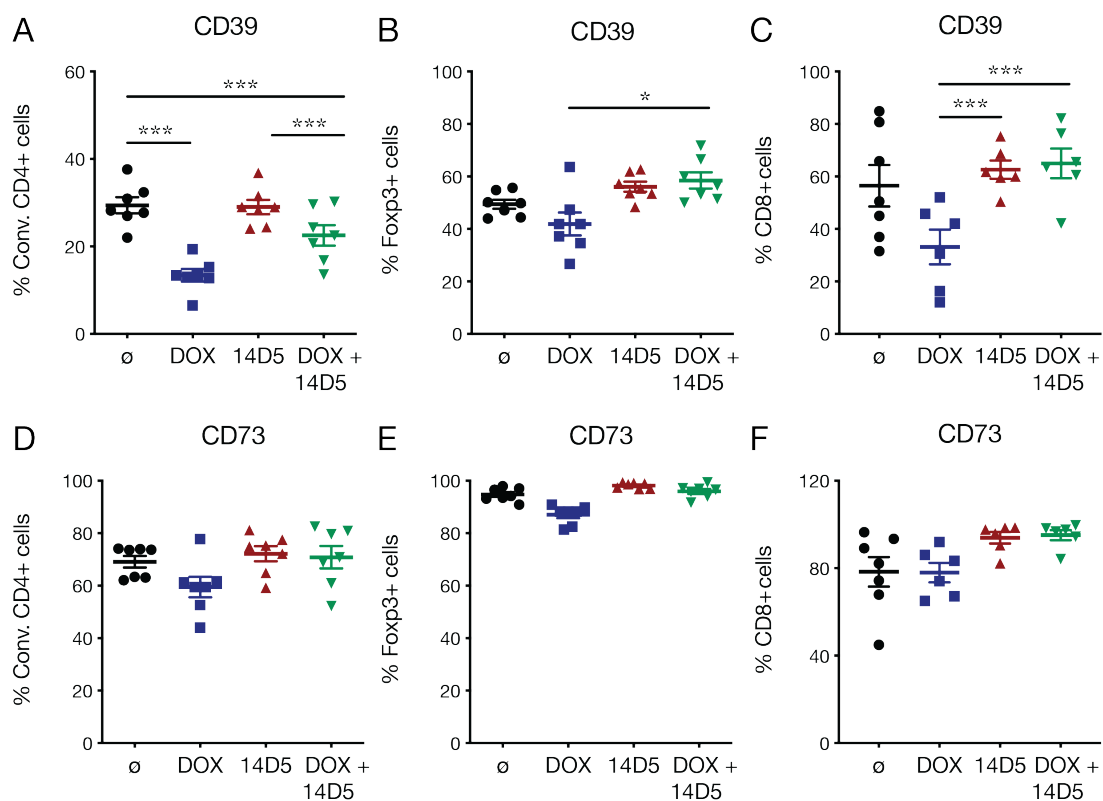


Figure 28. CD39 and CD73 expression on tumor infiltrating T lymphocytes:

The tumor samples shown in Figure 27 were stained for the surface markers CD39, and CD73 and analyzed by flow cytometry. **A-C** CD39 expression in different T cell populations treated with PBS (placebo), DOX, 14D5 or a combination of DOX and

14D5. **D-F**) Summary of CD73 expression on T cells (CD4⁺, Foxp3⁺ and CD8⁺). Statistics: one-way analysis of variance; posttest: Tukey. *, p<0.5, **, p<0.01, ***, p<0.001.

One of the important pathways of tumor immune suppression is the PD1 (programmed death-1)/PD-L1 (programmed death-ligand-1) signaling pathway, which can inhibit the T cell activation and facilitates the tumor immune escape (Jiang et al. 2019). In comparison to placebo, treatment with either DOX or 14D5 decreased the frequency of PD-1-expressing cells among conventional CD4⁺ cells, but had no major impact on PD-1 expression by Tregs (**Fig. 29A, B**). Treatment with 14D5 increased the expression of PD-1 on CD8⁺ cells (**Fig. 29C**).

The production and secretion of granzyme B (GRZB) is a mechanism that is used by cytotoxic T lymphocytes (CTLs) and natural killer (NK) cells to eliminate harmful target cells, including allogeneic, virally infected and tumor cells. GRZB is a protease that is directly involved in the activation of several pro-apoptotic pathways (Krepela and Krepela 2010; Lu et al. 2015). I checked the expression of GRZB in T cell subpopulations by flow cytometry. Interestingly, treatment with 14D5, either alone or in combination with DOX, significantly increased the expression of GRZB in all T cell subpopulations (**Fig. 29D-E**). By contrast, treatment with DOX alone tended to decrease GRZB in all subpopulations, but this effect only reached significance in CD8⁺ cells (**Fig.29 F**).

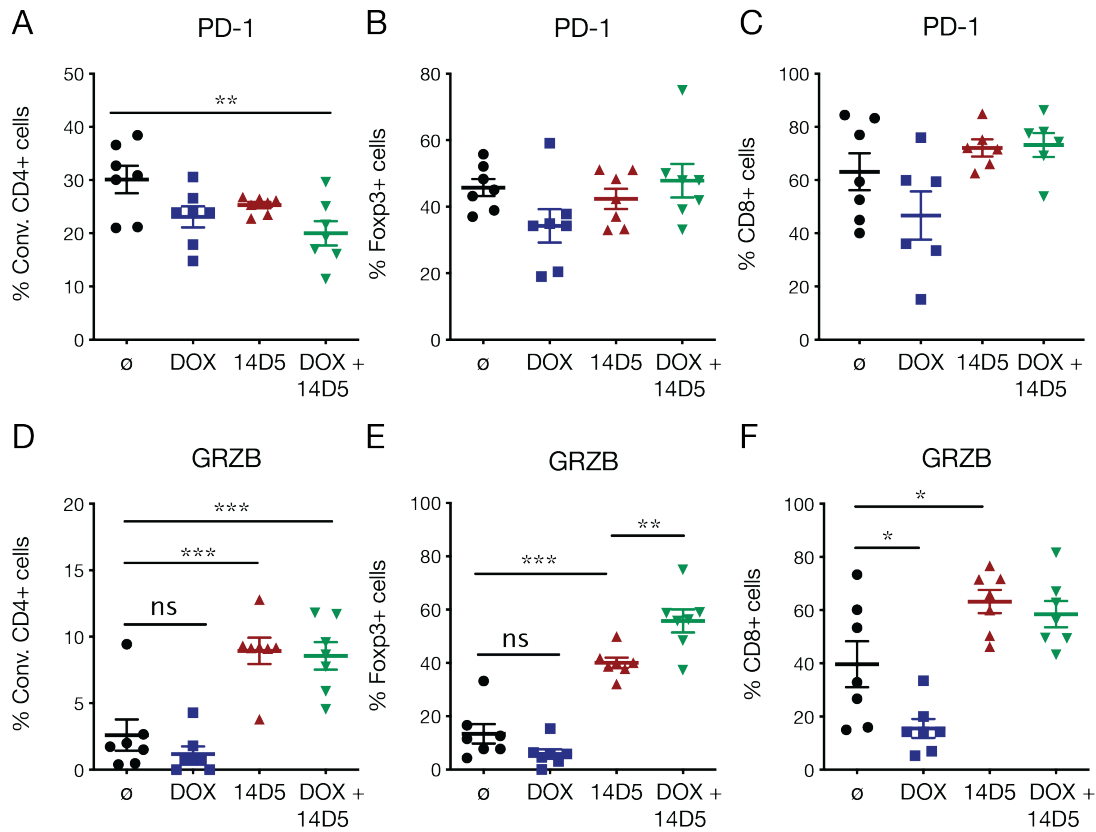


Figure 29. Expression of PD-1 and granzyme B (GRZB) on tumor infiltrating T lymphocytes: The tumor samples that are shown in Figure 27 were stained for the surface marker PD1, and then permeabilized and fixed for intracellular staining of granzyme B before analysis by flow cytometry. Summary of PD-1 expression by tumor infiltrating CD4 cells, Tregs and CD8 cells are shown in A, B and C respectively. Each data point in every group represents the percentage of PD-1⁺ cells in individual mice. D, E and F show granzyme B expression in conventional CD4⁺, Fxp3⁺ and CD8⁺ T cells respectively. Mice treated with 14D5 have significantly higher granzyme B expression compared to placebo and DOX alone. Statistics: one-way analysis of variance; posttest: Tukey. *, p<0.5, **, p<0.01, ***, p<0.001.

3.2.6. Subsets of lymphocytes in the spleen

To obtain a comparison between tumor-infiltrating T cells and T cells in the systemic circulation, lymphocytes from the spleens of the euthanized mice described in **Fig. 27** were collected and analyzed by flow cytometry. T cells (CD3⁺) were significantly increased in DOX-treated mice (**Fig. 30 B**). No treatment had a significant effect on the proportion of CD4 and CD8 T cells (**Fig. 30 C-D**). The frequency of Tregs among CD4⁺ cells was much lower in the spleen cells than in tumor-infiltrating lymphocytes (medians < 6% in spleen compared to > 40% in tumors, **Figs. 27 E** and **30 E**) (<10%). The frequency of Tregs among CD4⁺ cells was significantly reduced in 14D5+DOX treated mice compared to the other groups (**Fig. 30E**). Consistent with the hypothesis that CD69 is mainly expressed by tissue-resident memory cells, the frequencies of CD69⁺ cells in both CD4⁺ and CD8⁺ T cells were much lower in the spleen than in tumors (4-6% in spleen compared to 20-80% among tumor-infiltrating T cells; **Figs. 27 F, G** and **30 F, G**). Among spleen CD4⁺ T cells, the placebo group showed a slightly lower expression of CD69 compared to other groups (**Figure 30 F**).

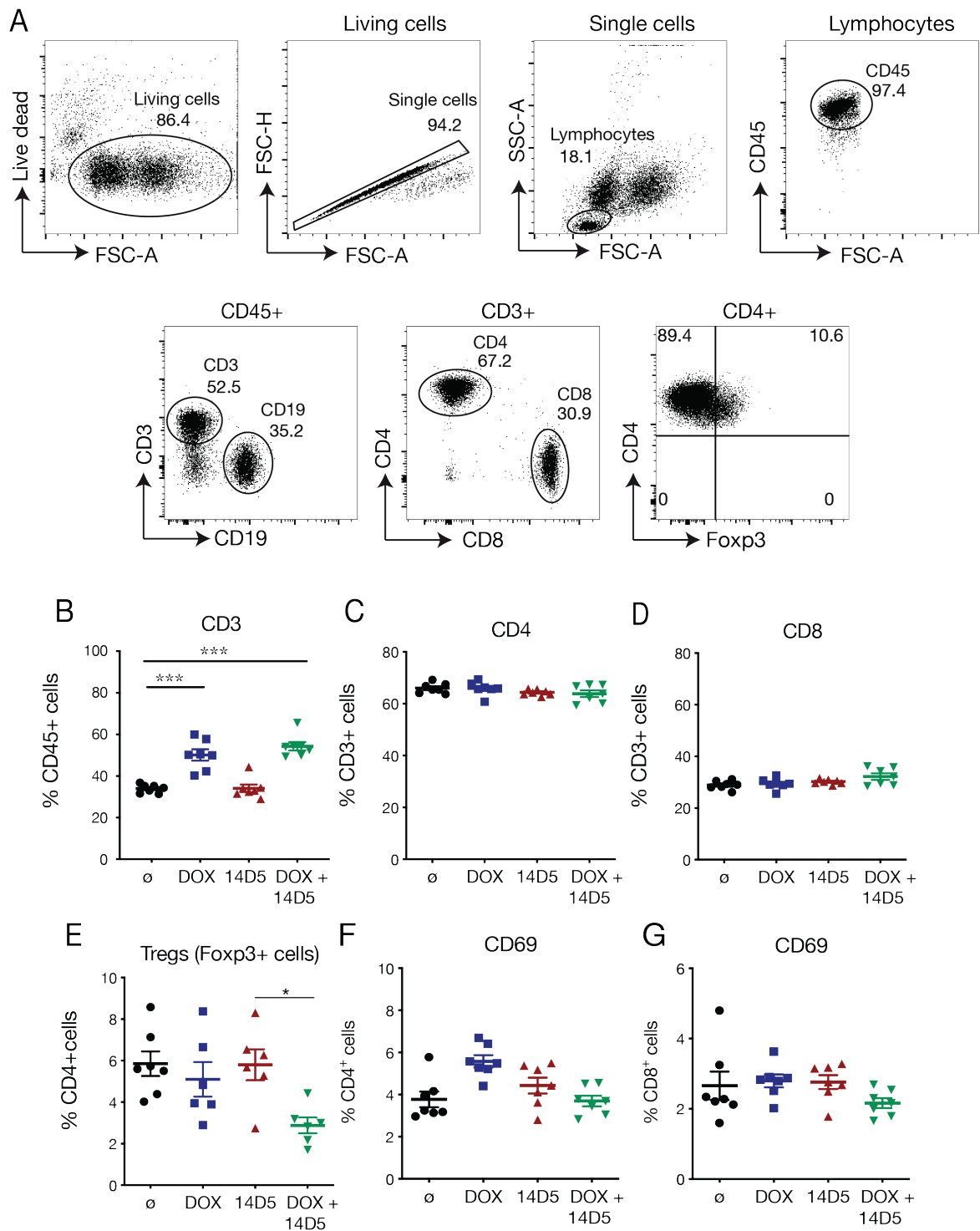


Figure 30. P2X₇ activation and chemotherapy do not affect T cell populations in spleen: After 31 days post injection, mice bearing 4T1 tumors (**Section 3.2.3**) were anesthetized and intraperitoneally injected with S+16, 30 min before euthanizing them. Single cells from spleens were stained for live dead staining and lineage markers. **A)** Representative gating strategy for B cells, T cells; CD4⁺ or CD8⁺ and regulatory T cells. **B-C)** Percentage of CD3⁺ and CD19⁺ cells in placebo and treated groups. **F)** Treg cells were gated as CD4⁺Foxp3⁺ cells. **G-H)** CD69⁺ cells were gated as CD45⁺CD3⁺CD4⁺CD69⁺ or CD45⁺CD3⁺CD8⁺CD69⁺ cells. Statistics: one-way analysis of variance; posttest: Tukey test. ***, p<0.001.

3.2.7. Phenotypic analysis of T cells in the spleen

As done for the tumor-infiltrating T cells, I also analyzed the expression profiles of splenic T cells with regard to the markers CD39, CD73, PD-1 and GRZB. CD39 expression was significantly increased in Tregs (medians around 70%) compared to CD4⁺ (medians around 10%) and CD8⁺ T cells (medians around 3%; **Fig. 31 A-C**). Conventional CD4⁺ T cells showed a decrease in CD39 expression in DOX+14D5 treated mice, while in Tregs a slight reduction in CD39 expression was observed in mice treated with DOX only (**Fig. 31 A-B**). CD73 expression was higher in Tregs and CD8⁺ T cells than in conventional CD4⁺ T cells (**Fig. 31 D-F**). No difference was observed between the different treatment groups. In CD4⁺ and CD8⁺ T cells PD1 expression was significantly lower in 14D5+DOX treated mice than in the other treatment groups (**Figure 31 G & I**). Spleen lymphocytes were also stained for granzyme B as mentioned in section 3.2.5. The T cells showed less than one percent granzyme B⁺ cells (Data not shown).

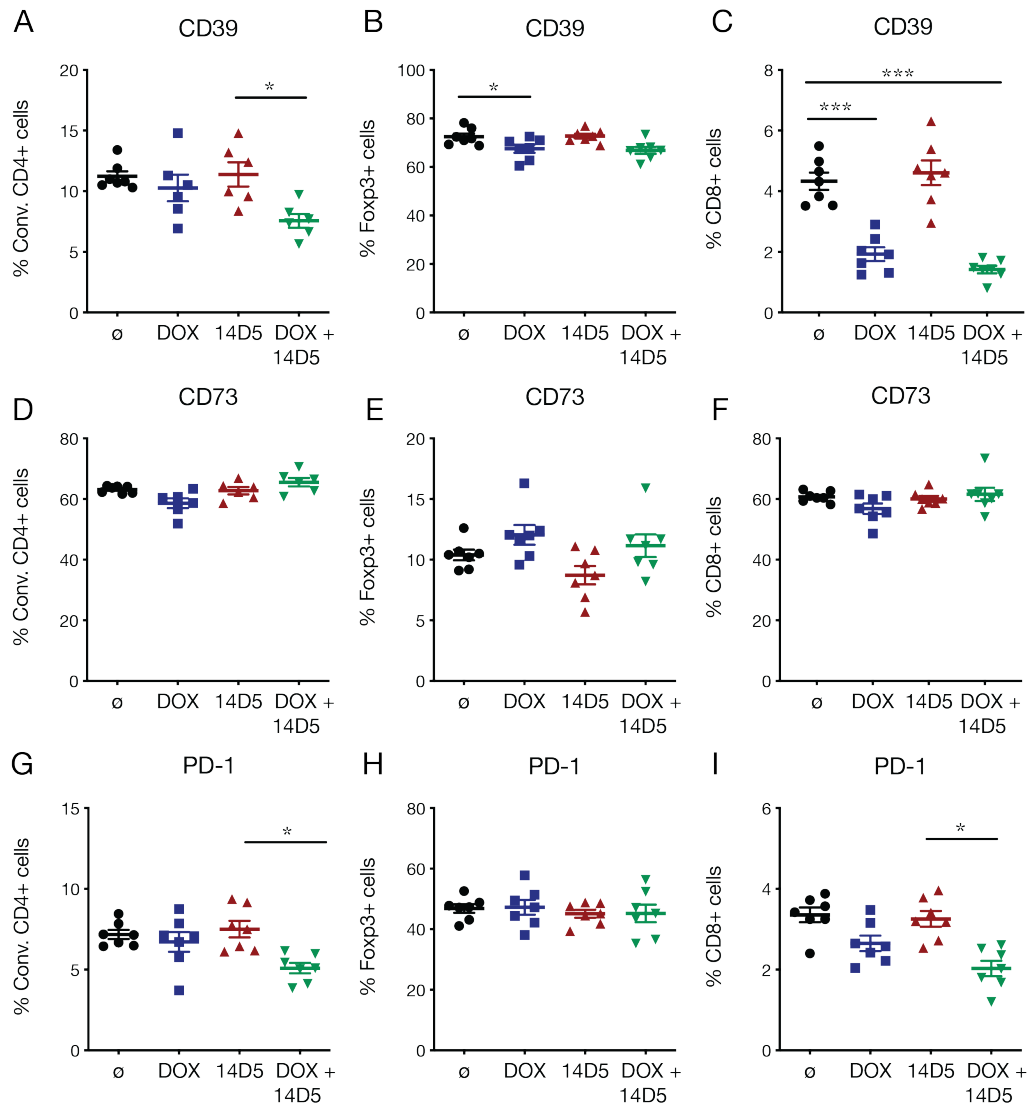


Figure 31. Phenotypic analysis of splenic T lymphocytes: Spleen samples that are shown in Figure 30, were stained for the surface markers CD39, CD73, and PD1, and analyzed by flow cytometry. Summary of CD39 (A-C), CD73 (D-F) and PD-1(G-I) expression by splenic CD4⁺, CD4⁺Foxp3⁺ and CD8⁺ T cells. Data presented as Mean±SEM. Statistics: one-way analysis of variance; posttest: Tukey test. *, p<0.5, **, p<0.01, ***, p<0.001.

3.2.8. Increased co-expression of CD39 and CD73 on tumor infiltrating Lymphocytes (TIL)

I also checked if the co-expression of CD73 and CD39 was changed among the different cell populations (i.e., CD4⁺, CD8⁺ and Tregs) in the spleen and primary tumors. In the spleen, treatment with DOX showed a tendency to decrease co-expression of CD73 and CD39, especially in combination with 14D5. This effect reached significance in Tregs from mice treated with DOX only, and in CD8⁺ T cells from mice treated with DOX+14D5 (Fig. 32D & G). In primary tumors, the co-

expression of CD39 and CD73 increased significantly in conventional CD4⁺ and CD8⁺ T cells compared to spleen (**Fig. 32 C, F and I**). Tregs did not show any difference in tumor or spleen samples. DOX-treated mice showed a decreased co-expression among all lymphocyte populations (**Fig. 32 B, E and H**).

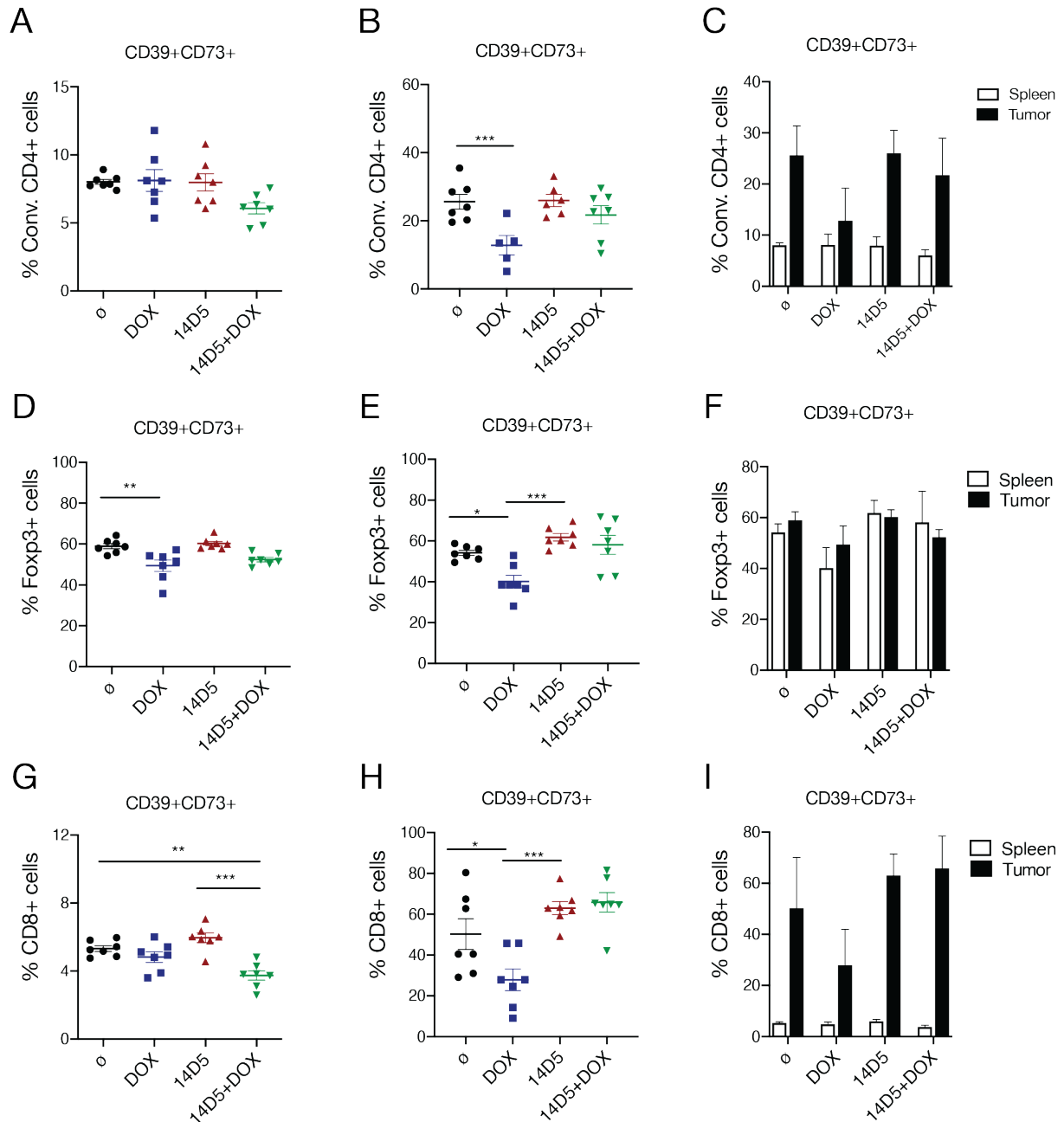


Figure 32: Co-expression of CD73 and CD39 on spleen and tumor cells: The samples shown in Fig. 28 and 31 were analyzed for co-expression of CD39 and CD73. **A, D and G)** Co-expression of CD73 and CD39 in spleen lymphocytes (conventional CD4⁺, Foxp3⁺ and CD8⁺ T cells). **B, E and H)** co expression of CD39 and CD73 in tumor infiltrating T cells. **C, F and I)** Comparison of CD39 and CD73 co-expression in tumor and spleen cells. Statistics: one-way analysis of variance; posttest for multiple comparisons: Tukey. *, p<0.5, **, p<0.01, ***, p<0.001.

4 Discussion

The present study examines the pharmacological role of purinergic receptor P2X₇ on tumor cells in the presence of chemotherapeutic agents that induce immunogenic cell death e.g., doxorubicin (DOX) and bortezomib (BTZ). In the first part I showed that P2X₇ activation synergistically enhanced the cytotoxicity of these drugs, *in-vitro*. This study also provides the evidence that P2X₇ is involved in unfolded protein response which contributes in immunogenic cell death. In the second part, the *in-vivo* results showed that the expression of P2X₇ (k) on tumor cells slows down the tumor growth. In the following section the results will be discussed in detail, considering the P2X₇ ion channel as a possible therapeutic target for combination cancer therapy and immunogenic cell death.

4.1. Synergistic cytotoxic effects

Continuous basal level stimulation of the P2X₇ receptor by ATP released from cells within the tumor microenvironment acts as a stimulus promoting the growth and survival of tumor cells under steady-state conditions (Di Virgilio et al. 2009a; Adinolfi et al. 2012, 2015). I examined the effect of low-level P2X₇ stimulation on the survival of tumor cells under the conditions of chemotherapeutic treatment. To this end I studied the effect of eATP on cell death induced by the cytostatic drug DOX in the P2X₇-expressing T lymphoma cell line Yac-1. I show that in the presence of DOX, low-level gating of P2X₇ does not protect tumor cells from death, but rather increases uptake of the drug and synergistically enhances its cytotoxic effects.

The mouse T lymphoma cell line Yac-1 is a good model to study the interaction between P2X₇ and DOX, since these cells endogenously express both, the P2X₇ receptor and ARTC2, and permit gating of P2X₇ by ATP and NAD⁺ with high sensitivity. Yac-1 cells are sensitive to the cytotoxic effects of ATP and DOX with EC₅₀s in the range of 300 μM and 200 nM, respectively (**Fig. 10 A-B; Fig. 8 A-B**). The cytotoxic effect of ATP is dependent on P2X₇, since it was effectively blocked by pre-incubation with a P2X₇-specific nanobody (**Fig. 8B**). Nanobodies are single-domain antibody fragments derived from camels or llamas that combine the selectivity of antibodies with a propensity to bind in molecular clefts, thereby often inhibiting the function of their target antigens (Wesolowski et al. 2009).

Co-incubation with ATP enhanced DOX-mediated cell death in Yac-1 cells in a supra-additive manner (**Fig. 9 A-C**). At concentrations of DOX and ATP that had little toxicity when administered alone, the combined application of both mediators killed nearly all cells in an overnight assay. The sensitizing effect of ATP was dependent on P2X₇, since it did not occur in cells pre-treated with the P2X₇-inhibitory nanobody 13A7. Blocking P2X₇ in the absence of exogenously added ATP had no effect on DOX-mediated toxicity (**Fig. 10 A-C**), indicating that, at least in this *in vitro* setting, the amount of ATP set free during DOX-mediated cell death was not sufficient to gate the P2X₇ receptor.

ATP and DOX induce cell death with different kinetics. ATP-induced cell death is rapid and can readily be observed within an hour, while DOX-mediated death requires many hours, e.g. an overnight incubation. Co-incubation of cells with ATP and DOX enhanced late death but had no effect on early death. Concentrations of ATP as low as 100µM sensitized Yac-1 cells to a non-toxic concentration of DOX (30nM) after overnight incubation (**Fig. 12 B**), while high concentrations of DOX (1µM) did not increase early death mediated by ATP (**Fig. 12 A**). These observations imply that the cytotoxic synergism of the two substances reflects an enhancement of DOX-mediated death by ATP.

Surprisingly, exposure to the combination of ATP and DOX for periods as short as one hour was sufficient to induce cell death (**Fig. 13 A, B**), although death did not become manifest until after overnight incubation. This might be explained by an effect of P2X₇ gating on DOX uptake. Gating of P2X₇ induces membrane pores that permit the passage of molecules up to a molecular mass of approximately 900 Da (Steinberg *et al.* 1987). These are large enough to accommodate DOX, which has a molecular mass of 580 Da. Indeed, I found that gating of P2X₇ substantially increased the initial uptake of DOX during the first four hours of co-incubation by a factor of eight (**Fig. 11 A**). However, this increased initial uptake was not reflected in the DOX content in the cells at the end of the overnight assay (**Fig. 11 B**), indicating that the cells had either externalized or metabolized DOX during the course of the assay.

Sensitization to DOX by extracellular ATP was also observed after transfection of P2X₇ into several other tumor cell lines that do not express P2X₇ endogenously. In these

experiments I observed that enhanced sensitivity to DOX was linked to a specific splice variant (k) of P2X₇ (**Fig. 14 D and 15G**).

The primary mode of action of ionotropic P2X receptors is as ATP-gated cation channels that permit equilibration of cation gradients across the cell membrane, in particular the influx of sodium and calcium and the efflux of potassium. In macrophages/monocytes, some effects of P2X₇ gating such as the induction of cell death or inflammasome assembly have been linked to P2X₇-mediated influx of calcium and/or efflux of potassium (Hanley *et al.* 2012; Muñoz-Planillo *et al.* 2013). I found none of these ion movements to be relevant for the synergistic action of P2X₇ on DOX-induced cell death (data not shown). This fits well to the observation that calcium influx is not necessary for P2X₇-mediated pore formation (Locovei *et al.* 2007), making it plausible that facilitation of DOX uptake is part of the mechanism underlying the sensitizing effect of ATP. However, in addition to its ion channel function, P2X₇ possesses a long C-terminal cytoplasmic tail that contains several signaling motifs that may interact with other signaling pathways (Denlinger *et al.* 2001). Conceivably, the synergistic effect of P2X₇ on DOX-induced death may also involve downstream signaling events triggered by its cytoplasmic tail.

4.2. Possible mechanisms of synergistic cell death

4.2.1. Increased Drug uptake

P2X₇ activation results in cell membrane pore formation which allows the influx of molecules up to 900 Dalton. The size of doxorubicin is about 543 Dalton. Therefore, the P2X₇-mediated pores formation could allow the increase influx of drugs that might be involved in synergistic cell death.

4.2.2. ER stress and immunogenic cell death

The cytotoxic mode of action of DOX has been linked to two mechanisms: inhibition of topoisomerase II with its consequences for DNA repair, and the induction of reactive oxygen species (Gewirtz 1999; Thorn *et al.* 2011). Especially, DOX induces a mode of apoptosis that has been termed immunogenic cell death (ICD). In contrast to classical apoptosis, which induces a tolerogenic phenotype in the immune cells that phagocytose the dead cell, ICD is accompanied by the exposition of various danger-associated molecular patterns (DAMPs) that stimulate a pro-inflammatory phenotype

in antigen-presenting cells, thereby enhancing the anti-tumor immune response (Kroemer et al. 2013). A phenotypic hallmark of ICD is the exposition of the ER resident chaperone protein calreticulin on the cell surface. In a 6 h assay, combination therapy (DOX+ATP), increased the cell surface exposure of calreticulin, suggesting that gating of P2X₇ can enhance the ICD phenotype elicited by other agents (**Fig. 16B**). In line with a supporting role for P2X₇ in the induction of ICD, I observed that gating of P2X₇ also increased cell death elicited by another known inducer of ICD, Bortezomib (**Fig. 17A-B**).

An important trigger of the ICD pathway is the induction of ER stress with consequent activation of the unfolded protein response (UPR) (Kroemer et al. 2013). Physiologically, the UPR has an ambivalent role. In the case of mild ER stress, it promotes cellular survival and protects cells from the harmful effects of an overload of misfolded proteins by inducing chaperone activity. Excessive or prolonged ER stress promotes cellular apoptosis and protects the organism by eliminating potentially harmful cells that cannot control their protein synthesis (Lin et al. 2008). In Yac-1 cells, I observed that the gating of P2X₇ alone results in the phosphorylation of eIF2 α and the translocation of CRT to the cell surface. Both of these effects were blocked by inhibition of PERK (**Fig. 19, 20 & 21**), suggesting that gating of P2X₇ is a trigger for the activation of PERK. Inhibition of PERK also reduced the synergistic cell death caused by combination therapy (ATP+DOX), suggesting that P2X₇ gating modulated the role of the UPR from cyto-protection towards apoptosis (**Fig. 22**).

Some tumors are non-responsive to chemotherapeutic drugs because they are resistant to ER stress-induced cell death. Cells resistant to ER stress are cross resistant to multiple chemotherapeutic drugs. In a study by Salaroglio and colleagues ER stress resistant cells showed a higher expression of PERK, and silencing of PERK reduced the tumor growth (Salaroglio et al. 2017). This is consistent with the results shown in **Fig. 22**, where inhibition of PERK increased the cytotoxic effect of DOX when this was administered alone. However, inhibition of PERK reduced synergistic cell death in response to the combination therapy of sub-threshold doses of ATP and DOX (**Fig. 22**), lending further support to the notion that P2X₇ gating can modulate the role of PERK from a cytoprotective to a pro-apoptotic one. It is conceivable that this may

occur through the CHOP/Caspase 3 axis, which is inhibited by PERK blockade. Further experiments will be necessary to clarify this point.

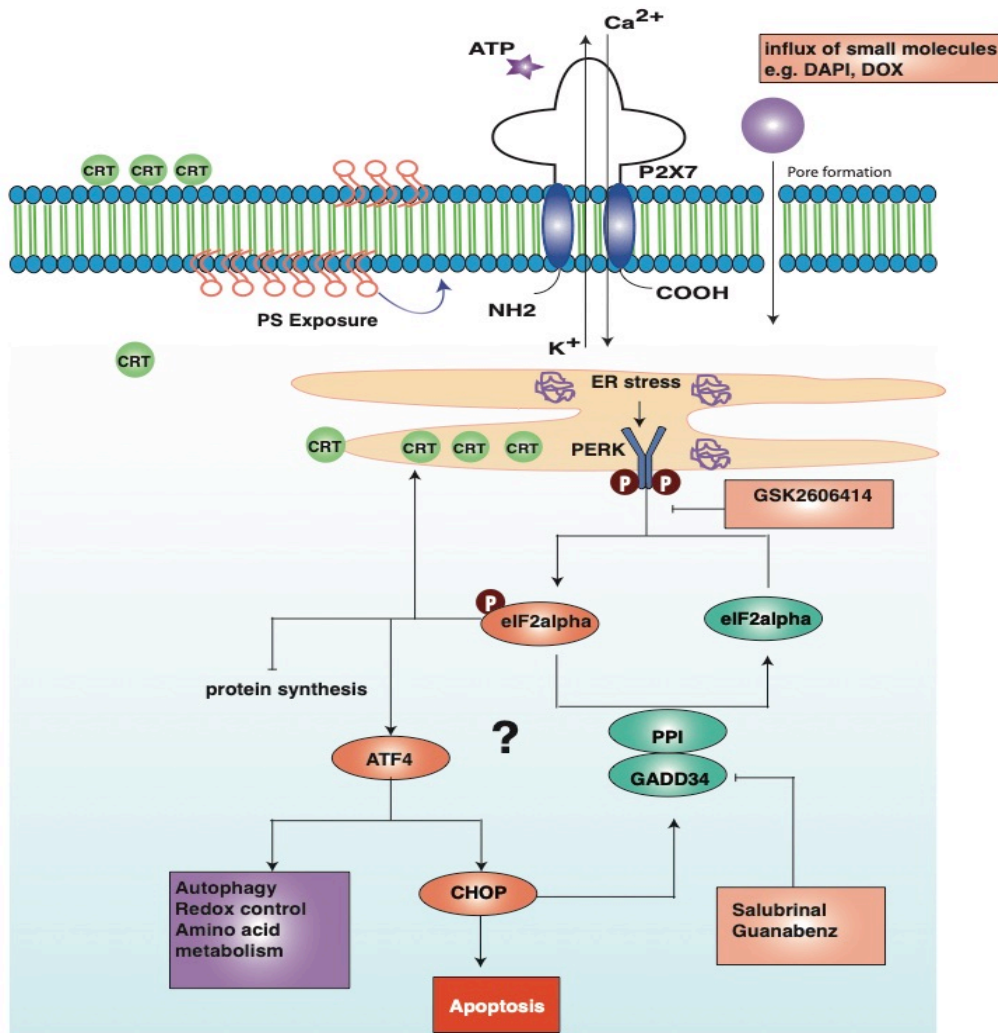


Figure 33. ER stress and link to immunogenic cell death: P2X7 activation results in cell membrane pores formation, that allow an increased influx of drugs (i.e., DOX and BTZ). ATP mediated P2X7 stimulation and increase accumulation of drug in the cytosol might be involved in increased ER stress and accumulation of misfolded proteins which lead to phosphorylation of PERK. Activation of PERK causes the phosphorylation of eIF2 α (eukaryotic initiation factor alpha). p-eIF2 α not only inhibits the synthesis of new proteins (except ATF4) but also promotes the calreticulin translocation to cell surface which is a major hallmark of immunogenic cells death. ATF4 expression is involved in upregulation of genes that regulate ER homeostasis as well as the genes that are involved in apoptosis i.e., CHOP. The unresolved stress leads apoptosis and autophagy. Adapted from (Hetz and Saxena 2017).

4.3. P2X7 expression on tumor cells

The role of P2X7 in the tumor microenvironment is ambiguous, depending on the intensity of signaling and on the cell-type by which it is expressed. Expression of P2X7 on tumor cells is probably mostly beneficial for the tumor. Low-level, basal P2X7 signaling raises the calcium concentrations in the cytosol and mitochondria and promotes aerobic glycolysis (Adinolfi *et al.* 2012a). These effects combine to increase ATP synthesis and provide a metabolic advantage for tumor cells. Only when the signaling intensity surpasses a certain threshold does calcium influx lead to mitochondrial calcium overload, causing opening of the mitochondrial permeability transition pore and cell death (Di Virgilio *et al.* 2009).

However, apart from tumor cells, P2X7 is also expressed on host immune cells such as dendritic cells. ATP released by tumor cells dying by ICD is a molecular danger pattern that enhances the anti-tumor response by gating P2X7 on host antigen-presenting cells (Kroemer *et al.* 2013) and enhancing T cell activation (Junger 2011). Thus, current evidence suggests that P2X7 expressed on tumor cells benefits tumor growth, while P2X7 expressed on host immune cells benefits the anti-tumor response.

However, I observed that the P2X7 antagonist 13A7 promoted the tumor growth and metastatic spread in SCID mice that cannot mount an adaptive anti-tumor immune response (**Fig. 23**). Although it cannot be excluded that this effect might be due to inhibition of P2X7 on innate immune cells, it seems likely that it might be the result of blocking the pro-apoptotic effect of P2X7 as discussed above.

In immune competent BALB/c mice, I further analyzed the tumor growth of 4T1 breast cancer cells that either expressed a functional version of P2X7 or a dead mutant. The tumors bearing P2X7 dead mutant showed significantly higher tumor growth compared to tumors expressing functional P2X7 (**Fig.24A**) In these experiments, I could link expression of P2X7 by tumors to an increase in T cell infiltration (CD3+ cells) and apoptosis (caspase 3) (**Fig.24 B**).

Presence of chemotherapy (DOX) significantly reduced the tumor growth in mice injected with 4T1 cells bearing non-functional P2X7 but remained ineffective in mice injected with 4T1 cells bearing functional P2X7 (**Fig. 25 A and B**). Doxorubicin mainly kills the dividing cells (Gewirtz 1999), therefore, increased apoptosis and less

proliferating cells in P2X₇ expressing tumors might be responsible for the DOX ineffectiveness.

In the next set of experiments, I studied the immune response and phenotypic changes in the immune cells in 4T1 tumors expressing functional P2X₇ (k). It has been previously shown that the treatment of cells with 14D5 nanobody (half-life extended (HLE)) significantly decreased the amount of ATP required for P2X₇ receptor activation (Danquah et al. 2016). Therefore, tumor-bearing mice were treated with P2X₇ enhancing nanobody 14D5 in the presence and absence of DOX to evaluate the effects of P2X₇ activation. P2X₇ receptor modulation with 14D5 further reduced the tumor growth in 4T1 breast cancer cells injected mice. This supports our previous results showing that P2X₇ activation is beneficial for growth inhibition (**Fig. 26 A**), while presence of DOX alone or in combination with 14D5 did not affect the tumor growth.

My results showed significantly higher T cell infiltration and apoptosis in P2X₇ expressing tumors compared to non-functional P2X₇ expressing tumors (**Fig. 24**). The presence of 14D5, DOX or the combination of 14D5 and DOX did not affect the infiltrating T cells in P2X₇ expressing tumors (**Fig 27 B**).

CD69 is a marker of early activation of lymphocytes and it is also expressed by tissue resident memory cells. Expression of CD69 was increased on tumor infiltrating T cells compared to peripheral T cells, in line with the notion that the former represents the activated tissue resident T cells. I also observed that DOX treated mice exhibited an increased expression of CD69 on primary tumor infiltrating lymphocytes as well as in spleen T cells compared to placebo treated mice (**Fig. 27 F and 30 F**).

Cytotoxic immune cells (CD8 T cells and NK cells) use different mechanisms to induce cell death in the tumor cells i.e., release of proapoptotic cytokines (TNF α and IFN- γ), perforin and granzymes (A and B). The activated cytotoxic T cells recognize the target cells that need to be eliminated from the system. For this, an immune synapse is formed between the T cell and the target cell, and the T cell secretes granules containing granzyme B into the synaptic space, where perforin facilitates the fusion of granzyme B with the target cell and induces the cell death (Stinchcombe and Griffiths 2007; Cai et al. 2009). To check the anti-tumor activity of T cells, I stained the tumor infiltrating and peripheral T cells for granzyme B expression. I observed an increase in granzyme B expression on conventional CD4⁺ and CD8⁺ T cells was

observed in 14D5 treated mice, possibly explaining the slow tumor growth in these mice (**Fig. 29 D and F**).

Local immunosuppression in the tumor microenvironment is a feature of many cancers. Immunosuppressive pathways in tumors significantly impact the efficacy of immunotherapy. Foxp3⁺ regulatory T cells-mediated immunosuppression is a dominant pathway by which growing tumors escape immunotherapy (Tanchot et al. 2013). In healthy peripheral organs 10% of total CD4⁺ cells are Tregs this proportion was increased in the tumor microenvironment up to 50% (Quezada et al. 2006). In my results, 30 to 50% CD4⁺ cells in primary tumors were tregs (Foxp3⁺) while CD8⁺ cells did not show any Foxp3 expression. DOX or 14D5 treatment alone did not affect the total percentage of Tregs in either spleen or tumor T cells (Figs. 27F and 30F). In the spleen the frequencies of Foxp3⁺ cells were much lower than in tumors (2 - 10% vs 20 - 50% of CD4⁺ cells). In the spleen, the combination therapy (DOX+14D5) significantly reduced the percentage of Tregs compared to 14D5 or DOX alone.

The B cells infiltration was increased in the DOX only treated mice. B cells do not only inhibit tumor growth by releasing immunoglobulin but Bregs (B regulatory cells) that secrete immunosuppressive cytokines can also regulate T cells to suppress immune responses (Sarvaria et al. 2017). In our experiments, the presence of high infiltrating B cells in DOX treated mice might contribute to the ineffectiveness of chemotherapy.

Tumor microenvironment plays an important role in deciding the fate of tumor growth or anti-tumor immune response. It has been well established that ATP concentration in solid tumor microenvironments are increased up to 500 μ M / liter, which is high enough to induce P2X7 receptor activation and proinflammatory response (Pellegatti et al. 2008). At the same time, ATP is quickly degraded to prevent the overstimulation of target molecules. ATP is degraded into AMP by ectonucleoside triphosphate diphosphohydrolase-1 (ENTPD-1, CD39), and AMP is efficiently dephosphorylated by CD73 to generate adenosine (Vijayan et al. 2017). The CD39 is highly expressed by regulatory T cells but not by conventional CD4 and CD8 cells in steady state conditions. In tumor microenvironment, the levels of CD39 and CD73 are upregulated by hypoxia inducible factor 1 alpha (HIF1 alpha) and transcription factor SPI. Therefore, ATP degradation and accumulation of adenosine, could lead to immune suppression (Synnestvedt et al. 2002). Apart from the immune suppression ability of CD39, it is also involved in T cell activation. It has been published that CD39⁺ and

CD103+ tumor-infiltrating CD8 T cells are tumor reactive cells in primary and metastatic tumors. These tumor reactive CD8 cells may help to improve cancer therapy (Duhon et al. 2018). Increased co-expression of CD39 and CD73 improves prognosis in cancer patients. I observed that 14D5 treated mice have higher co-expression of CD39 and CD73.

Given the high concentrations of extracellular ATP in tumor tissues (Pellegatti et al. 2008), the pharmacological modulation of purinergic signaling appears as an attractive principle for the development of novel therapeutic strategies (Di Virgilio 2012). Indeed, based on the findings that expression of P2X₇ by tumor cells promotes tumor growth, several drug companies are developing potent P2X₇ antagonists as anti-cancer therapeutics. However, our findings with Yac-1 and 4T1 cells suggest that this approach must be carefully evaluated. Our results show that even when it is expressed on tumor cells, functional P2X₇ may slow the growth of tumors by promoting tumor cell death while at the same time enhancing the anti-tumor immune response of the host. In addition, blocking P2X₇ in the context of chemotherapy may blunt a potentially synergistic interaction between P2X₇ and the chemotherapeutic drug.

5 Materials and Methods

5.1. Materials

Table 1 :General Equipment

Equipment	Model/Type	Company
Analytical scale	Analytical Plus	Ohaus
Autoclave	Model 2540 EL	Tuttnauer Europe
Centrifuge	Rotanata 460 R	Hettich
Cell imaging system	Evos ®FL	Thermo Fischer Scientific
CO ₂ incubator	MCO-20AIC	Sanyo
Confocal Microscope	Leica TCS Sp5	Leica Microsystem
ELISA plate reader	Victor 3 1420	Perkin-Elmer
Flow cytometer	FACS Canto	BD Bioscience
Flow cytometer	FACS Celesta	BD Bioscience
Heat Block	Thermomixer Compact	Eppendorf
Horizontal electrophoresis system for agarose gel	40-0708	Peqlab Biotechnology
Laminar Flow hood	Gelaire Typ BST6	Gelman
Liquid Nitrogen Tank	K series	Taylor Wharton
Multichannel pipette 10µl-300µl	Research Type	Eppendorf
Micropipettes	Research type	Eppendorf
Microwave	M 637 EC	Miele
Microscope	Zeiss AxioScope A1	Carl Zeiss Microscopy
Neubauer cell chamber		LaborOptic
Optical imaging system	IVIS-200	Caliper Life Sciences
pH meter	Toledo MP220	mettler
Photometer	Nanodrop 2000c	Peqlab biotechnology
Pipette controller	Pipetboy	Integra
Power supply for agarose gel electrophoresis		Biometra
Roller	Mixer SRT 6	Staurt
Scanner	CanonScan 9800F	Canon
Shaker incubators	HT INFORS	Unitron
Sterile work bench	Hera safe	Thermo Fischer science
Table centrifuge	Heraeus Pico17	Thermo Fischer scientific
Table centrifuge	5417R	Eppendorf
Thermal cycler	T3/T gradient	Biometra
UV-transilluminator	Type TI 1	Biometra
Vortex mixer		Stuart
Water bath	23621	GFL

Table 2: Consumables

Consumables	Type	Manufacturer
Cell culture well plate	Various sizes	Thermo Fischer Scientific
Cell culture flask	T-25, T-75, T-225	Greiner bio one / Nunc™
Cell culture petri dish	Various sizes	Greiner bio one
Cell sieves	70µM, 30 µM	Falcon
Cell culture tubes	12 ml	Greiner bio one
Cover slips	12mm	Glaswaren fabrick karl Hecht
FACS tubes	5 ml	BD Bioscience
Falcone tubes	15 ml, 50 ml	Greiner
Gloves	Nitratex	
Microcentrifuge tubes	Various sizes	Eppendorf
Nunc 96 well plate		Thermo Fischer Scientific
Nunc 96 well plate		Thermo Fischer Scientific
Pipette tips	Various sizes	Eppendorf
Microscope Slides	76×26 mm	ROTH
Scissors, forceps, scalpels	Various sizes	FST Fine science tool
Serological pipettes	Various sizes	BD Falcon
Sterile filtration	Steriflip, stericup	Millipore
Syringes and needles	Various sizes	Braun / BD science

Table 3: Chemicals used

Chemicals	Manufacturer
4',6-Diamino-2Phenylidole, Dihydrochloride (DAPI)	Thermo Fischer Science
Adenosine triphosphate (ATP)	Sigma Aldrich/Merck
Aqua ad injectabilia	Braun
β mercaptoethanol	Gibco™
Bovine serum albumin (BSA)	Sigma-Aldrich/Merck
Bortezomib	EMD Millipore
Carbenicillin	Sigma-Aldrich /Merck
Collagenase D	Roche
Dimethyl sulfoxide (DMSO)	Sigma-Aldrich /Merck
DMEM medium	Gibco™ / Thermo Fischer Scientific
DNA Gel loading Dye, 6x	New England Biolabs
DNA typing grade Agarose	Gibco™ / Thermo Fischer Science
DNase 1 (D) 600 U/mg	Roche
Doxorubicin (DOX)	Teva®
Ethanol (70%) for disinfection	Roth

Chemicals	Manufacturer
Ethylenediaminetetraacetic acid (EDTA)	Sigma-Aldrich / Merck
GSK2606414 (PERK inhibitor)	EMD Millipore
p- Nitrophenyl phosphate (phosphatase substrate), 5 mg tablets	Sigma Aldrich
Fetal Calf serum (FCS)	Gibco™ / Thermo Fischer Scientific
HEPES 1 M	Gibco™ / Thermo Fischer Scientific
LB agar	BD Difco
LB broth	BD Difco
L-Glutamin, 200 mM	Gibco™ / Thermo Fischer Scientific
MEM, non-essential amino acid, 10 mM	Gibco™ / Thermo Fischer Scientific
Paraformaldehyde (PFA)	Sigma Aldrich / Merck
Penicillin (100U/ml) Streptomycin (10000 µg/ ml)	Gibco™ / Thermo Fischer Scientific
Phalloidin	Invitrogen
Phosphate buffer Saline (PBS) (1x, 10x)	Gibco™ / Thermo Fischer Scientific
Poly-L lysin solution 0.01%	Sigma Aldrich
RMPI 1640 with phenol red	Gibco™ / Thermo Fischer Scientific
SOC-medium	Sigma Aldrich / Merck
Sodium chloride 0.9%	Braun
Sodium pyruvate, 100mM	Gibco™ / Thermo Fischer Scientific
TAE-buffer Ultra-pure DNA typing grade, 50 x	Thermo Fischer Science
Trypsin, 10 x	Invitrogen/ Thermo Fischer Science

Table 4:Cell culture media

Bacterial culture media	Composition
LB-agar	10 g/l tryptone 5 g/l yeast extract 10 g/l NaCl 15 g/l agar-agar (pH 7)
LB-medium	10 g/l Tryptone 5 g/l yeast extract 10 g/l NaCl (pH 7)
SOC medium	8.6 mM NaCl 2.5 mM KCl 20 mM MgSO ₄ 20 mM Glucose 2 % Tryptone 0.5 % yeast extract

Eukaryotic cell culture media	Composition
Complete RPMI	RPMI medium 2 mM L-Glutamine 1mM Sodium pyruvate 5% FCS
Complete DMEM	1x NEM (non-essential amino acids) 5% FCS 1mM sodium pyruvate 2 mM L-Glutamine 10 mM HEPES

Table 5: Buffers

Buffers	Composition
ACK erythrocyte lysis buffer	155 mM NH ₄ Cl 10mM KHCO ₃ 0.1 mM EDTA pH 7.2 in deionized H ₂ O
Digestion solution (tumor)	RPMI 0.2mg/mg collagenase D 10 U/ml DNase 1
Cell Transfection	300 mM NaCl in deionized H ₂ O 7.5 mM linear PEI (polyethyleneimine, 25 kDa) in deionized H ₂ O
Annexin V buffer (10x)	25mM CaCl ₂ 1.4 M NaCl in 100 mM HEPES (pH 7.4) diluted in de-ionized H ₂ O to get 1x solution before use
FACS Buffer	0.02% BSA 1mM EDTA in PBS-/-
Fixation buffer	2% and 4% PFA in PBS-/-
Blocking buffer	0.1% Triton X-100 1 % BSA

Buffers	Composition
Acid phosphatase buffer	5 mM p-nitrophenyl phosphate 0.1 % Triton X-100 In 0.1 M sodium acetate (pH 5)

Table 6: Standards for gel electrophoresis

DNA Standards	Manufacturer
GeneRule, 1kB, SmartLadder	Thermo Fischer Science Thermo Fischer Science

Table 7: Primers used for polymerase chain reactions

Primer name	Sequence	Description
f.p2x7_infusion_pCSE	TCCTGCAGGCCTCGAGAT CCACTAGTCCAGTGTG	Forward primer for infusion cloning of P2X7 receptor in pMXs vector
r.p2x7_infusion_pCSE	CGCGCCGGCCCTCGATA GAAGGCACAGTCGAGG	Reverse primer for infusion cloning of P2X7 receptor in PMXs vector
S1811	GACGGCATCGCAGCTTGG ATACAC	Forward Primer for sequencing of PMXs vector
IRES-5'-R	ATTCCAAGCGGCTTCGGC	Reverse Primer for sequencing of PMXs vector
f. P2X7-sequence: P and L morphism	GGAAAATTTGACATCATCC AGC	Sequence primer to check the P and L polymorphism in P2X7 receptor cloned in PMXs vector
f. P2X7a_PCR	CACATGATCGTCTTTTCCT AC	Forward primer for amplification of P2X7 (a)
f. P2X7k_PCR	GCCCGTGAGCCACTTATG C	Forward primer for amplification of P2X7 (k)
r. P2X7ak_PCR	CCTTGTCTTGTCATATGGA AC	Reverse primer for P2X7 (a) and (k) amplification

Table 8: Polymerase enzymes for PCR

Polymerases	Manufacturer
KOD Hot Start	Novagen
Pfu Turbo	Agilent Technologies

Table 9: Restriction enzymes used for cloning

Restriction enzymes	Manufacturer
Xho 1	New England Biolabs
Not1 HF	New England Biolabs

Table 10: Vectors

Plasmids	Specification
pMXs	pMXs retroviral vector is based on Moloney murine leukemia virus (MMLV). The vector provides the viral package signal, transcription and processing elements, and MCS for cloning of a target gene
LeGo-iG2	HIV derived third generation lentivector for the expression of cDNA. An integral ribosome entry site (IRES) is used to express the marker gene.

Table 11: kits

Kit	Manufacture
FLICA caspase 3 kit	Immuno chemistry technologies
Foxp3/transcription Factor staining buffer set	e Bioscience San Diego USA
High-capacity cDNA Reverse Transcription kits	Applied Biosystem
Infusion Cloning kit	Takara Bio USA, Inc.
Nucleo Spin ®Gel and PCR clean up	Macherey Nagel
Plasmid mini kit	Qiagen
Plasmid Maxi kit	Qiagen
RNA synthesis kit	Analytikjena

Table 12: Nanobodies

Name	Description	source
13A7	Half-life extended (HLE), Fc	Ag Koch-Nolte
14D5	Half-life extended	Ag Koch-Nolte

Table 13: Antibodies

Antibodies used for flow cytometry cell analysis

Antigen	Conjugate	Clone	Manufacturer
CD3	BV785	17A2	Biolegend
CD4	BV605	RM4-5	Biolegend
CD8	BV650	53-6.7	Biolegend
CD19	FITC	1D3	eBioscience
CD45	AF700	30-F11	eBioscience
CD39	APC	24DMS1	eBioscience
CD73	BV421	eBioTY/11.8	eBioscience
Granzyme B	PE	GB12	MolProb
PD-1	PE/Cy7	RMPI-30	Biolegend
Annexin V	FITC	-	BD
Annexin V	APC	-	Biolegend
Calreticulin	-	D3E6	Cell signaling
p-eIF2 α	-	SZ01-06	NovusBio
Rabbit IgG (H+L)	PE	-	Dianova
Rabbit IgG (H+L)	APC	-	MolProb
P2X7	APC	RH23	AG Nolte
Foxp3	FITC	FJR-16S	eBioscience
CD69	PE-CY7	H1.2F3	Biolegend

Table 14: Bacterial cells

Prokaryotic cells	Manufacturer
XL-2 Blue E. coli	Stratagene

Table 15: Cell lines

Eukaryotic cell lines	Source
Yac-1	Provided by Dr. Klaus Harbers, Hamburg
4T1 wt	Provided by Prof. Sonja Loges, Hamburg
4T1 P2X ₇ a	Ag Haag
4T1 P2X ₇ a (R294A)	Ag Haag
A20 wt	Ag Haag
A20 P2X ₇ a	Ag Haag
A20 P2X ₇ k	Ag Haag
3T3	Provided by Dr. Ingke Braren, Hamburg
3T3 P2X ₇ k	Ag Haag

Table 16: mouse strain

Mouse strains	Provider
SCID	Charles River
Balb/C wt	Charles River

Table 17: Software

Software	Manufacturer
FACSDiva™ Software V.8.0.1	BD Bioscience
FlowJo V10.6.1	FlowJo, LLC, Ashland, USA
GraphPad Prism v8.3.0	Graphpad Software. Inc., La Jolla, USA
Axio Vision software	Carl Zeiss Microscopy
Living image 4.2 software	Caliper Life Sciences

5.2. Methods

5.2.1. Methods in Molecular Biology

5.2.1.1. PCR amplification of target fragment

In vitro amplification of target DNA fragment by thermal cycler was performed by Polymerase Chain Reaction (PCR) using oligonucleotide primers (specific for infusion cloning) which anneal to the denatured opposite strands of target DNA at the particular region of interest. A high-grade temperature between 90°C to 95°C is applied to denature double stranded DNA template to two single strands. The temperature is then lowered down to 50°C to 65°C so that oligonucleotides could anneal to the complementary strands of the template DNA to flank the segment to allow the amplification. Deoxyribonucleotide triphosphates (dNTPs) are incorporated to the 5' end of the single stranded flanked DNA and creates a copy following 3' direction. This step of elongation is carried out at temperatures between 69°C to 72°C. Various rounds of cycles are performed for annealing and elongation in which newly manufactured DNA fragments act as template for further amplification. The optimal performance of polymerase is attained by using buffer with MgCl₂. PCR reactions have been used for incorporation of restriction sites, tags and peptide linkers, site directed mutagenesis of plasmid DNA and amplification of DNA fragments.

The following PCR reactions have been used in this project:

Table 18: PCR reaction

Reagent	Volume (μl)	Final concentration
10x Buffer for KOD polymerase	5	1x
dNTPs (2 mM)	5	0.2 mM
MgSO ₄ (25 mM)	2	1 mM
Forward primer (10 μM)	2	400 nM
Reverse primer (10 μM)	2	400 nM
KOD DNA polymerase	1	0.02 U/μl
DNA (app. 1 ng)	x	
ddH ₂ O	up to 50 μl	

Table 19: PCR amplification

Reaction steps	Temperature (C°)	Time (s)	Cycle
First denaturation	95	120	1
Denaturation	95	30	
Annealing	50-65	15	30
Elongation	70	20-30/kb	
Final elongation	70	300	
On hold	4	∞	

5.2.1.2. Linearization of vector for cloning

2 µg of pMXs vector was linearized using Xho1 restriction enzyme (NEB) for 3 hours at 37°C for cloning and agarose gel electrophoresis was performed to check the linearized vector.

5.2.1.3. Agarose gel electrophoresis of DNA fragments

Agarose gel electrophoresis has been used to separate DNA fragments according to their size. 1% agarose matrices have been prepared using 50 and 100 ml Tris Acetate EDTA (TAE) buffer added with 2.5 and 5 µl of Roti®-Gel stain (Carl Roth GmbH + Co KG) respectively. For tracking the migration of DNA in the gel, samples were dyed using loading buffer (Thermo Fischer Scientific) for visualization of the bands. A DNA ladder as a marker has also been used for the comparison of the band sizes. The movement intensity of the DNA samples has been kept at 60 – 90 V for 40-50 minutes. The visualization and photographing of the DNA bands for documentation has been performed using a UV-transilluminator along with Video-image system (BioVision 3000). The required bands were excised using razor blade for further purification.

5.2.1.4. DNA extraction from agarose gel

The purification of the excised bands has been carried out using PCR clean-up and Gel extraction kit (Macherey Nagel) according to the manufacturer's protocol. The elution of the cleaned-up PCR products and restricted DNA fragments has been done in 15µl of sterile deionized water.

5.2.1.5. DNA enzymatic restriction

It is a fact that double stranded DNA can be cleaved at palindromic sequences using endonucleases or restriction enzymes. In order to clone the desired genes, restriction

of the target DNA fragments has been performed using appropriate restriction enzymes and their corresponding buffers following the instructions of manufacturer New England BioLabs (NEB) at optimal temperatures. The online tool “Double Digest Finder” from NEB was used to select the restriction digestion conditions and heat inactivation of enzymes after they are done with their functions. Considering the fact that 1U of endonuclease is sufficient enough to cleave 1µl of DNA, a volume of 20-23 µl of restriction reaction mixture has been used. Moreover, thermocycler was used for setting-up the restriction and heat inactivation steps of the restriction digestion reactions.

5.2.1.6. Dephosphorylation of DNA fragment

It is important to dephosphorylate the enzyme digested plasmid DNA to reduce the chance of re-ligation of vector so that the desired gene can be successfully cloned into it. The enzyme phosphatase (1 µl) along with 2.2 µl and 4.2 µl of antarctic phosphatase buffer were added into the completed restriction digestion reaction for a reaction volume of 20 µl and 40 µl respectively. An incubation of 2 h at 37°C following the enzyme inactivation at 65°C for 20 min has been carried out for dephosphorylation step.

5.2.1.7. Quantification of DNA

The estimation of the concentration of double stranded DNA was made by measuring the absorbance at 260 nm through spectrophotometer 'Nanodrop 2000c' (Thermo Fisher Scientific). A wavelength of 260 nm (A_{260}) was used for measuring absorbance because DNA presents the peak of light absorption at this point. The conversion relationship A_{260} of 1 = 50 µg/ml was used to calculate the concentration of double stranded DNA. as there are chances of the presence of the contaminants in the DNA preparation such as proteins which absorb light at 280 nm, the evaluation of the DNA purity was done by finding out the ratio between A_{260} and A_{280} . The high-quality DNA preparations were considered between the values of $A_{260}/A_{280} = 1.7 - 2.0$.

5.2.1.8. Ligation of DNA fragments

In order to generate recombinant DNA plasmids, ligation of the DNA fragment into plasmid was performed.

For restriction enzyme cloning: Ligation reactions were prepared using T4 ligase (NEB) and corresponding T4 buffers according to the instructions of the manufacturers. The formation of the ligated product is established by T4 ligase which creates a covalent bond between the complementary ends of the desired restricted DNA fragment and digested plasmid backbone. A final volume of 20 μ l with a molar ratio of 1:3 of vector backbone to insert was taken as a ligation mixture. A temperature of either 16°C for overnight or room temperature for 3 h was applied to the ligation reaction mixture and T4 ligase was inactivated at 65°C for 10 min once it had accomplished its task.

For infusion cloning: The amplified DNA fragment was ligated with linearized vector for 15 min at 50°C using infusion cloning kit (Takara Bio USA, Inc.).

The reaction mixture used for ligation is shown in Table:

Mixture contents	Concentrations
Insert	100ng
Vector	100ng
Enzyme premix	2 μ l
Deionized H ₂ O	Up to 10 μ l

5.2.1.9. Transformation of chemically competent bacteria

The plasmid DNA was transformed into chemically competent *E. coli* XL-2 Blue cells (Stratagene) by heat shock strategy. A frozen vial (at -80°C) of 100 μ l was thawed on ice and 1-10 ng of ligation product or plasmid DNA was added to the cells and placed on ice for incubation for a period of 30 min. The heat shock at 42°C was applied to the cells in water bath for 30 s followed by the incubation on ice for 2 min. An amount of 500 μ l of pre-warmed SOC medium at 37°C was poured into the transformed cells and the resulted cell suspension was kept at 450 rpm and 37°C in a heating block for a time period of 1 h. The transformed cells were spread onto LB agar plates having appropriate antibiotic under aseptic conditions and the plates were placed at 37°C for the growth of the potential transformed cells.

5.2.1.10. Cultivation of bacterial cultures for plasmid DNA preparation

The isolated single colonies of the potential clones were picked up from the plates and inoculated into 5 ml or 100 ml of LB medium containing carbenicillin depending upon the small-or large-scale plasmid preparation respectively. The incubation of the cultures was performed at 37°C overnight under shaking conditions. The very next

day, the culture samples were centrifuged at 4600 rpm for 20 min to harvest the cells while supernatant was discarded for each culture. The extraction of plasmid DNA was performed using QIAprep® Spin Miniprep or Maxiprep Kits (Qiagen) according to the manufacturer's protocol.

5.2.1.11. DNA sequencing

In order to sequence the cloned DNA samples, the services of Eurofins (Ebersberg) and SeqLab (Göttingen) were hired. Eurofins required 50 - 100 ng of DNA with 10 μ M of sequencing primer in a total volume of 17 μ l of sterile deionized water. For sequencing performed by SeqLab, 500 - 700 ng/ μ l of DNA were submitted in a volume of 7 μ l sterile deionized water containing 20 pmol of sequencing primer. The analysis of DNA sequences was carried out using the program 4Peaks (Nucleobytes).

5.2.1.12. Isolation of RNA from cell lines

2×10^6 yac-1 cells were transferred into clean 1.5ml Eppendorf tubes and washed with PBS using table top centrifuge. RNA extraction was performed using RNA mini direct kit (analytikjena) under sterile conditions (RNA Bench), according to the manufacturer's instructions. The concentration of RNA was determined by nanodrop (section 3.2.1.7).

5.2.1.13. Synthesis of cDNA

The reverse transcription of the RNA into cDNA was carried out according to the manufacturer's instructions using the High-Capacity cDNA Reverse Transcription Kits from Applied Biosystems. The following reaction steps were used for cDNA synthesis.

Table 20: cDNA synthesis

Reaction steps	Temperature (C°)	Time (min)
Step 1	25	10:00
Step 2	37	120:00
Step 3	85	5
Step 4	4	∞

5.2.1.14. Reverse transcriptase PCR (RT-PCR)

RT-PCR is also known as reverse transcriptase PCR. IN RT-PCR, cDNA is amplified to study gene expression. I used end point PCR to amplify cDNA from Yac-1 cells to

check the expression of P2X7 splice variant by using primers specific for P2X₇ (a) and (k) isoforms. Therefore, the principle and the procedure are the same as mentioned in **section 5.2.1** except I used complementary DNA (cDNA) instead of DNA. The primers used for the amplification are mentioned in **table 7**.

5.2.2. Methods in cell biology

The cell culture was performed under sterile condition in a laminar flow hood. Medium was purchased sterile and self-prepared solutions were sterilized using Stericup or Steriflip vacuum filter.

5.2.2.1. Cell Culture

Adherent cells were cultivated in complete DMEM (except 4T1 breast cancer cell line which was cultured in RPMI complete medium with 10% FCS and pen/strep) medium containing 5% FCS in T-25 or T-75 cell culture flasks with filter caps (Nunc™ EasYFlasks™). Cultures were sub-cultivated 1:5-1:20 every 2 to 4 days when cells were 80% confluent. Cells were washed with PBS and treated with trypsin for 1-3 min to detach the cells from flask surface. Addition of FCS containing DMEM or RPMI inactivated the trypsin and cell suspension was centrifuged at 1300rpm for 5 min. supernatant was discarded and cell pellet was resuspended in appropriate volume (5 or 10ml DMEM/RPMI medium in T-25 flask or T-75 flasks respectively).

The non-adherent suspension cell lines (Yac-1 and A20) were cultivated in complete RPMI medium with 5% FCS using 10 or 20cm uncoated petri dishes. Cells routinely split in 1:10-1:20 every two to four days according to the cell density. Cells were resuspended in medium and respective dilutions transferred to the fresh petri dishes. Transfected cells were maintained by addition of respective antibiotics (i.e. 1:3000 puromycin). Cells were cultured in a stream-saturated incubator at 37°C with 5% CO₂.

5.2.2.2. Determination of cell numbers

To determine the cell numbers, Neubauer counting chamber was used (LaborOptik). Cell suspension (10µl) was diluted with 1:10 with trypan blue and 10µl of cell suspension was loaded on the chamber to analyze cell viability. The cells were counted under the microscope and cells in 4 major quadrants were averaged. The cell number per ml is calculated as follows: mean of the cell number in major quadrants x 10⁴ x dilution factor.

5.2.2.3. Transfection of eukaryotic cells

P2X₇ splice variants (a and k) and Calreticulin (GFP) were cloned into the expression vector pMXs using infusion cloning or restriction enzymes (Xho1 and Not I HF) respectively, and expressed by retroviral transduction in adherent 4T1 and 3T3 cells and non-adherent A20 cells. For retroviral transduction of cells, Platinum E cell line was used for virus packaging. The platinum E cells were cultivated in T-25 flask. When cells reached the confluency 40%, transfected with respective plasmid using jetPEI following the manufacturer protocol. The packed viruses were released in the supernatant. 48 h post transfection, the supernatant was collected, centrifuged and transferred to a new 10 ml cell culture tube. 1 ml of supernatant was replaced with 1 ml of medium in each well of 6 well plate containing 1×10^5 cells (A20 or 4T1) in 2 ml medium. 1 μ l of polybrene/ sample was added to increase the efficiency of transfection. After 24 h, cells were stained for the surface proteins and analyzed by flow cytometry.

5.2.2.4. Lentiviral transduction of luciferase in Yac-1 cells

For in-vivo imaging of mouse the Lymphoma cell line (yac-1) was transfected with luciferase (LeGo-iG2-Puro+luc2+GFP) provided by Dr. Kristoffer Riecken, Center for Oncology, Interdisciplinary Clinic and Polyclinic for Stem Cell Transplantation, University Medical Center, Hamburg-Eppendorf, Germany. At day one 5×10^4 cells per well in 500 μ l medium in 24 well plate was added and waited for cell attachment (in case of adherent cells). Polybrene (8 μ g/ml) was added to each well. Supernatant containing viral particles was added to the cells in 1:10 or 1:100 dilution. Each dilution was prepared in triplicate. At day 2, medium was changed and 1 ml of fresh medium was added. At day four, cells were analyzed by flow cytometry to check the transfection efficiency, Puromycin (1:3000) was added for positive selection.

5.2.2.5. Cryopreservation of eukaryotic cells

For cryopreservation, approximately, 1×10^6 cells were re-suspended in 1 ml freezing medium (10% DMSO, 20% complete medium (RMPI or DMEM) and 70% FCS) and transfer into cryotubes (Nunc cryotube™). Cells were immediately frozen at -80°C for short term and then transferred to nitrogen tank for long term storage.

5.2.2.6. Flow cytometry

Flow cytometry (fluorescence activated cell sorting (FACS)) is a technique that is used to detect and analyze the characteristics of a population of cells. It allows the differentiation of cell size, granularity, markers present on cell surface, cytoplasm or in the nucleus. Generally, cells are labeled with fluorochrome conjugated antibodies against target antigen. Fluorochromes are the molecules that are excited at specific wavelength and emit a fluorescent signal that is detected by flow cytometer. The intensity of signal is directly proportional to the number of target antigens. The flow cytometry was performed by using FACS Canto II and FACS Celesta.

5.2.2.7. Organ preparation from mice

Following S+16 (ART 2 blockers, that protect the cells from NAD⁺ induced cell death) nanobody administration, the mice were anesthetized and sacrificed by cervical dislocation. Tumors and spleen were collected, weighed and transferred to the 50 ml falcon tubes containing 15 ml digestion solution or 10 ml PBS, respectively (for single cell analysis) or histology cassettes (for histology analysis). Histology slides were prepared with the help of the department of Mouse Pathology, University Medical Center Hamburg-Eppendorf.

5.2.2.7.1. Preparation of Tumor cells

To prepare the single cells from the solid tumor, tissue was transferred to 50ml falcon tube containing 15 ml digestion solution and cut into small pieces using scissors. The sample was rotated at 37°C for 1h with continuous shaking. After 1 h the digestion solution was collected in new 50 ml falcon tube and stored on ice, 15 ml additional digestion solution was added to the falcon tube containing tumor tissue. The tubes were placed in shaker at 37°C for 1h. Solution was collected and placed on ice and 10 ml PBS containing DNase-1 was added to the tissue containing tube and placed on shaker again for 30 min. All the collected solutions were passed through the 70µM cell strainer (EASY strainer, GBO) and centrifuged at 1600rpm for 5 min at 4°C. Then, cells resuspended in 3 ml of Erythrocyte lysis Buffer (ACK). After 3 min incubation at RT, 10 ml of FACS Buffer was added to stop the lysis. Cells were centrifuged at 1600 rpm for 5 min. The pellet was then resuspended in 500µl FACS buffer and cells were stained for flow cytometry analysis.

5.2.2.7.2. Preparation of spleen cells

To prepare the splenocytes, the spleens were compressed through a 70 μ M cell strainer (EASY strainer, GBO) using the plunger of a 5 ml syringe in a 10 cm petri dish. The suspension was centrifuged at 1600 rpm for 5 min at 4°C. The cell pellet was treated with 3 ml lysis buffer (AKT) for 3 min at room temperature for the lysis of erythrocytes. 10ml of PBS was added to stop the lysis reaction and centrifuged at 1600 rpm for 5 min. The cell pellet was resuspended in 2ml FACS buffer.

5.2.2.8. Staining of cell surface proteins

2×10^5 cells/ 100 μ l FACS buffer in FACS tubes were stained with fluorochrome conjugated antibodies (**Section 5.1, Table 13**) for staining of surface markers (CD62L, P2X₇) at 4°C for 30 min or at room temperature for 20 min. The antibody amount used was based on manufacturer recommendation of titrated dilution. Cells were washed with 2 ml washing buffer and centrifuged at 1300 rpm for 5 min at 4°C. Supernatants were discarded and pellet was resuspended in 200-400 μ l buffer for FACS analysis. In case of 2-step staining, cells were first incubated with unconjugated antibody (calreticulin 1:600) in 100 μ l FACS buffer on ice for 30 min or at room temperature for 20 min. Cells were washed once as described above. Cell pellet was resuspended in 100 μ l of FACS buffer and stained with species-specific fluorochrome-conjugated secondary antibody (Rabbit IgG (H+L), APC for calreticulin staining) for the detection of bound antibody.

5.2.2.8.1. Mouse splenocytes and tumor cells

10^6 splenocytes or tumor cells resuspended in 50 μ l washing buffer were transferred to the FACS tubes and treated with Fc-block (1:100) for 10 min on ice to reduce the nonspecific staining by fluorochrome conjugated antibodies. Master mix of antibodies in 50 μ l washing buffer was added to the cell suspension to a final volume of 100 μ l. Cells were incubated on ice for 30 min and washed with 2 ml washing buffer and resuspended in 200-400 μ l buffer for FACS analysis. The fluorochrome conjugated antibodies (**section 5.1, table 13**) were used to stain cell surface markers (CD45, CD3, CD4, CD8, CD19, CD69, CD39, CD73 and PD1) on spleen and tumor by flow cytometry.

5.2.2.9. Staining for intracellular molecules

For the intracellular staining, cells were stained for cell surface protein/ molecules and live dead dye as described in section **3.2.2.10**. After washing with 2ml cold PBS, cell pellet was resuspended in 1 ml fixation/permeabilization buffer (Foxy3/transcription factor staining buffer set (eBioscience)), and incubated on ice for 30 min in dark. After washing with 1x permeabilization buffer, fluorochrome-conjugated antibodies against transcription factors (Granzyme B, Foxy3 and p-eIF2 α) were added and incubated on ice for 30 min in dark. The cells were washed in 1x permeabilization buffer. In case of unconjugated antibodies (p-eIF2 α), cells were incubated further with fluorochrome conjugated species-specific secondary antibody (rabbit IgG (H+L) PE for p-eIF2 α staining) for 30 min at 4°C in dark. The cells were washed in 1x permeabilization buffer and resuspended in 200-400 μ l FACS buffer and analyzed by flow cytometry.

5.2.3. *In-vitro* assays

5.2.3.1. Uptake of 4', 6-diamino-2-phenylindole (DAPI), exposition of Phosphatidylserine and CD62L shedding

4',6-diamino-2-phenylindole (DAPI) is a fluorescent dye that binds to double stranded DNA. The DAPI uptake is a read out to evaluate the P2X₇ mediated pore formation on different cell types. 2*10⁵ Yac-1 cells (T lymphoma cell line), P2X₇ (a) and (k) transfected A20 cells (B lymphoma cell line), or P2X₇ transfected 4T1 cells were resuspended in complete RPMI medium and incubated in the presence or absence of P2X₇ blocking nanobody 13A7 for 15 min at shaking roller at room temperature. Afterwards cells were loaded with DAPI (1:400) and incubated for different time points (2 min-30 min) at 37°C in the presence of 50 μ M-3mM ATP. Immediately after prescribed time, cells were place on ice to stop the reaction. Cells were washed with cold buffer and stained for CD62L antibody (conjugated with APC) for 30min on ice. After washing with annexin V buffer, cells were resuspended in 100 μ l FACS buffer and stained for surface translocation of phosphatidylserine (PS) by using annexin v antibody (conjugated with FITC) at room temperature for 15min. Cells were kept on ice and analyzed by flow cytometry.

5.2.3.2. Assays for cell viability

To investigate the ATP mediated cell death in P2X₇ expressing cancer cell lines (YAC-1, P2X₇ transfected A20), cells were pre-treated with 1 μ g/10⁶ of P2X₇ blocking

nanobody 13A7.Fc for 15 min at room temperature. $1 \times 10^5/500\mu\text{l}$ cells with and without P2X₇ blocking nanobody were transferred in 24 well plates. 500 μl of 0.06-6mM ATP in complete medium was transferred in the 24 well plates containing cell suspension, to get the final concentration 0.03-3mM. cells were incubated for 24 h in stream-controlled incubator at 37°C and 5% CO₂. Cells were transferred in the FACS tubes, centrifuged at 1300rpm for 5 min and supernatant was discarded. Cells were washed with 2 ml of washing buffer. Cells were resuspended in 200 μl of FACS buffer and stained for DAPI (1:100) to check the dead cells by flow cytometry. To check the chemotherapy induced cell death, cells were treated with Doxorubicin (0.03-3 μM) or Bortezomib (0.03-100nM) for 24 or 48 h as described above.

To investigate the synergistic cytotoxic effect of chemotherapeutic drugs by P2X₇ activation, cells were treated with and without P2X₇ blocking nanobody 13A7 for 15 min at room temperature. 1×10^5 cells / sample in RPMI were treated with DOX alone (0.03-3 μM), DOX plus 200 μM ATP or DOX plus 200 μM ATP in 13A7 pretreated cells for 24 h or 48 h. After washing with 2 ml washing buffer, cells were resuspended in 200 μl FACS buffer and stained for DAPI (1:100) to analyze the dead cells by flow cytometry. All the samples were prepared in triplicates.

5.2.3.3. Apoptosis

To investigate the apoptosis by doxorubicin treatment, 1×10^5 Yac-1 cells were incubated in a 24-well microtiter plate in 500 μL complete medium containing ATP, or DOX at the indicated concentrations (**Section 3.1.13**). To block gating of P2X₇, cells were pre-incubated with 1 $\mu\text{g}/\text{ml}$ of the antagonistic nanobody 13A7 for 20 min at room temperature. The samples were incubated for 6 h at 37°C, 5% CO₂. Cells were stained for Caspase 3 using the FLICA kit. Cells were analyzed by flow cytometry.

5.2.3.4. Acid Phosphatase assay

The acid phosphatase assay is based on the principle of measuring the cell numbers by cell membrane associated acid phosphatase. The substrate for the assay is p-nitrophenyl phosphate which is colorless in balanced salt solution or medium. Acid phosphatase in cell membrane cleaves the substrate and produce yellow colored compound (p-nitrophenol), which is detected by plate reader (victor3). An increase or decrease in the cell number is directly proportional to the cleaved substrate and color intensity, indicating the level of cell death in response to treatments. To investigate

the cell cytotoxicity by DOX in 4T1 and A20 cell lines (wild type and P2X7 transfected) in the presence or absence of ATP and/or P2X₇ blocking nanobody 13A7, Cells were seeded in 96 well plate (1×10^4 cells/well) and treated with different concentration of DOX +/- ATP +/- 13A7 overnight. The culture medium was removed in one swing. Cells were washed once with 200 ml phosphate-buffered saline (PBS, pH 7.2). In each well, 100 μ l of buffer (0.1 M sodium acetate (pH 5.0), 0.1% Triton X-100, and 5 mM *p*-nitrophenyl phosphate) was added. The plate was incubated at 37°C for 2 h. The reaction was stopped by adding 10 μ l of 1 M NaOH. Yellow color formation was determined by using plate reader.

5.2.3.5. Microscopy

Fixed cell imaging was performed using confocal microscope (Leica sp5). P2X₇ (k) and calreticulin (eGFP) transfected 3T3 cells were seeded (1×10^5 cells per well) on a 24-well plate containing 12 mm cover slips coated with 0.1 mg/ml poly-L-lysine 24 h prior to measurement. Cells containing coverslips were incubated with respective treatments for indicated time (Section 3.1.11), washed with cold PBS and fixed with 2% PFA (paraformaldehyde) for 15 min. For phalloidin staining, cells were permeabilized with 1% triton for 5 min and blocked with blocking buffer (1% BSA and 0.1% Triton in PBS) for 40 min at room temperature. coverslips were washed with PBS and stained with Phalloidin (1:50) for 30 min. Coverslips were washed again with PBS and mounted on slides with mounting medium containing DAPI and imaged by using confocal microscope (Leica TCS sp5).

5.2.4. Methods in animal experiments

The animal testing was performed in collaboration of Prof. Loges, Institute of Oncology, University Medical Center Hamburg-Eppendorf with the assistance of Dr. Isabel Ben Batalla and Nikolaus Berenbrok. *In-vivo* imaging was performed by Mr. Michael Horn-Glander, IVIS facility, University Medical center Hamburg-Eppendorf. The nanobodies (13A7 half-life extended and 14D5 half-life extended) were provided by Prof. Friedrich Koch-Nolte.

5.2.4.1. Generating tumor models, injection of nanobodies and chemotherapeutic agents.

5.2.4.1.1. Yac-1 lymphoma model and *in-vivo* imaging

The *in-vivo* experiment was conducted in SCID mice obtained from Charles River Laboratories (Sulzfeld, Germany). All experiments were performed according to the animal welfare and institutional guidelines; and approved by licensing authority (project number: **G13/017**). For generation of tumor grafts, mice were injected *i.v.* in the tail vein with 2.5×10^5 luciferase transduced Yac-1 cells in 0.1 ml of 0.9% sodium chloride solution. Bioluminescence imaging (BLI) was performed after 3 days and at indicated time points (section 3.2.1). For imaging, mice were anesthetized with isoflurane, injected with luciferin (6 mg/mouse) for 15 min and positioned in the imaging chamber of a small animal imaging system (IVIS-200, Caliper Life Sciences, Hopkinton, Massachusetts, USA). According to the BLI, mice were randomized into two groups, control (PBS treated mice) and treated (P2X₇ blocking nanobody (13A7.HLE) mice. PBS or 50 µg of 13A7.HLE was injected in control or treated mice respectively. The treatments were given via *i.p.* route in 0.1 ml, twice a week, and imaged for tumor growth. After qualitative imaging *in-vivo*, quantitative analyses were performed by placing ROIs (region of interest). Total flux was measured with Living Image 4.2 software (Caliper Life Sciences).

5.2.4.1.2. 4T1 tumor model

To conduct tumor graft experiments, 6 weeks old female Balb/c mice were purchased from Charles river Laboratories (Sulzfeld, Germany). All experiments were performed according to the animal welfare and institutional guidelines; and approved by licensing authority (project number: **N 069/2018**). 0.5×10^6 4T1 cells (4T1 P2X₇ dead mutant or 4T1 P2X₇ (k)) was injected orthotopically into the mammary fat pad of syngeneic Balb/c mice. Mice were randomized into four group according to the size of the tumors (80 to 100 mm³) and treated *i.p.* with PBS (control group), 14D5 (50µg), DOX (3mg/kg) or combination of 14D5 and DOX, in 200µl volume. The treatments were injected twice a week. The tumor size was measured every alternative day (three times a week) using Vernier caliper. Volume of the tumor was measured using the formula $V = (\text{longer length} \times \text{shorter length}) / 2$. When the first tumor size reached to maximum allowed size (1500 mm³), mice were injected with S+16 (ART2 blocker), 30 min before

sacrificing them (to protect from NAD released cell death). Mice were sacrificed according to given guidelines, after scarifying the mice, tumor and spleen were weighed, and collected for histology and flow cytometry analysis.

5.2.4.2. Histology

Tumor samples were fixed in 1 % PFA overnight, and send to the Pathology Department for preparation and staining of slides. slides were stained for caspase 3 (to check the apoptosis) and CD3 (to check the T cell infiltration in primary tumor). The stained slides were imaged using Zeiss Axio Scope A1 for immunohistochemistry (IHC). Image analysis was carried out using AxioVision software (Carl Zeiss Microscopy). Counting of CD3 positive cells in Tumor sections was performed manually in 10-12 fields of each tumor section (20x magnification). The caspase3+ area was also manually assessed in 10-12 fields of each tumor slide (20x magnification).

5.3. Statistical analysis

Data representation and statistical analysis were performed by using graph pad prism 8.3.0 software. Analysis of variance (One way or two-way ANOVA) was used for the comparison among multiple groups with repeated measures. In *in-vitro* experiments, n=3 (each condition or treatment was performed in triplicate in single experiment) and also each experiment was reproduced minimum of three times to confirm the results. For *in-vivo* experiments, n= 7 (each group consists of 7 mice). To check the significance among different groups and treatments, Bonferroni posttest was applied for multiple comparisons with less repetitive measures (n=3) and Tukey posttest was applied for multiple comparisons where n=7. Dunnett's' test was used to compare the treatments with control. A p-value ≤ 0.05 was considered significant. *, p<0.05, **, p<0.01, ***, p<0.001.

6 References:

- Adinolfi E, Amoroso F, Giuliani AL (2012a) P2X7 Receptor Function in Bone-Related Cancer. *J Osteoporos* 2012:1–10. doi: 10.1155/2012/637863
- Adinolfi E, Capece M, Franceschini A, et al (2015) Accelerated tumor progression in mice lacking the ATP receptor P2X7. *Cancer Res* 75:635–644. doi: 10.1158/0008-5472.CAN-14-1259
- Adinolfi E, Raffaghello L, Giuliani AL, et al (2012b) Expression of P2X7 receptor increases in vivo tumor growth. *Cancer Res* 72:2957–2969. doi: 10.1158/0008-5472.CAN-11-1947
- Adriouch S, Dox C, Welge V, et al (2002) Cutting edge: a natural P451L mutation in the cytoplasmic domain impairs the function of the mouse P2X7 receptor. *J Immunol* 169:4108–4112. doi: 10.4049/jimmunol.169.8.4108
- Adriouch S, Scheuplein F, Bähring R, et al (2009) Characterisation of the R276A gain-of-function mutation in the ectodomain of murine P2X7. *Purinergic Signal* 5:151–161. doi: 10.1007/s11302-009-9134-6
- Allard B, Longhi MS, Robson SC, Stagg J (2017) The ectonucleotidases CD39 and CD73: Novel checkpoint inhibitor targets. *Immunol. Rev.*
- Anson DS (2004) The use of retroviral vectors for gene therapy-what are the risks? A review of retroviral pathogenesis and its relevance to retroviral vector-mediated gene delivery. *Genet Vaccines Ther* 2:1–13. doi: 10.1186/1479-0556-2-9
- Apetoh L, Ghiringhelli F, Tesniere A, et al (2007) Toll-like receptor 4-dependent contribution of the immune system to anticancer chemotherapy and radiotherapy. *Nat Med* 13:1050–1059. doi: 10.1038/nm1622
- Bezu L, Gomes-da-Silva LC, Dewitte H, et al (2015) Combinatorial strategies for the induction of immunogenic cell death. *Front Immunol* 6:1–11. doi: 10.3389/fimmu.2015.00187
- Bilbao PS, Katz S, Boland R (2012) Interaction of purinergic receptors with GPCRs, ion channels, tyrosine kinase and steroid hormone receptors orchestrates cell function. *Purinergic Signal* 8:91–103. doi: 10.1007/s11302-011-9260-9
- Boeynaems JM, Communi D, Gonzalez NS, Robaye B (2005) Overview of the P2 receptors. *Semin. Thromb. Hemost.* 31:139–149
- Burnstock G (2007) Purine and pyrimidine receptors. *Cell Mol Life Sci* 64:1471–1483. doi: 10.1007/s00018-007-6497-0

- Cai SF, Fehniger TA, Cao X, et al (2009) Differential expression of granzyme B and C in murine cytotoxic lymphocytes. *J Immunol* 182:6287–97. doi: 10.4049/jimmunol.0804333
- Chao CC, Huang CC, Lu DY, et al (2012) Ca²⁺ store depletion and endoplasmic reticulum stress are involved in P2X7 receptor-mediated neurotoxicity in differentiated NG108-15 cells. *J Cell Biochem* 113:1377–1385. doi: 10.1002/jcb.24010
- Chao MP, Jaiswal S, Weissman-Tsukamoto R, et al (2010) Calreticulin Is the Dominant Pro-Phagocytic Signal on Multiple Human Cancers and Is Counterbalanced by CD47. *Sci Transl Med* 2:63ra94-63ra94. doi: 10.1126/scitranslmed.3001375
- Chen DS, Mellman I (2013) Oncology meets immunology: The cancer-immunity cycle. *Immunity* 39:1–10. doi: 10.1016/j.immuni.2013.07.012
- Cibrián D, Sánchez-Madrid F (2017) CD69: from activation marker to metabolic gatekeeper. *Eur J Immunol* 47:946–953. doi: 10.1002/eji.201646837
- Cohen IJ, Blasberg R (2017) Impact of the Tumor Microenvironment on Tumor-Infiltrating Lymphocytes: Focus on Breast Cancer. *Breast Cancer (Auckl)* 11:1178223417731565. doi: 10.1177/1178223417731565
- Danquah W, Catherine MS, Rissiek B, et al (2016) Nanobodies that block gating of the P2X7 ion channel ameliorate inflammation. *Sci. Transl. Med.* 8:366ra162-366ra162
- Denlinger LC, Fisette PL, Sommer JA, et al (2001) Cutting Edge: The Nucleotide Receptor P2X 7 Contains Multiple Protein- and Lipid-Interaction Motifs Including a Potential Binding Site for Bacterial Lipopolysaccharide. *J Immunol* 167:1871–1876. doi: 10.4049/jimmunol.167.4.1871
- Di Virgilio F (2012) Purines, purinergic receptors, and cancer. *Cancer Res* 72:5441–5447. doi: 10.1158/0008-5472.CAN-12-1600
- Di Virgilio F, Boeynaems JM, Robson SC (2009) Extracellular nucleotides as negative modulators of immunity. *Curr Opin Pharmacol* 9:507–513. doi: 10.1016/j.coph.2009.06.021
- Di Virgilio F, Chiozzi P, Ferrari D, et al (2001) Nucleotide receptors: An emerging family of regulatory molecules in blood cells. *Blood* 97:587–600. doi: 10.1182/blood.V97.3.587

- Di Virgilio F, Sarti AC, Falzoni S, et al (2018) Extracellular ATP and P2 purinergic signalling in the tumour microenvironment. *Nat Rev Cancer* 18:601–618. doi: 10.1038/s41568-018-0037-0
- Duhen T, Duhen R, Montler R, et al (2018) Co-expression of CD39 and CD103 identifies tumor-reactive CD8 T cells in human solid tumors. *Nat Commun* 9:2724. doi: 10.1038/s41467-018-05072-0
- Eltzschig HK, Sitkovsky M V, Robson SC (2012) Purinergic Signaling during Inflammation. doi: 10.1056/NEJMra1205750
- Fantini MC, Dominitzki S, Rizzo A, et al (2007) In vitro generation of CD4+ CD25+ regulatory cells from murine naive T cells. *Nat Protoc* 2:1789–1794. doi: 10.1038/nprot.2007.258
- Farrell AW, Gadeock S, Pupovac A, et al (2010) P2X7 receptor activation induces cell death and CD23 shedding in human RPMI 8226 multiple myeloma cells. *Biochim Biophys Acta - Gen Subj* 1800:1173–1182. doi: 10.1016/j.bbagen.2010.07.001
- Gardai SJ, McPhillips KA, Frasch SC, et al (2005) Cell-surface calreticulin initiates clearance of viable or apoptotic cells through trans-activation of LRP on the phagocyte. *Cell* 123:321–34. doi: 10.1016/j.cell.2005.08.032
- Garg AD, Krysko D V., Vandenabeele P, Agostinis P (2016) Extracellular ATP and P2X7 receptor exert contextspecific immunogenic effects after immunogenic cancer cell death. *Cell Death Dis* 7:1–3. doi: 10.1038/cddis.2015.411
- Garg AD, Krysko D V., Verfaillie T, et al (2012) A novel pathway combining calreticulin exposure and ATP secretion in immunogenic cancer cell death. *EMBO J* 31:1062–1079. doi: 10.1038/emboj.2011.497
- Gever JR, Cockayne DA, Dillon MP, et al (2006) Pharmacology of P2X channels. *Pflugers Arch Eur J Physiol* 452:513–537. doi: 10.1007/s00424-006-0070-9
- Gewirtz D (1999) A critical evaluation of the mechanisms of action proposed for the antitumor effects of the anthracycline antibiotics adriamycin and daunorubicin. *Biochem Pharmacol* 57:727–741. doi: 10.1016/S0006-2952(98)00307-4
- Haag F, Adriouch S, Braß A, et al (2007) Extracellular NAD and ATP: Partners in immune cell modulation. *Purinergic Signal* 3:71–81. doi: 10.1007/s11302-006-9038-7
- Hanley PJ, Kronlage M, Kirschning C, et al (2012) Transient P2X₇ Receptor

- Activation Triggers Macrophage Death Independent of Toll-like Receptors 2 and 4, Caspase-1, and Pannexin-1 Proteins. *J Biol Chem* 287:10650–10663. doi: 10.1074/jbc.M111.332676
- Hetz C, Saxena S (2017) ER stress and the unfolded protein response in neurodegeneration. *Nat Rev Neurol* 13:477–491. doi: 10.1038/nrneurol.2017.99
- Hitomi J, Katayama T, Taniguchi M, et al (2004) Apoptosis induced by endoplasmic reticulum stress depends on activation of caspase-3 via caspase-12. *Neurosci Lett* 357:127–130. doi: 10.1016/j.neulet.2003.12.080
- Jiang X, Wang J, Deng X, et al (2019) Role of the tumor microenvironment in PD-L1/PD-1-mediated tumor immune escape. *Mol Cancer* 18:10. doi: 10.1186/s12943-018-0928-4
- Joseph SM, Pifer MA, Przybylski RJ, Dubyak GR (2004) Methylene ATP analogs as modulators of extracellular ATP metabolism and accumulation. *Br J Pharmacol* 142:1002–1014. doi: 10.1038/sj.bjp.0705865
- Junger WG (2011) Immune cell regulation by autocrine purinergic signalling. *Nat Rev Immunol* 11:201–212. doi: 10.1038/nri2938
- Kepp O, Semeraro M, Bravo-San Pedro JM, et al (2015) eIF2 α phosphorylation as a biomarker of immunogenic cell death. *Semin Cancer Biol* 33:86–92. doi: 10.1016/j.semcancer.2015.02.004
- Klapperstück M, Büttner C, Schmalzing G, Markwardt F (2001) Functional evidence of distinct ATP activation sites at the human P2X(7) receptor. *J Physiol* 534:25–35. doi: 10.1111/j.1469-7793.2001.00025.x
- Krepela I, Krepela E (2010) Granzyme B-induced apoptosis in cancer cells and its regulation (Review). *Int J Oncol* 37:1361–1378. doi: 10.3892/ijo_00000788
- Kroemer G, Galluzzi L, Kepp O, Zitvogel L (2013) Immunogenic cell death in cancer therapy. *Annu Rev Immunol* 31:51–72. doi: 10.1146/annurev-immunol-032712-100008
- Lin JH, Walter P, Yen TSB (2008) Endoplasmic Reticulum Stress in Disease Pathogenesis. *Annu Rev Pathol Mech Dis* 3:399–425. doi: 10.1146/annurev.pathmechdis.3.121806.151434
- Liu Z, Lv Y, Zhao N, et al (2015) Protein kinase R-like ER kinase and its role in endoplasmic reticulum stress-decided cell fate. *Cell Death Dis* 6:e1822–e1822. doi: 10.1038/cddis.2015.183

- Locovei S, Scemes E, Qiu F, et al (2007) Pannexin1 is part of the pore forming unit of the P2X₇ receptor death complex. *FEBS Lett* 581:483–488. doi: 10.1016/j.febslet.2006.12.056
- Lu L, Zou Y, Yang W, et al (2015) Anisamide-Decorated pH-Sensitive Degradable Chimaeric Polymersomes Mediate Potent and Targeted Protein Delivery to Lung Cancer Cells. *Biomacromolecules* 16:1726–1735. doi: 10.1021/acs.biomac.5b00193
- Michaud M, Martins I, Sukkurwala AQ, et al (2011) Autophagy-Dependent Anticancer Immune Responses Induced by Chemotherapeutic Agents in Mice. *Science* (80-) 334:1573–1577. doi: 10.1126/science.1208347
- Motz GT, Coukos G (2013) Deciphering and Reversing Tumor Immune Suppression. *Immunity* 39:61–73. doi: 10.1016/j.immuni.2013.07.005
- Muñoz-Planillo R, Kuffa P, Martínez-Colón G, et al (2013) K⁺ Efflux Is the Common Trigger of NLRP3 Inflammasome Activation by Bacterial Toxins and Particulate Matter. *Immunity* 38:1142–1153. doi: 10.1016/j.immuni.2013.05.016
- Muyldermans S (2013) Nanobodies: Natural Single-Domain Antibodies. *Annu Rev Biochem* 82:775–797. doi: 10.1146/annurev-biochem-063011-092449
- North RA (2002) Molecular physiology of P2X receptors. *Physiol Rev* 82:1013–67. doi: 10.1152/physrev.00015.2002
- Obeid M, Tesniere A, Ghiringhelli F, et al (2007) Calreticulin exposure dictates the immunogenicity of cancer cell death. *Nat Med* 13:54–61. doi: 10.1038/nm1523
- Panaretakis T, Joza N, Modjtahedi N, et al (2008) The co-translocation of ERp57 and calreticulin determines the immunogenicity of cell death. *Cell Death Differ* 15:1499–1509. doi: 10.1038/cdd.2008.67
- Panaretakis T, Kepp O, Brockmeier U, et al (2009) Mechanisms of pre-apoptotic calreticulin exposure in immunogenic cell death. *EMBO J* 28:578–590. doi: 10.1038/emboj.2009.1
- Peidis P, Papadakis AI, Muaddi H, et al (2011) Doxorubicin bypasses the cytoprotective effects of eIF2 α phosphorylation and promotes PKR-mediated cell death. *Cell Death Differ* 18:145–154. doi: 10.1038/cdd.2010.76
- Pellegatti P, Raffaghello L, Bianchi G, et al (2008) Increased level of extracellular ATP at tumor sites: In vivo imaging with plasma membrane luciferase. *PLoS One* 3:1–9. doi: 10.1371/journal.pone.0002599

- Pulaski BA, Ostrand-Rosenberg S (1998) Reduction of established spontaneous mammary carcinoma metastases following immunotherapy with major histocompatibility complex class II and B7.1 cell-based tumor vaccines. *Cancer Res* 58:1486–93
- Pulaski BA, Ostrand-Rosenberg S, Miller F, et al (2000a) Mouse 4T1 Breast Tumor Model. *Curr Protoc Immunol* 39:1–16. doi: 10.1002/0471142735.im2002s39
- Pulaski BA, Terman DS, Khan S, et al (2000b) Cooperativity of Staphylococcal aureus enterotoxin B superantigen, major histocompatibility complex class II, and CD80 for immunotherapy of advanced spontaneous metastases in a clinically relevant postoperative mouse breast cancer model. *Cancer Res* 60:2710–5
- Quezada SA, Peggs KS, Curran MA, Allison JP (2006) CTLA4 blockade and GM-CSF combination immunotherapy alters the intratumor balance of effector and regulatory T cells. *J Clin Invest* 116:1935–1945. doi: 10.1172/JCI27745
- Ri M (2016) Mechanism of action of bortezomib in multiple myeloma therapy. *Int J Myeloma* 6:1–6
- Rissiek B, Haag F, Boyer O, et al (2015) P2X7 on Mouse T Cells: One Channel, Many Functions. *Front Immunol* 6:204. doi: 10.3389/fimmu.2015.00204
- Robson SC, Sévigny J, Zimmermann H (2006) The E-NTPDase family of ectonucleotidases: Structure function relationships and pathophysiological significance. *Purinergic Signal* 2:409–30. doi: 10.1007/s11302-006-9003-5
- Sakaguchi S, Wing K, Onishi Y, et al (2009) Regulatory T cells: How do they suppress immune responses? *Int Immunol* 21:1105–1111. doi: 10.1093/intimm/dxp095
- Salaroglio IC, Panada E, Moiso E, et al (2017) PERK induces resistance to cell death elicited by endoplasmic reticulum stress and chemotherapy. *Mol Cancer* 16:91. doi: 10.1186/s12943-017-0657-0
- Sambucci M, Gargano F, De Rosa V, et al (2018) FoxP3 isoforms and PD-1 expression by T regulatory cells in multiple sclerosis. *Sci Rep* 8:3674. doi: 10.1038/s41598-018-21861-5
- Sarvaria A, Madrigal JA, Saudemont A (2017) B cell regulation in cancer and anti-tumor immunity. *Cell Mol Immunol* 14:662–674. doi: 10.1038/cmi.2017.35
- Scheuplein F, Schwarz N, Adriouch S, et al (2009) NAD⁺ and ATP released from

- injured cells induce P2X7-dependent shedding of CD62L and externalization of phosphatidylserine by murine T cells. *J Immunol* 182:2898–2908. doi: 10.4049/jimmunol.0801711
- Schwarz N, Drouot L, Nicke A, et al (2012) Alternative splicing of the N-terminal cytosolic and transmembrane domains of P2X7 controls gating of the ion channel by ADP-ribosylation. *PLoS One* 7:. doi: 10.1371/journal.pone.0041269
- Seman M, Adriouch S, Scheuplein F, et al (2003) NAD-Induced T Cell Death. *Immunity* 19:571–582. doi: 10.1016/S1074-7613(03)00266-8
- Serrano-del Valle A, Anel A, Naval J, Marzo I (2019) Immunogenic Cell Death and Immunotherapy of Multiple Myeloma. *Front Cell Dev Biol* 7:50. doi: 10.3389/fcell.2019.00050
- Steinberg TH, Newman AS, Swanson JA, Silverstein SC (1987) ATP₄- permeabilizes the plasma membrane of mouse macrophages to fluorescent dyes. *J Biol Chem* 262:8884–8
- Stinchcombe JC, Griffiths GM (2007) Secretory Mechanisms in Cell-Mediated Cytotoxicity. *Annu Rev Cell Dev Biol* 23:495–517. doi: 10.1146/annurev.cellbio.23.090506.123521
- Surprenant A, Rassendren F, Kawashima E, et al (1996) The Cytolytic P2Z Receptor for Extracellular ATP Identified as a P2X Receptor (P2X7). *Science* (80-) 272:735–738. doi: 10.1126/SCIENCE.272.5262.735
- Synnestvedt K, Furuta GT, Comerford KM, et al (2002) Ecto-5'-nucleotidase (CD73) regulation by hypoxia-inducible factor-1 mediates permeability changes in intestinal epithelia. *J Clin Invest* 110:993–1002. doi: 10.1172/JCI15337
- Szegezdi E, Logue SE, Gorman AM, Samali A (2006) Mediators of endoplasmic reticulum stress-induced apoptosis. *EMBO Rep* 7:880–5. doi: 10.1038/sj.embor.7400779
- Tanchot C, Terme M, Pere H, et al (2013) Tumor-infiltrating regulatory T cells: phenotype, role, mechanism of expansion in situ and clinical significance. *Cancer Microenviron* 6:147–57. doi: 10.1007/s12307-012-0122-y
- Tesniere A, Schlemmer F, Boige V, et al (2010) Immunogenic death of colon cancer cells treated with oxaliplatin. *Oncogene* 29:482–91. doi: 10.1038/onc.2009.356
- Thorn CF, Oshiro C, Marsh S, et al (2011) Doxorubicin pathways: pharmacodynamics and adverse effects. *Pharmacogenet Genomics* 21:440–6.

doi: 10.1097/FPC.0b013e32833ffb56

- Tijink BM, Laeremans T, Budde M, et al (2008) Improved tumor targeting of anti-epidermal growth factor receptor Nanobodies through albumin binding: taking advantage of modular Nanobody technology. *Mol Cancer Ther* 7:2288–2297. doi: 10.1158/1535-7163.MCT-07-2384
- Urta H, Dufey E, Avril T, et al (2016) Endoplasmic Reticulum Stress and the Hallmarks of Cancer. *Trends in Cancer* 2:252–262. doi: 10.1016/j.trecan.2016.03.007
- Van Bockstaele F, Holz J-B, Revets H (2009) The development of nanobodies for therapeutic applications. *Curr Opin Investig Drugs* 10:1212–24
- Vijayan D, Young A, Teng MWL, Smyth MJ (2017) Targeting immunosuppressive adenosine in cancer. *Nat Rev Cancer* 17:709–724. doi: 10.1038/nrc.2017.86
- Walter F, O'Brien A, Concannon CG, et al (2018) ER stress signalling has an activating transcription factor 6 α (ATF6)-dependent “off-switch.” *J Biol Chem* jbc.RA118.002121. doi: 10.1074/JBC.RA118.002121
- Wang M, Kaufman RJ (2014) The impact of the endoplasmic reticulum protein-folding environment on cancer development. *Nat Rev Cancer* 14:581–597. doi: 10.1038/nrc3800
- Wesolowski J, Alzogaray V, Reyelt J, et al (2009) Single domain antibodies: Promising experimental and therapeutic tools in infection and immunity. *Med Microbiol Immunol* 198:157–174. doi: 10.1007/s00430-009-0116-7
- Yegutkin GG (2008) Nucleotide- and nucleoside-converting ectoenzymes: Important modulators of purinergic signalling cascade. *Biochim. Biophys. Acta - Mol. Cell Res.*
- Yip L, Woehrle T, Corriden R, et al (2009) Autocrine regulation of T-cell activation by ATP release and P2X7 receptors. *FASEB J* 23:1685–1693. doi: 10.1096/fj.08-126458
- Zhu X, Lang J (2016) The significance and therapeutic potential of PD-1 and its ligands in ovarian cancer: A systematic review. *Gynecol Oncol* 142:184–189. doi: 10.1016/j.ygyno.2016.04.002
- Zimmermann H, Zebisch M, Sträter N (2012) Cellular function and molecular structure of ecto-nucleotidases. *Purinergic Signal* 8:437–502. doi: 10.1007/s11302-012-9309-4

Zitvogel L, Galluzzi L, Kepp O, et al (2015) Type I interferons in anticancer immunity.
Nat Rev Immunol 15:405–414. doi: doi:10.1016/j.ccell.2015.10.012

7 Appendix

7.1. List of Figures

Figure 1. P2X ₇ structure, splice variants and mutants	14
Figure 2. Purinergic signaling.....	15
Figure 3. P2X ₇ activation.....	16
Figure 4: Immune activation by chemotherapeutic drugs (i.e., DOX):.....	19
Figure 5: Unfolded protein response	21
Figure 6. Cell surface expression and splice variants of P2X ₇ in T cell lymphoma (Yac-1).....	23
Figure 7. P2X ₇ R mediates ATP-induced CD62L shedding, PS exposure, and dye uptake.....	24
Figure 8. ATP induced toxicity in Yac-1 cells	25
Figure 9. Gating of P2X ₇ enhances the cytotoxicity of doxorubicin in Yac-1 cells: ..	26
Figure 10. Doxorubicin cytotoxicity:	27
Figure 11. Gating of P2X ₇ enhances uptake of doxorubicin at early timepoints	28
Figure 12. ATP-induced cell death is rapid, but death due to ATP/DOX synergism is a late event.	29
Figure 13. Transient gating of P2X ₇ marks cells for doxorubicin-induced death.....	30
Figure 14. The synergistic effect of P2X ₇ on doxorubicin cytotoxicity is dependent on the P2X ₇ isoform	32
Figure 15. P2X ₇ splice variants differ in their effects on synergistic cytotoxicity.	34
Figure 16: P2X ₇ and doxorubicin co-operate in the induction of phagocytosis-promoting signals	36
Figure 17. Enhanced ER stress in fibroblast cell line	37
Figure 18. P2X ₇ activation results in enhanced Bortezomib toxicity.....	38
Figure 19. P2X ₇ and doxorubicin synergize to activate caspase-3.....	39
Figure 20. P2X ₇ activation results in CRT surface translocation.....	40
Figure 21. P2X ₇ -mediated DAPI uptake, PS flashing and CRT translocation are blocked by inhibition of PERK	41
Figure 22. Inhibition of PERK blocked the synergistic effect of P2X ₇ on doxorubicin-mediated cytotoxicity	42
Figure 23. Inhibition of P2X ₇ in Yac-1 cells promotes tumor growth	44

Figure 24. Tumors carrying a functional P2X7R exhibit slower growth in-vivo.....	46
Figure 25. DOX does not affect the tumor growth in P2X7 (k) expressing tumors ...	47
Figure 26. P2X7 enhancing nanobody slows down the tumor growth.	48
Figure 27. T cell infiltration in solid tumors	50
Figure 28. CD39 and CD73 expression on tumor infiltrating T lymphocytes:.....	51
Figure 29. Expression of PD-1 and granzyme B (GRZB) on tumor infiltrating T lymphocytes:	53
Figure 30. P2X7 activation and chemotherapy do not affect T cell populations in spleen:	55
Figure 31. Phenotypic analysis of splenic T lymphocytes.	57
Figure 32: Co-expression of CD73 and CD39 on spleen and tumor cells.....	58
Figure 33. ER stress and link to immunogenic cell death.	63

7.2. List of tables

Table 1 :General Equipment	68
Table 2: Consumables.....	69
Table 3: Chemicals used	69
Table 4:Cell culture media	70
Table 5: Buffers.....	71
Table 6: Standards for gel electrophoresis.....	72
Table 7: Primers used for polymerase chain reactions.....	72
Table 8: Polymerase enzymes for PCR.....	73
Table 9: Restriction enzymes used for cloning.....	73
Table 10: Vectors.....	73
Table 11: kits	73
Table 12: Nanobodies.....	73
Table 13: Antibodies.....	74
Table 14: Bacterial cells.....	74
Table 15: Cell lines.....	74
Table 16: mouse strain	75
Table 17: Software.....	75
Table 18: PCR reaction.....	76
Table 19: PCR amplification	77
Table 20: cDNA synthesis.....	80

7.3. Safety and Disposal

All the experiments were carried out considering the safety data sheets of the respective chemicals, as well as in laboratories of security level 1 and 2, chemicals, solutions and buffers were disposed of in the designated containers and all materials were autoclaved before disposal. Contaminated surfaces were disinfected with 70% Ethanol.

Chemicals	CAS-Nr.	-statement	P-statement
β -Mercaptoethanol	60-24-2	301-310-330-315-318-410	261-305+351+338
Ethanol	64-17-5	225	210
Formaldehyde	50-00-0	301-311-314-317-331-314-350	201, 260, 280, 301 + 310 + 330, 303 + 361 + 353, 304 + 340 + 310, 305 + 351 + 338, 308 + 311, 403+233
Gentamicin	1403-66-3	317,334,360,372,400,410	201, 202, 260, 261, 264, 270, 272, 273, 280, 281, 302 + 352, 304 + 341, 308 + 313, 314, 321, 333 + 313, 342 + 311, 363, 391, 405, 501
Collagenase D	900-12-1	317,334	261,280,302 + 352, 304 + 34, 342 + 311
Penicillin	69-57-8	317,334	280, 302 + 352, 304 + 341, 333 + 313, 342 + 31, 501
Streptomycin	3810-74-0	361,302	305 + 351+338,280,308+313
Doxorubicin	25316-40-9	302,315,319,340,350,360	201, 202, 264, 270, 280, 281, 301 + 312, 302 + 352, 305 + 351 + 338, 308 + 313, 321, 330, 332 + 313, 337 + 313, 362, 405, 501

Chemicals	CAS-Nr.	-statement	P-statement
Bortezomib	179324-69-7	300,315,319,361,372,411	201, 202, 260, 264, 270, 273, 280, 301 + 310, 302 + 352, 305+ 351 + P338, 308 + 313, 314, 321, 330, 332 + 313, 337 + 313, 362, 391, 405, 501
Ethidium bromide	1239-45-8	331,341	261,280,304 + 340 + 311, 403 + 233
Hydrochloric acid (HCl)	7647-01-0	290,314,335	234, 260, 304 + 340, 303, 361 + 353, 305 + 351 + 338, 309 + 311, 501
Phalloidin	17466-45-4	300,310,330	260,262,264,280,284,301 +310,302+352,304+340, 310,330,361+364
Puromycin	53-79-2	302	

Hazards statements

- H225 Highly flammable liquid and vapor
- H290 May be corrosive to metals
- H300 Fatal if swallowed
- H301 Toxic if swallowed
- H302 Harmful if swallowed
- H310 Fatal in contact with skin
- H311 Toxic in contact with skin
- H314 Causes severe skin burns and eye damage
- H315 Causes skin irritation
- H317 May cause allergic skin reaction
- H318 Causes severe eye damage
- H319 Causes severe eye irritation
- H330 Fatal if inhaled
- H331 Toxic if inhaled
- H334 May cause allergy or asthma symptoms or breathing difficulties if inhaled
- H335 May cause respiratory irritation
- H340 May cause genetic defects
- H341 Suspected of causing genetic defects
- H350 May cause cancer

- H360 May damage fertility or the unborn child
- H361 Suspected damage fertility or the unborn child
- H372 Causes damage to organs through prolonged or repeated exposure
- H400 Very toxic to aquatic life
- H410 Very toxic to aquatic life with long lasting effects
- H411 Toxic to aquatic life with long lasting effects

Precautionary statements

- P201 Obtain special instructions before use
- P202 DO not handle until all safety precautions have been read and understood
- P233 Keep container tightly closed
- P234 Keep only in original container
- P235 Keep cool
- P260 Do not breath dust/fume/gas/mist/vapors/spray
- P261 Avoid breathing dust/fume/gas/mist/vapors/spray
- P262 Do not get in eyes, on skin, or on clothing
- P264 Wash hands thoroughly after handling
- P270 Do not eat, drink or smoke when using this product
- P272 Contaminated work clothing should not be allowed out of workplace
- P273 Avoid release to the environment
- P280 Wear protective gloves/protective clothing/eye protection/face protection
- P284 In case of inadequate ventilation, wear respiratory protection
- P301 If swallowed
- P302 If on skin
- P303 If on skin (or hair)
- P304 If inhaled
- P305 If in eyes
- P308 If exposed concerned
- P309 If exposed or if you feel unwell
- P310 Immediately, call a poison center or doctor/physician

- P311 Call a poison center or a doctor/physician
- P312 Call a poison center or a doctor/physician, if you feel unwell
- P313 Get medical advice/attention
- P314 Get medical advice/attention, if you feel unwell
- P321 Specific treatment (as mentioned on the label)
- P330 Rinse mouth
- P332 If skin irritation occurs
- P333 If skin irritation or rash occurs
- P337 If eye irritation persists
- P338 Remove contact lenses, if present and easy to do, continue rinsing
- P340 Remove victim to fresh air and keep at rest in a position comfortable for breathing
- P341 If breathing is difficult, remove victim to fresh air and keep at rest in a position comfortable for breathing
- P342 If experiencing respiratory symptoms:
- P351 Rinse cautiously with water for several times
- P352 Wash with plenty of water
- P353 Rinse skin with water (or shower)
- P361 Take off immediately, all contaminated clothing
- P362 Take-off contaminated clothing
- P363 Wash contaminated clothing before reuse
- P364 and wash it before reuse
- P370 In case of fire:
- P378 Use.. to extinguish
- P391 Collect spillage
- P403 Store in a well-ventilated place
- P405 Store locked up.
- P501 Dispose of contents/containers...respectively

7.4. Curriculum vita

7.5. Acknowledgement

First, I would like to thank Prof. Friedrich Haag for believing in me and providing me the opportunity to fulfill my professional dream of doing PhD studies in Cancer Immunotherapy. Prof. Haag, I could have never done it without continuous support and guidance you have provided me over the last few years. Thank you listening my ideas and encouraging me to pursue them. You provided me the confidence and taught me how to critically develop the scientific ideas. I also want to thank you for encouraging me to attend the conferences and present my work. Last but not the least, I am really grateful for the support at the personal level with your advice during all this time.

I would like to acknowledge Prof. Koch-Nolte for his valuable feedback on my research work during departmental meetings. I would also like to thank him for providing nanobodies for the experiments.

I would like to acknowledge Dr. Carolina Pinto Espinoza. Caro, thank you for being a great and sincere friend, and a wonderful roommate. I really appreciate your support and encouragement during my thesis writing.

I also want to acknowledge the unconditional support from lab fellows, particularly Mrs. Gudrun Dubberke and Mr. Klaus Kaschubowski. Gudrun, thank you for being a great colleague and teacher, and all the help and support you provided during my stay in the lab. Thank you, Klaus, you have been always supportive and ready to help during all these years. It will be a memorable time for me.

I would also like to thank Dr. Björn Rissiek, Dr. Stephan Menzal and Dr. Nicole Schwarz for their help in solving technical issues related to research. I also extend my thanks to Mrs Fabienne Seyfried and Joanna Smith for the exceptional technical assistance. I would also like to acknowledge my office fellow Dr. Stefanie Klinge for nice time and for proofreading my thesis.

I would like to thank Dr. Isabel Ben Batalla and Nikolaus Berenbrok for their support and help in *in-vivo* experiments. I am very thankful to Mr. Michael Horn-Glander for his help in optical imaging.

Hello besties! Umber Saleem, Madiha Fayyaz and Hina Mir, you all were always there for me in good and bad times. I am grateful to all of you for the nice time. I will miss you all.

Dear Mom and Dad, I am very grateful to you that you believed in me and gave me the impulse to fulfil my dreams. Without your support, it could have been very difficult to accomplish my doctoral studies. I feel proud to have parents like you. I also thank my siblings for the nice time during my visits to Pakistan.

I very much appreciate the financial support from the DAAD, University of Hamburg and Prof. Haag, that allowed me to complete my doctoral research.

Sana Javed

7.6. Declaration

I hereby take the oath that I am writing this dissertation myself and not to have any tools other than those specified. I confirm that the dissertation was not submitted in an earlier doctoral procedure.

Date, Signature